Micromechanics of Natural-Synthetic Fiber-hybrid Reinforced Polymer Composites Laminae

A dissertation presented to The University of Manchester for the Bachelor of Science degree in the Faculty of Science and Engineering, within the Department of Mechanical, Aerospace, and Civil Engineering.

Juan Ignacio Doval Roque

10752534

Supervised by Dr. Kali-Babu Katnam

Department of Solid and Structures 2024

University of Manchester

TABLE OF CONTENT

LIST OF TABLES

LIST OF FIGURES

ABSTRACT

Fiber-hybrid reinforced polymer composites have proven to be an innovative design solution in structural application across the industry and sectors such as the Aerospace, Automotive, Sports, and Energy industry, because they have experimentally proven to be able to enhance damage tolerance compared to non-hybrid solutions. Computational micromechanical models, in particular two- and three-dimensional repeating unit cells (RUCs) with periodic microstructures are developed in Abaqus/Standard, a commercial FEA software, to model the micromechanics of unidirectional natural synthetic fiber-hybrid reinforced polymer composites with intralaminar hybridization. The aim of the study is to understand the lamina properties and micro stress fields of such when in-plane and out-of-plane tensile, and shear loadings are applied to the composite lamina. Throughout the study we will explore the differences between two- and three-dimensional RUCs and compare against commonly used analytical models, with the use of Python, programming language. Specifically, Chamis, Rule of Mixture, and modified Rule of Mixture

DECLARATION

I declare that no portion of the work referred to in the dissertation has been submitted in support of an application for another degree or qualification of this or any other university or other institutes of learning.

DEDICATION

To my parents Adolfo and Patricia,

My brother Adolfo,

And my girlfriend Kamila,

Who always support me.

To my friends who have always been of help and support.

I dedicate this work.

APPRECIATIONS

Firstly, I would like to express my sincere gratitude to my supervisor Dr. Kali-Babu Katnam for his endless support throughout my individual project journey, without his assistance the completion of this project would have never been possible.

I would like to say thanks to Giuseppe Romano, PhD Student, for his shared knowledge and constant feedback, guidance with formatting, support across the use of Abaqus/Standard and Python providing tutorials for a deeper understanding. As well as incentivising me to create my own Figures with the use of PowerPoint.

I would also like to thank Yang Yang for his verbal support, incentivising me to 'Tell a story' Instead of 'just producing a research paper'.

I express sincere gratitude to Akin Atas, my second marker, for his feedback provided during my poster presentation.

I express sincere gratitude to Miguel Herráez from https://tecnodigitalschool.com/ for his tutorials on Python scripting for Abaqus, which have been invaluable in modifying and post-processing intricate computational models. His expertise and guidance have played a pivotal role in advancing my project.

Special thanks to my colleague Mohamed Sadik Mohamed Ali who provided inspiring discussion and support throughout this project.

Another special thanks to my girlfriend, family and friends who always support me unconditionally.

Lastly, I want to extend my appreciation to The University of Manchester for providing the resources and facilities that made this study possible. The Mechanical Aerospace and Civil Engineering (MACE) department has fostered an environment conducive to academic development, and I am thankful for the opportunities it has offered.

COPYRIGHT

i. The author of this dissertation (including any appendices and/or schedules to this dissertation) owns certain copyright or related rights in it (the "Copyright") and s/he has given The University of Manchester certain rights to use such Copyright, including for administrative purposes. AERO62000 Dissertation 2023 38.

ii. Copies of this dissertation, either in full or in extracts and whether in hard or electronic copy, may be made only in accordance with the Copyright, Designs and Patents Act 1988 (as amended) and regulations issued under it or, where appropriate, in accordance with licensing agreements which the University has entered into. This page must form part of any such copies made.

iii. The ownership of certain Copyright, patents, designs, trademarks, and other intellectual property (the "Intellectual Property") and any reproductions of copyright works in the dissertation, for example graphs and tables ("Reproductions"), which may be described in this dissertation, may not be owned by the author, and may be owned by third parties. Such Intellectual Property and Reproductions cannot and must not be made available for use without the prior written permission of the owner(s) of the relevant Intellectual Property and/or Reproductions.

iv. Further information on the conditions under which disclosure, publication and commercialisation of this dissertation, the Copyright, and any Intellectual Property and/or Reproductions described in it may take place is available in the University IP Policy, in any relevant Dissertation restriction declarations deposited in the University Library, and The University Library's regulations.

NOMENCLATURE

i, j, k	As subscripts	Vector and tensor indices
$1, 2, 3$	As subscripts	Longitudinal, transverse
f, m, i	As subscript/ superscript	Fibre, matrix, and interphase
E	$[GPa]$	Elastic modulus
G	$[GPa]$	Shear modulus
v	[-]	Poisson's ratio
R	$[m]$	Radius
U	$[m]$	Distance, Displacement
ε	[-]	Strain
V	[-]	Volume fraction
A	$[m^2]$	Area
F	$[N]$	Force
Γ	$[m^2]$	Boundary
Ω	$[m^3]$	Volume
$\boldsymbol{u}$	$[m]$	Displacement vector
u_i	$[m]$	Displacement vector components along i
x_1		Coordinate axis along longitudinal direction
x_2, x_3		Coordinate axis along transverse direction
$\boldsymbol{\sigma}$	$[MPa]$	Stress tensor
$\boldsymbol{\varepsilon}$	[-]	Strain Tensor
$[C]$	$[MPa]$	Compliance tensor
N_i	[-]	Nodes
$\widehat{\ }$	$[MPa]$	Homogenised/macro
$\boldsymbol{\sigma}$	$[MPa]$	Micro (local) stress
σ_{ij}	$[MPa]$	Micro (local) stress components along i, j
σ_n	$[MPa]$	Normal stress at the fibre-matrix interface
τ_{nt}	$[MPa]$	Shear stress at the fibre-matrix interface
L	$[m]$	Width of RUC
H	$[m]$	Height of RUC
t	$[m]$	Thickness of RUC

τ	$[N]$	Traction force
ρ	$[g/cm^3]$	Density
$\boldsymbol{n}$	[-]	Unit normal vector (surface normal)
$\langle \quad \rangle$		Volume average

GLOSSARY

PMC – Polymer Matrix Composite

MMC – Metal Matrix Composite

CMC – Ceramic Matrix Composite

NF – Natural Fibers

HC – Hybrid Composite

PBC – Periodic Boundary Condition

RUC – Repeating Unit Cell

RVE – Representative Volume Element

ROM – Rule of Mixture

$ROMm$ – Modified Rule of Mixture

Ch – Chamis

FEA – Finite Element Analysis

FEM – Finite Element Method

UD – Unidirectional

1 INTRODUCTION

Experimental data is crucial for both developing and validating models, yet it comes with inherent limitations such as cost, complexity, and the challenge of replicating certain geometries. The advent of commercial software for structural analysis, commonly known as Finite Element Analysis (FEA), has revolutionized the study of complex components. FEA yields representative results for materials and structures, albeit with computational constraints in terms of power and time. [30]

In modelling composite materials, one approach has been employed, Repeating Unit Cells (RUCs), in both two- and three-dimensional models, with diagonal fiber packing arrangement [24]. This paper focuses on polymer-matrix composites reinforced with natural and synthetic fibres, involving hybridization at the microscale to derive macroscopic material properties through homogenization. [5]

Polymer-matrix composites have demonstrated remarkable strength-to-weight and stiffness-to-weight ratios, offering versatile opportunities for tailoring material properties through hybridization. This versatility extends across various sectors and structures, making them increasingly attractive for diverse applications. [5][6]

However, alongside their advantages, these single fiber composites also present drawbacks such as fragility and poor damage tolerance and repairability, which are undesirable traits.

In recent years, the modelling of fiber hybrid composites has witnessed the adoption of different strategies based on the scale of the composite considered, including macro, meso, and micro-scale approaches. This trend is exemplified by the utilization of glass fibres as thin-wall tubes to replace conventional metals like aluminium. This substitution aims to reduce costs and weight, thereby enhancing operational efficiencies without compromising mechanical properties. [26]

The study in this paper entails a micromechanical investigation of fiber-hybrid composites. It delves into the use of 2D and 3D Repeating Unit Cells, discussing their advantages and limitations. The simulation process is thoroughly documented, encompassing considerations of periodicity and boundary conditions applied to the models under study.

In conjunction with computational models, the paper employs analytical models, Rule Mixture, modified Rule of Mixture and Chamis model for validation. It presents and discusses the behaviour of these models compared to the Repeating Unit Cells, offering insights into their efficacy.

1.1 CONTEXT

1.1.1 Composites Materials

Many materials, whether they are artificially produced or found in nature, can be classified as composites. These materials are typically composed of two distinct components. Composites are the outcome of combining two different materials, and this combination results in an improved design and enhanced mechanical properties when compared to the individual constituents tested separately. It is commonly recognized that within composites, one of the components, referred to as the reinforcement, possesses characteristics such as stiffness, discontinuity, and strength, often taking an elongated form. In contrast, the second component, known as the matrix, is typically less rigid, weaker, and extends uniformly throughout the composite material. It's important to note that due to chemical interactions between these two constituents, a new phase, known as the interphase, may develop at the interface where both constituents come into contact. As illustrated in Figure 1, a cross-section of a composite material allows for the observation of the reinforcement embedded within the matrix, including the presence of the interphase.

For instance, wood consists of a cellulose fiber, as reinforcement, which is embedded in lignin, as matrix [9]. Regarding the properties of a given composite, factors such as geometry, properties of the individual materials and the distribution of each constituent across the plane will take an important role on the properties of the material [26]. Due to the distribution of the constituents throughout the composite, as mentioned before, often fibres tend to be elongated due to their crystal structure, many composites will show *anisotropy* as the fiber and matrix will both depend on direction and position in a fixed system of coordinates [11]. *Anisotropy* is defined as the change or differing in physical and mechanical properties when different orientations are considered across the composite, whereas *isotropy* demonstrates consistent properties of the composite over

various planes. Therefore, the behaviour of anisotropic composites when load is applied may vary depending on orientation of such force.

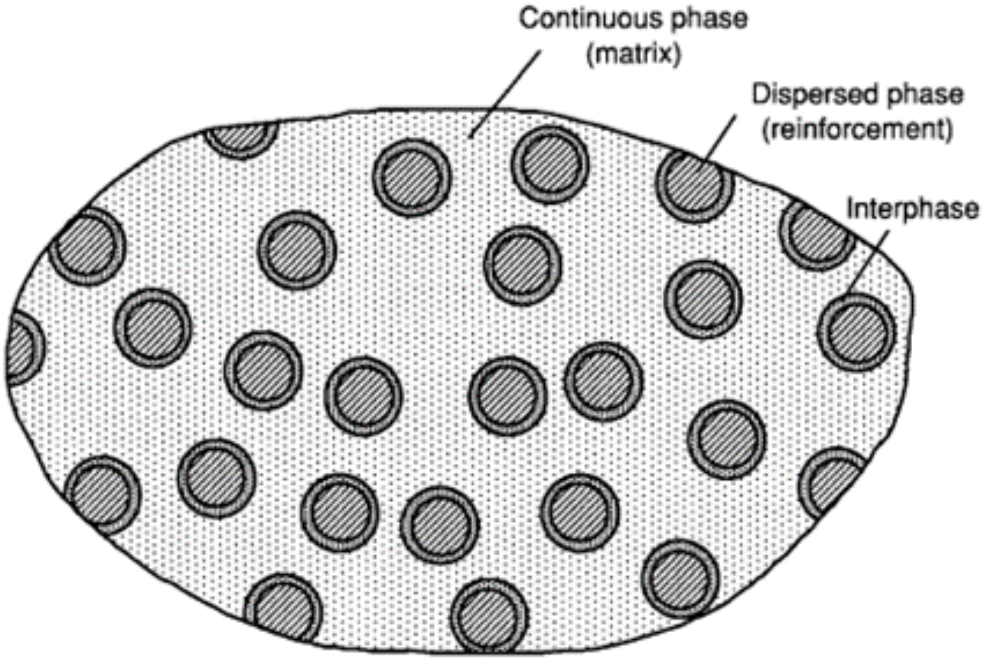

Figure 1: *Distribution of Constituents in a composite material [26].*

Composites can present different volume fractions, which is considered one of the most important parameters to follow up when studying a given composite. This refers to the ratio between reinforcement, matrix, and interphase that a material possess. This can be represented in similar manners depending on the number of phases a composite possesses by the Equation (1).

$$V_f + V_m + V_I = 1 \quad (1)$$

Where V_f – is the volume fraction of the reinforcement or fiber, V_m – is the volume fraction of the matrix and V_I – Represents the volume fraction of the interphase. It is important to note that the sum of these values is 1 which account for the 100% of the volume of a given composite. In addition, if the composite in question does not possess an interphase, then V_I is equal to zero.

The volume or weight fraction will determine how homogeneous or heterogenous the composite is, and it follows, the more uniform the fibrous constituent is across the

composite, the more homogeneous the material, and vice versa. Thus, heterogeneous composite can present disadvantages such as structural failure in areas where reinforcement is absent or scattered.

Revisiting our prior discussion regarding wood, this composite material exhibits both anisotropy and a consistent structure, properties that have been harnessed by humanity for millennia, dating back as far as 10,000 years ago. These properties allow the wood to provide significant strength along the axis cellulose fibres. Axis that is often shared with the trunk or branch axis, instead of, throughout the transverse direction of the wood [9]. Therefore, a trunk will be able to withhold a significant load across its axial direction, where the stress will be distributed across of such axis, acting as a cantilever, rather than throughout the trunk's thickness.

Modifying the physical characteristics of a particular composite to meet specific requirements and deviate from traditional approaches offers numerous benefits to the industry, shown in Figure 2. This includes the enhancement of material properties, customization of composite performance, weight reduction, and consequently, improvements in the strength-to-weight ratio and cost-effectiveness. Hence, the development of synthetic composites, often referred to as man-made composites, necessitates the need for modelling and testing to assess failure modes and define the properties of various hybrid combinations.

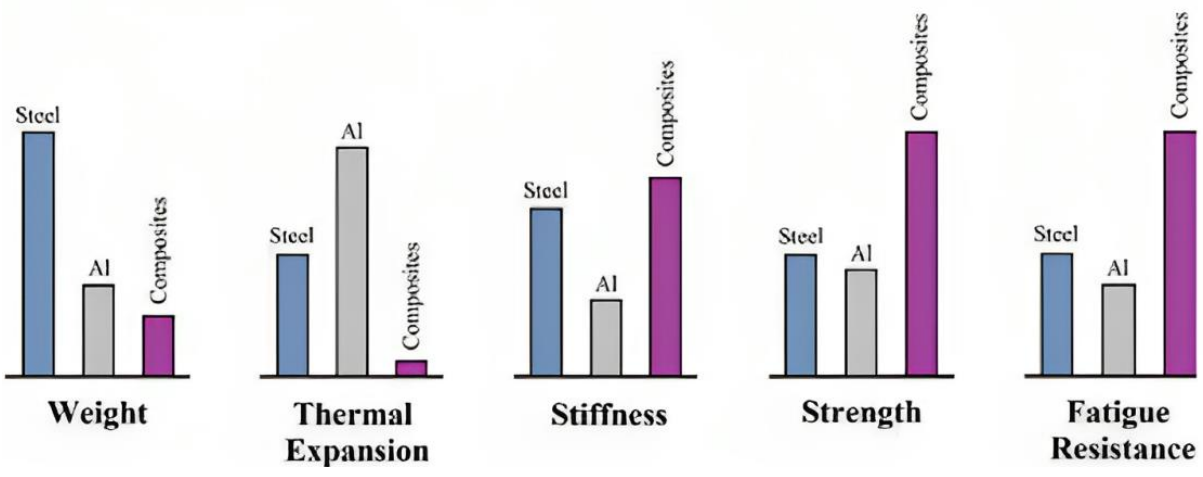

Figure 2: *Comparison between monolithic materials (Aluminium & Steel) vs Composite materials [8].*

1.1.2 Applications

Modern Composites are used across a wide range of engineering disciplines due to their desirable physical, mechanical, electrical, and thermal properties. Through history different applications has been discovered for the use of composite. For example: In the Aerospace industry, composite materials such as epoxy/carbon and titanium/graphite encompass around 50% of Boeing 787's weight [26].

1.1.3 Overview of Composite Analysis

In STEM field engineering have developed a way to facilitate the analysis and representation of physical and mechanical properties such as Young Modulus of elasticity, Poisson's ratio and thermal expansion coefficient that occurs in a specific point in a material. This has been done by setting a boundary within the structure in order to separate the structure from the material. A good example of this would be a beam of aluminium, when subjected to analysis of its properties, such as flexural rigidity, both the shape of the structure and the property of aluminium are accounted for, shown in Equation (2). More specifically, moment of inertia, I, is exclusive from the shape of the given beam, while E (Young's Modulus) is provided from the material of choice, for this case, aluminum (70 GPa).

$$D = EI \tag{2}$$

The discussion above remains relevant to the study as an internal boundary will be required in order to demonstrate closely the arrangement and displacement of both reinforcement, matrix, and the interphase in between when a load is applied. This is ideal as each constituent can be analysed as continua, which allows the use of continuum mechanics, and account for their respective properties, which in combination to the general arrangement of the constituents together, will demonstrate the general behaviour of the composite in use.

1.1.4 Classification of Composites

Composites are classified in regard to 2 different aspects, the first one is with respect to the matrix constituent, and the second with respect to the reinforcement.

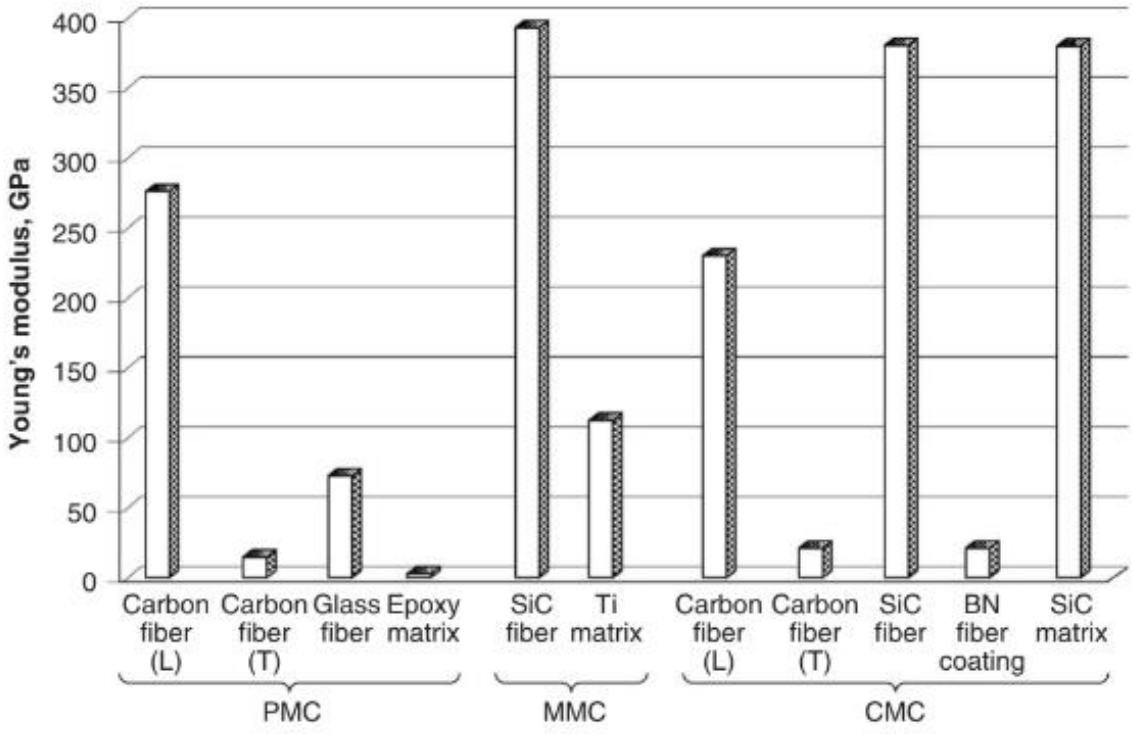

Figure 3: *Young's Modulus of common PMC, MMC, and CMC isotropic composites, and in both Longitudinal and Transverse directions for carbon fiber composites that are anisotropic [2].*

Moreover, within the matrix classification, the types of composites are characterized by the matrix of choice, thus, the following 3 categories: PMC – polymer matrix composites, MMC – metal matrix composites, and CMC – ceramic matrix composites. In the other hand, Reinforcement composites are classified by the following list of aspects: continuous fibres, discontinuous fibres, also known as whiskers, or textile, which refers to the pattern in which fibres were arranged/braided within the yarn [2]. Yarns in composites are continuous length of interlocked fiber and matrix, that facilitates the sewing of lamina. For instance, the common ways of braiding fiber are the following: Coiled into a helix, or Tubular – continuous and consistent fibres from one end of the yarn to the other. In Figure 3, it is possible to observe the influence in Young Modulus of elasticity of the use of different matrix constituents (PMC , MMC , and CMC) for composites, in both longitudinal orientation (L) and Transverse orientation (T) for anisotropic composites.

1.1.5 Environmental Impact

As mentioned before, composites have improved quality and life span of structures across the different engineering disciplines throughout the world. By 2000, it was estimated that the production of composites materials was about 7 million tons within the various industrial sectors. Even though the composites reduce fuel consumption on aircrafts and automobiles, due to their reduced weight, or improve the resistance to larger loads in structures, they possess a treat to the environment as composites present a challenge during its recycling. Individual materials within the composites have been recycled efficiently, but composites remained an exception. This occurs due to the complexity of the structure, as the composites have to be recycled accounting for both the matrix and reinforced constituents that present inherent heterogeneity and complex structure. Down recycled – the use of waste materials to produce a material inferior to the original, has been the possible recycle method for composites material, but this method introduces a new challenge as extensive fuel is consumed for a return of little material recovered, for example: fibres.

Thus, the advances of recycling composites are promising, the methods inherently present high costs and lower quality, therefore the introduction of natural fiber reinforced composites such as Basalt and Flax, branching the categories of composites and bringing a more sustainable opportunity for the industry. In the past 2 decades, a promising eco-friendly alternative to conventional matrix constituents called geo-polymers. These polymers are capable of improving both fracture toughness and flexural strength, in addition to, to their ability to retain CO_2 emissions.

1.1.6 Advantages and Limitations

As mentioned before, composites present different advantages in comparison to pure or monolithic materials such as steel or aluminium. More specifically, regarding their higher strength, stiffness, fatigue resistance, lower density. In addition, these composites can be designed for specific situations where there is a stronger wear or corrosion resistance, therefore, their adaptability. Regarding their structural composition when directly compared to monolithic materials, the parameter to take into consideration is the weight-to-strength ratio, which is usually seen as the requirement to perform the same task as a monolithic material but reducing the weight of the structure by a given percentage of

lesser weight. Despite the composite's advantages across multiple areas, they possess various limitations when different aspects or scales are considered.

Composites can be tested and studied across different scales, moreover, Macro-scale, Mesoscale and Micro-scale in order to determine failure modes and characterization. Throughout this study, the focal point will be regarding the microscale, and therefore, the micromechanics of the composites.

1.2 MICROMECHANICS

The microscale of a composite ranges between millimetres (mm) to micrometre (μm), where fibres can be observed, and consequently the matrix functioning as a 'glue' for the fibres. Again, fibres tend to contain low fracture toughness, and therefore, the use of a ductile matrix that facilitates the transfer of stresses across the structure of the composite and dissipate energy. Ultimately, the ability of the matrix to transfer the stresses of an applied load prevents the failure of the structure in different locations.

2 LITERATURE REVIEW

2.1 NATURAL FIBERS IN POLYMER COMPOSITES

Natural Fibers (NF), also known as plant, animal, or mineral fibres, are expanding rapidly as they come with abundant advantages regarding their environmental impact, availability, cost, and energy required for production. Additionally, these fibres possess valuable mechanical and physical properties such as reduced weight, high resilience against wear and tear, and a high specific modulus. Similarly, natural fibres have some significant drawbacks in comparison to synthetic fibres such as carbon that is commonly used due to their composition, as they are constructed from materials prompt to moisture like lignin and cellulose, which are found on trees, pectin, and waxy, causing a weaker bond between the polymer matrix and the natural fibres. This moisture can overshadow the mechanical properties of the fiber as the fiber swells from the ineffectiveness of the interphase, due to chemical reactions between reinforcement and matrix, at conveying the stresses, and ultimately generate micro-cracks [14]. In Table 1, both advantages and drawbacks of the NF composites have been listed for general reference.

Table 1: Advantages and Drawback of Natural Fibers [14].

Advantages	Drawbacks
• Low specific weight produces greater specific strength and rigidity than glass • Renewable resources and production need little energy and emit little CO2 • Low-cost production with low investment • Processing is gentle, there is no tool wear, and there is no skin irritation • Electrical resistance is high • Excellent thermal and acoustic insulation qualities • Biodegradable • Thermal recycling is possible	• Lower strength, particularly impact strength • Variable quality affected by climatic conditions • Insufficient resilience to moisture, which results in fibre swelling • Temperature limit placed on the manufacturing procedure • Reduced durability • Fire resistance is poor • Inadequate fibre/matrix adhesion • Variations in prices brought about by the outcomes of harvests or by agricultural politics

The relevant parameters to consider during the testing of the natural fibre composites are the tensile strength, the flexibility and elasticity, wicking or moisture absorption, thermal properties, chemical resistance, UV resistance and Biodegradability. Though, despite the recognition of the different parameters, the study will focus specifically on the homogenised properties the composites porsses and the behaviour of such during transverse loading.

2.2 HYBRID COMPOSITES

Hybrid composites is the combination of fibres or matrix constituents to achieve different and improved composites, with superior physical and mechanical properties. Combining the natural fibres and matrix constituents with superior strengths can ultimately counteract drawbacks mentioned in previous section [14].

In the realm of fiber-hybrid composites, three main configurations are worth considering, as depicted in Figure 4. The first configuration, illustrated in Figure 4(a), is interlayer fiber-hybrid composites, which is not only the most economical but also the simplest among the three. It involves stacking layers of different fibres on top of each other.

Figure 4(b) showcases intralayer fiber-hybrid composites, where two distinct fibres are combined within the same layer. In this setup, the yarns of these different fibres are interwoven to create a fabric. It's worth noting that a configuration with parallel yarns of different fibres is also a viable option within the intralayer approach.

The third configuration, which is of primary relevance to this study, is the intrayarn configuration, as depicted in Figure 4(c). In this case, different fibres are mixed within the same yarn and are assumed to be transversely isotropic, thus cylindrical. In addition, it is assumed no debonding in the interface between the fiber and the matrix. This configuration is considered the most complex of the three [20].

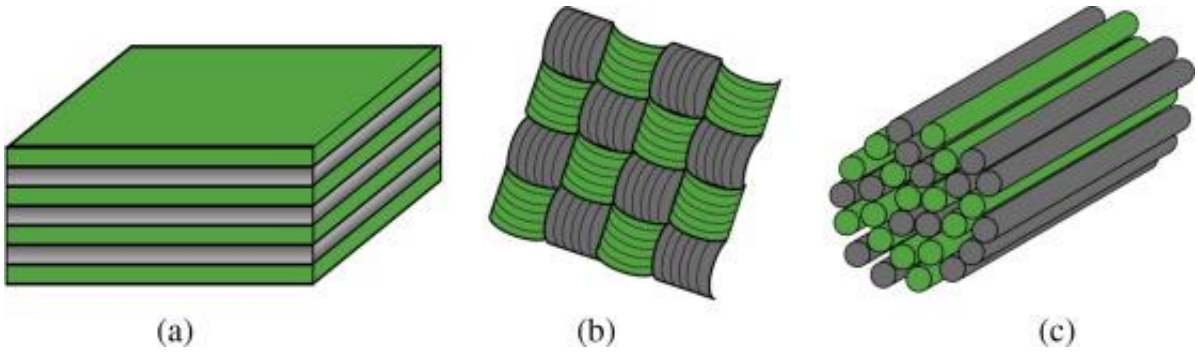

Figure 4: *Three main hybrid configurations: (a) Inter-layer (b) Intra-layer, and (c) Intra-yarn [20].*

More specifically, these hybrid composites can consist of either a combination of various fibres and one matrix phase, a fibre of choice allocated within different matrix phases, or a combination of different fibre phases and various matrix phases. Despite the wide range of combination, the engineers interest remains in natural composites with one matrix phase and various natural fibres as the qualities of such fibres can be balanced by overshadowing the inferior qualities of a fibre by the superior qualities of the other fibre in specific properties, thus, the use of two fibres remains approved. Hybrid Composites can be found in applications like plastic tanks, automobile and aviation parts, and construction components [14]. Common natural fibres are aramid, carbon, and glass.

Hybridization can be used to reduce weight as pure single fibre composites can be expensive depending on the higher-quality fiber of choice, and therefore the combination of low- and high-quality fibres for the same component without compromising the performance and satisfy its purpose. This can result in a significant reduction of the price of parts. For instance, exchanging carbon fibres for cheaper glass fibres within a laminate can reduce costs by a significant margin [20]. On the other hand, hybridization can be used to enhance maximize performance by combining high-quality fibres for critical applications such as spacecraft parts where performance will becloud price as human life may present safety risks.

Regarding fibres, not only dissimilar fibres but similar fiber with other physical properties such as fibre's dimensions may affect the performance of the reinforcement. For instance, carbon fibres may be found with different diameters as this will impact the fibre's stiffness [14].

2.3 Periodic Boundary Conditions and Boundary Conditions

The concept of boundary conditions is often downplayed and simplified when teaching, but in reality, boundary conditions play a crucial role in not only determining solutions but also in shaping the methods used to solve equations [13].

Various micromechanical techniques have been developed to analyse and predict the overall behaviour of composite materials. Energy variational principles have been used to establish upper and lower bounds for the elastic modulus, as demonstrated by Hashin and Shtrikman in 1963 and Hashin and Rosen in 1964. Additionally, Whitney and Riley, in 1966, employed an energy balance approach and elasticity theory to derive analytical expressions for the elastic modulus of composites. However, it's worth noting that extending this method to viscoelastic, elastoplastic, and nonlinear composites is a challenging task [24].

In 1991, Aboudi introduced a comprehensive micromechanical theory that was centred on the examination of interacting periodic cells. This theory enabled the prediction of the overall behaviour of both elastic and inelastic components within composite materials. Aboudi's approach involved applying homogeneous boundary conditions to the Representative Volume Element (RVE) or unit cell models. Between 1987 and 1996, several researchers, including Needleman and Tvegaard, Sun and Vaidya, and Suquet,

pointed out that the use of 'plane in plane' boundary conditions had certain limitations [16][18][19]. Specifically, these conditions led to over-constrained boundary conditions and violated stress/strain boundary conditions [24].

The micromechanical models mentioned earlier are typically known as mechanical or engineering models. In contrast, a mathematical model called 'asymptotic homogenization theory' was introduced in the 1970s as an alternative approach. Pioneers in this mathematical model include Suquet (1987), Benssousan et al. (1978), Sanchez-Palencia (1980), and Bakhvalov and Panasenko (1984) [6][7][17]. This asymptotic homogenization theory explicitly incorporated periodic boundary conditions when modelling both linear and non-linear composite materials. As a direct result, it was demonstrated by Suquet in 1987 that distinctive patterns of deformation do not occur along planar boundaries after deformation. Following this, in 1991, Guedes and Kikuchi investigated the utilization of the finite element method (FEM) for solving issues related to composite materials [24].

In 1999, Hori and Nemat-Nasser showed that the anticipated effective elastic modulus could change depending on the conditions applied to the boundary, denoted as B_{δ}, of a unit cell. Consequently, the utilization of periodic boundary conditions is favored as it provides more precise results, particularly when applied in the context of hybrid theory [24].

Periodic boundary conditions (PBC) involve replicating a 3D modelled 'box' representing the composite, often referred to as a unit cell, endlessly throughout space. This can be visualized as a periodic arrangement of a repeated unit cell (RUC). When a cell, as depicted in the figure, moves beyond the boundary, it reappears on the opposite side of the 'cloned box,' following the same direction and displacement.

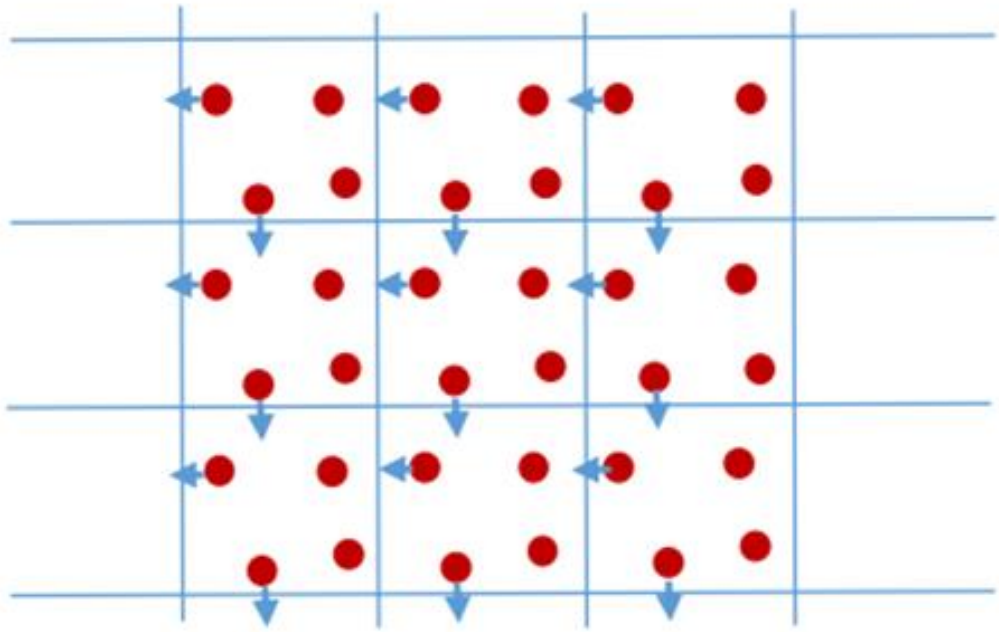

Figure 5: *2D periodic boundary condition cell of a randomly distributed RVE [3].*

The Periodic Boundary Condition is governed by the equations (3)(4)(5). The equations are capable of representing the displacement or strain that arises within the framework of the periodic boundary condition and maintaining distance $\Delta \boldsymbol{x}$ constant between the nodes of opposite edges.

$$u_i(\boldsymbol{x} + \Delta \boldsymbol{x}) - u_i(\boldsymbol{x}) = \varepsilon_{ij} \Delta x_j \tag{3}$$

$$u_i(\boldsymbol{x} + \Delta \boldsymbol{x}) = u_i(\boldsymbol{x}) \tag{4}$$

$$\tau(\boldsymbol{x} + \Delta \boldsymbol{x}) = -\tau(\boldsymbol{x}) \tag{5}$$

In Equations 3-5, u_i – is the displacement at $\boldsymbol{x}$, ε_{ij} – signifies the applied macro-strain component to the RVE, $\boldsymbol{x} + \Delta \boldsymbol{x}$ and $\boldsymbol{x}$ – are position vectors of opposite unit cell's faces τ – denotes the traction force, and B_{δ}^{1} – is boundary chosen with its normal oriented in the '1' direction, illustrated in figure 6.

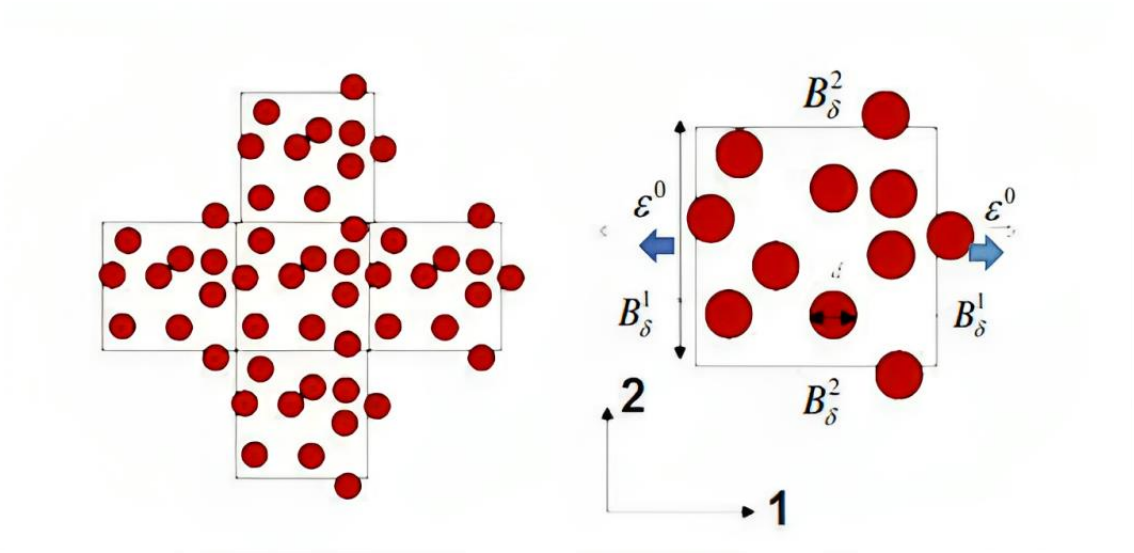

Figure 6: *2D periodic boundary condition cell of a randomly distributed RVE, with set coordinate directions and notation [3].*

Randomness in the distribution of fibres within a transverse cross-section of actual composites is a common occurrence. However, when modelling these materials with periodic boundary conditions, this randomness can introduce complexities. The approach called falsified periodicity has been proposed as a solution to this issue, but it's essential to note that this approach is fundamentally incorrect, and we will explore this matter further in the Section 2.4.

2.4 Representative Volume Elements (RVEs) vs Repeating Unit Cells (RUCs)

An essential aspect of multiscale modelling involves defining the appropriate representative volume. When this volume is precisely defined as a mathematical domain with specific dimensions, it is referred to as the Representative Volume Element (RVE). The primary objective is to make the RVE closely mirror the material's behaviour at a larger length scale, ensuring both the homogeneity and uniformity of the composite, whether on a physical or statistical basis. In other words, the RVE represents a finite-sized portion of the material at a lower length scale, which is considered mathematically infinitesimal at larger length scales [13].

The characteristics of the materials under consideration, such as heat capacity and Young's modulus in the fiber direction of unidirectional (UD) fiber-reinforced composites, are primarily influenced by the volume fraction of the selected constituents

as a high-volume fraction of fibres will provide a more brittle composite, while low fiber fractions will provide less strong composites. For properties like Young's modulus, which rely on the statistical uniformity of transverse fibres in unidirectional composites, it may be necessary to have larger material volumes for the Representative Volume Element (RVE) to be considered truly representative of the composite.

In the context of the study and at smaller length scales, researchers often define a unit cell, which serves as a specific type of RVE. This unit cell is designed based on the regular and repeating structure of the material, where "regularity" pertains to the geometric

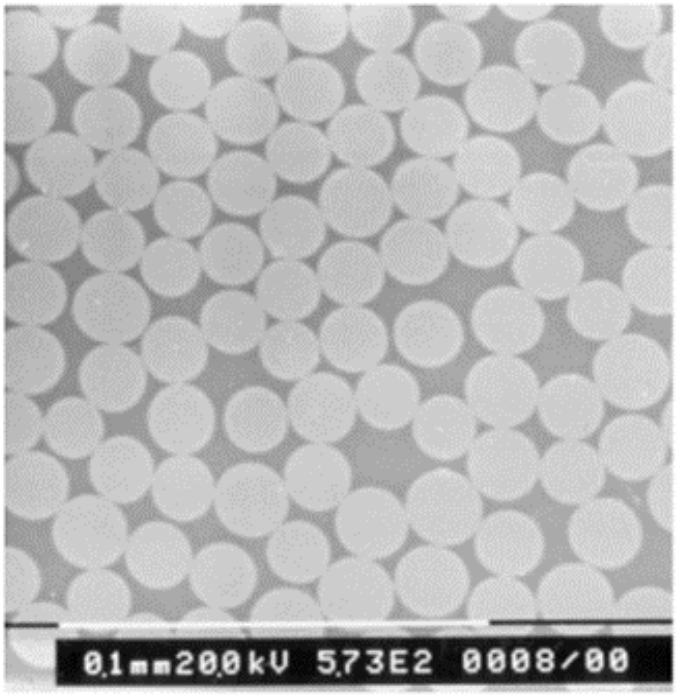

Figure 7: *Random fibre distribution over the transverse cross section of a real unidirectional composite [13].*

arrangement of the composite's fibres and matrix phase. RVEs are typically used to address issues associated with random structures, such as those found in unidirectional fiber-reinforced composites at the microscale, as illustrated in Figure 7.

When dealing with the challenges of falsified periodicity in randomly distributed fibres within real composites, complexities arise. As per the definition of the Representative Volume Element (RVE), it should accurately represent and retain key characteristics, such as randomness, which can be compromised when simplifying the RVE for ease of analysis.

As mentioned earlier, at smaller length scales, Periodic Boundary Conditions (PBCs) may be introduced, but this necessitates adjusting the boundaries to mimic periodicity. This adjustment involves duplicating all the features truncated by the boundary on the opposite side, as depicted by the darker circles in Figure 8(b). However, this previous approach can undermine the volume fraction of the composite constituents, thereby failing to preserve the composite's essential characteristics.

Figure 8(e) exemplifies the issues with falsified periodicity, where repeating Figure 8(b) across the space results in overlapping, which, again, affects the volume fractions of constituents. To address this, Figure 8(c) demonstrates how truncated features that happen to overlap are managed through the following criteria: existing features are artificially relocated to free space, overlapping features are either deleted or prevented, as shown in Figure 8(c). When this process is repeated periodically, it generates Figure 8(f), where there is no overlapping, and the volume fraction is preserved. It's important to note that when truncating the features along the boundary of Figure 8(c), an RVE emerges, as illustrated in Figure 8(b) [13].

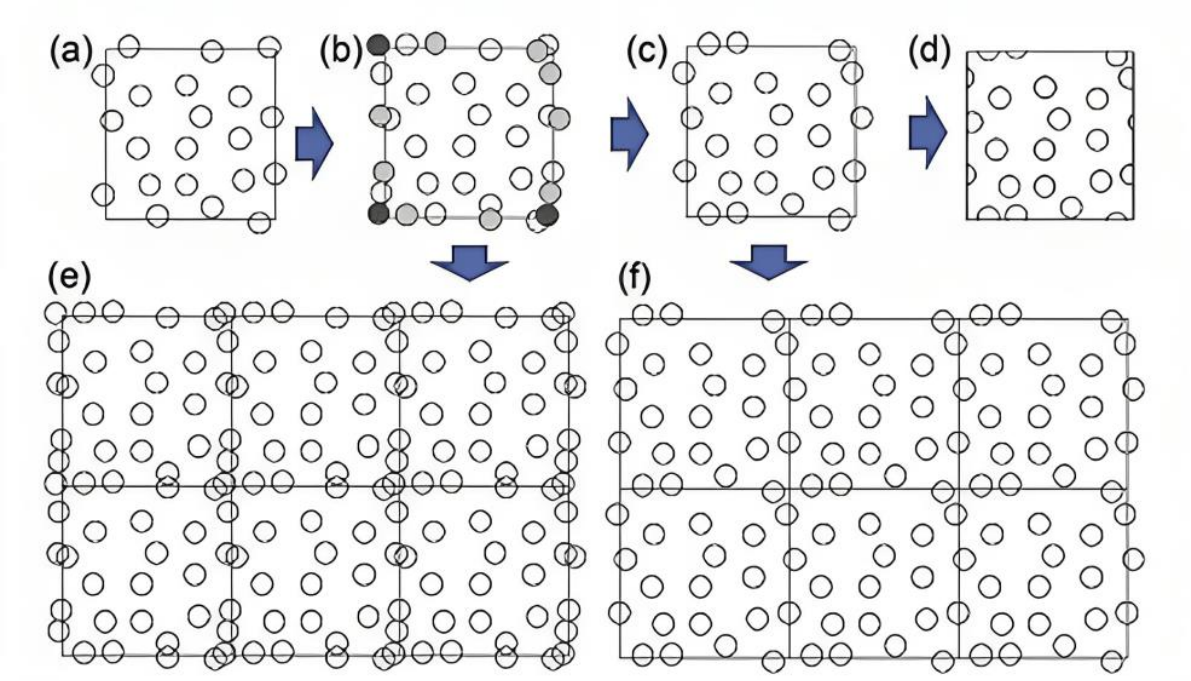

Figure 8: *Falsified periodicity in RVEs [13].*

As mentioned before a unit cell (UC) is a portion of material at its lower length scale which reproduces all other parts of the material through appropriate symmetry transformations, so that the UC and its images fill up the space the material occupies in

exactly the same way as the original material without leaving gaps or causing overlaps, which causes regularity across the structure of the material. This involves asserting the correct interpretation of symmetries present in the structure.

As RVE may require larger volumes to capture the essence of the micromechanics of a given composite and rise computational time, and often this will not ensure it is rightly representative. RUC can be modelled smaller length scales, and a periodicity condition can be applied to it in order to generate the overall structure of the composite which can reduce the modelling time significantly. Shown in Figure 9, it is possible to locate both the RVE and the RUC. Here the RUC is represented by size d, while D represents the size of the RVE. It is worth noting that if the ratio d/D is much less than 1, then the RVE will require plenty RUCs in order to represent an inherent heterogeneous composite as homogeneous.

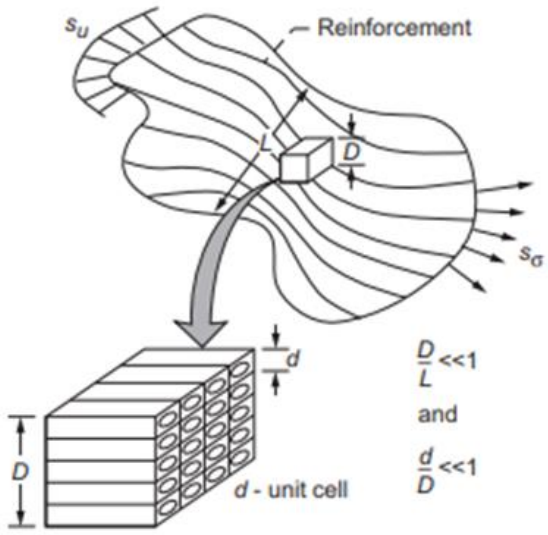

Figure 9: *RVE and RUC dimensions [1].*

RUCs can present idealized organization of the constituent within the cell to provide homogeneity across the materials when repeated periodically, and these cells possess different shapes, often used are the following: square, and hexagonal shape.

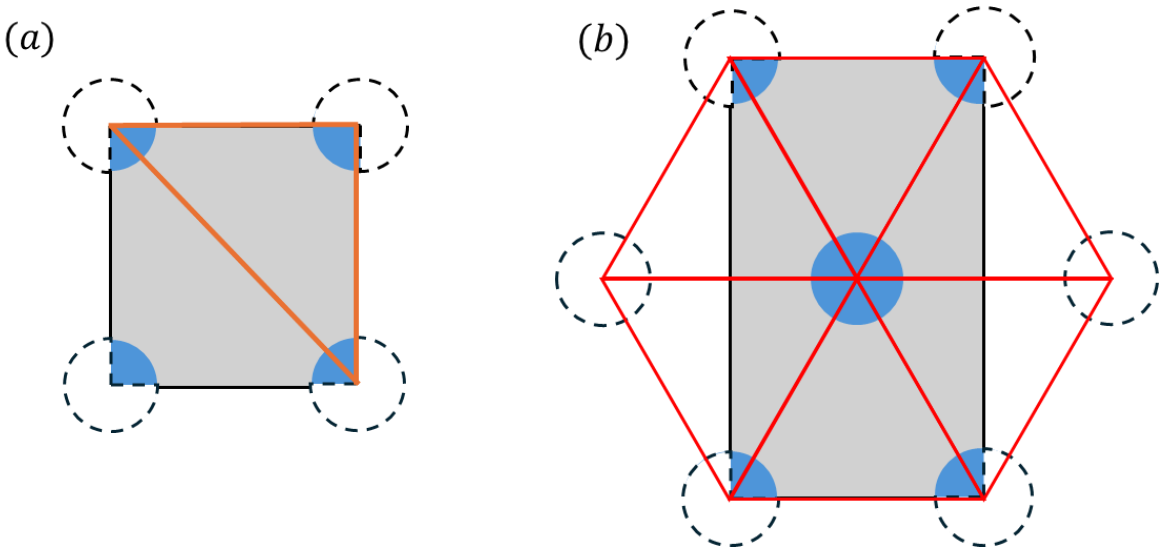

Figure 10: *(a) Square and (b) Hexagonal packing of a 2D RUC.*

The primary distinction between the two shapes lies in their spatial arrangement. Illustrated in Figure 11, square packing results in fibres being situated at inherently varying distances from the centre of each fiber to its surroundings. Specifically, diagonally positioned surrounding fibres are farther away compared to those located vertically or horizontally due to the application of the Pythagorean theorem. Consequently, this arrangement lacks isotropic transverse properties. In contrast, the hexagonal shape's unit cell generates fibres with consistent spacing to every surrounding fiber, thereby ensuring transverse isotropy.

2.4.1 Selection of the shape

Shape of the unit cell is dictated by microstructure of the composite in order to represent the characteristic of such for both a realistic RVE or a reasonable RUC idealization. Regarding an Idealized model, some general considerations are required to choose the appropriate shape from Figures 10. For UD composites, where fibres are located randomly across the yarn, a hexagonal packing would represent the randomness as idealistic as a square packing. However, for transversely isotropic composites with fibres like basalt and E-Glass, the random distributed fibres across the transverse plane will remain isotropic, and hexagonal packing will be more representative than a square packing. For 2D shapes Abaqus is not able to capture axial shear, therefore the use of 3D shapes can provide a solution in the analysis of axial parameters [1].

2.5 ANALYTICAL MODELS

In this section, numerous micromechanical models will be discussed and evaluated. It is important to note that each of these models relies on specific assumptions that hold true for particular types of composite structures. We will outline the assumptions inherent to each model, as well as their respective advantages and drawbacks [21].

In the context of micromechanical model analysis, certain fundamental principles are introduced. To begin, the composite material is assumed to exhibit linear elasticity and possess transverse isotropy in the unidirectional (UD) plane. Additionally, the fiber is regarded as transversally isotropic, while the matrix phase is assumed to be isotropic in all directions. In terms of composite properties, there are five distinct independent properties: E_1 as the axial modulus and E_2 for the transverse modulus. G_{12} and G_{23}, representing the axial and transverse shear modulus of the fiber. v_{12} as the in-plane Poisson ratio. [21]

Thus, E_1^f, E_2^f, G_{12}^f, G_{23}^f and v_{12}^f. The superscript ƒ denotes fiber and for superscript m, as the matrix phase, goes as followed: E^m, v^m and G^m, where G^m is:

$$G^m = \frac{E^m}{2(1 + v^m)} \tag{6}$$

Another way to define a composite material is through the volume fraction V_f, as described by equation 1. However, an alternative approach is to account for the void volume fraction, representing the absence of material, denoted as V_v.

2.5.1 Analytical models based on Rule of Mixture

Rule of Mixture is an intuitive approach for the homogenization of composites that' has become popular due to its simplicity. This simplicity comes with assumptions that may not be favourable, and thus the different models derived from it, to try and correct this for different approaches. For simple geometries these models can be very practical. Thus, a description below is provided for each model derived from ROM [21].

2.5.1.1 Rule of Mixture (ROM)

The Rule of Mixture relies on a straightforward solid mechanics analysis, assuming that the fiber and matrix can be modelled either in parallel or in series, as depicted in Figure X, depending on the applied load [21]. However, this approach inherently results in a

limited representation of the transverse plane of the composite material. The governing equations for the engineering constants are as follows.

***Figure 11**: Rule of Mixture Parallel element assumption.*

$$E_1 = E_1^f\, V_f + \left(1 - V_f\right)E^m \tag{7}$$

$$v_{12} = v_{12}^f\, V_f + \left(1 - V_f\right)v^m \tag{8}$$

$$E_2 = \frac{E_2^f E^m}{E_2^f\left(1 - V_f\right) + E^m V_f} \tag{9}$$

$$G_{12} = \frac{G_{12}^f E^m}{G_{12}^f\left(1 - V_f\right) + G^m V_f} \tag{10}$$

2.5.1.2 Modified Rule of Mixture (ROMm)

A modified Rule of Mixture (ROMm) is proposed to enhance parameter adjustment for better alignment with experimental data. This adjustment involves introducing an experimental constant ξ, which, when set to 1, makes ROMm equivalent to the conventional Rule of Mixture (ROM), specifically for the parameters E_2 and G_{12}. ROMm, akin to the Halpin-Tsai model, incorporates the Volume Fractions of the fibers, with the added capability of modifying the ratio between the matrix and fibers. In terms of its assumptions, ROMm utilizes ROM for estimating E_2 and G_{12}, while the Chamis (Ch) model is employed for estimating G_{23}, albeit with V_f utilized instead of $\sqrt{V_f}$ [21]. The governing equation for G_{23} is:

$$G_{23} = G^m\left(\frac{1}{1 + \xi_{G_{23}}\left[\left(\frac{G^m}{G_{23}^f}\right) - 1\right]V_f}\right) \tag{11}$$

$$v_{23} = \left(\frac{E_2}{2G_{23}}\right) - 1 \tag{12}$$

2.5.1.3 Chamis (Ch):

The proposal involves considering void impact on equivalent properties and adopting a nonlinear effect of fibre volume fraction on transverse properties. If microstructural voids are neglected ($V_v = 0$), the Chamis model closely resembles the Rule of Mixture with some differences in parameter estimation.

Chamis introduced an inverse modelling approach, where laminate properties are measured first and then used to calculate constituent properties. This method helps avoid issues with fibre property measurement but introduces errors from the micromechanical model. An inverse methodology is also suggested.

$$E_1 = E^m + (1 - V_v)V_f\left(E_1^f - E^m\right) \tag{13}$$

$$E_2 = \frac{E^m}{1 - \sqrt{(1 - V_v)V_f}[1 - (E^m/E_2^f)]} \tag{14}$$

$$G_{12} = \frac{G^m}{1 - \sqrt{(1 - V_v)V_f}[1 - (G^m/G_{12}^f)]} \tag{15}$$

$$G_{23} = \frac{G^m}{1 - \sqrt{(1 - V_v)V_f}[1 - (G^m/G_{23}^f)]} \tag{16}$$

$$v_{12} = v^m + (1 - V_v)V_f\left(v_{12}^f - v^m\right) \tag{17}$$

2.5.2 Analytical Models Based on the Theory of Elasticity

Numerous methodologies have been suggested to determine the homogenized characteristics of composite materials. These methods encompass both upper and lower bounds derived from variational approaches [21]. In this subsection, a couple of analytical models grounded in elasticity theory are presented, providing concise descriptions, outlining the underlying assumptions for each, and presenting their governing equations.

2.5.2.1 Mori-Tanaka:

The concept involves deriving a collective behaviour by considering the behaviours of both the fibres and the matrix. Consequently, stress and strain tensors can be determined based on their average values, which are evaluated for both the matrix and the fibres.

The fundamental assumption in macroscopic homogenization is to establish a connection between the average stress and average strain tensors. Assuming that the constituents are linear and elastic, it is feasible to formulate average equations for the fibres and the matrix. This allows us to calculate the longitudinal and transverse elastic modulus, in-plane Poisson's ratio, in-plane, and out-of-plane shear modulus using the following equations.

$$E_1 = V_f E_1^f + (1 - V_f) E^m + 2V_f (1 - V_f) Z_1 \left(v_{12}^f - v^m\right)^2 \tag{18}$$

$$E_2 = \frac{E_1}{[1 - (v^m)^2](Y_1 + Y_2)} \tag{19}$$

$$v_{12} = v^m + 2V_f \frac{Z_1}{E^m} \left(v_{12}^f - v^m\right)[1 - (v^m)^2] \tag{20}$$

$$G_{12} = \frac{E^m}{2(1 - V_f)(1 + v^m)} [1 + V_f - \frac{4V_f}{1 + V_f + 2(1 - V_f) \frac{G_{12}^f}{E^m} (1 + v^m)}] \tag{21}$$

$$G_{23} = E^m [2(1 + v^m) + \frac{V_f}{\frac{1 - V_f}{8[1 - (v^m)^2]} + \frac{V_f}{E^m - 2G_{23}^f (1 + v^m)}}]^{-1} \tag{22}$$

2.5.3 Halpin-Tsai:

The proposed set of equations differs from those in the reference [21]. Additionally, we introduce the parameter ζ_{E_2} and $\zeta_{G_{12}}$ [21] that are parameters that can be adjusted through experimental data calibration. We offer a general recommendation for cases where experimental calibration data is not available in the following sections. The different equations proposed are:

$$E_2 = E^m\left(\frac{1 + \zeta_{E_2}\eta_{E_2}V_f}{1 - \eta_{E_2}V_f}\right) \tag{22}$$

$$G_{12} = G^m\left(\frac{1 + \zeta_{G_{12}}\eta_{G_{12}}V_f}{1 - \eta_{G_{12}}V_f}\right) \tag{23}$$

Moreover, from this analytical model, Vignoli carried out experiments in order to determine the appropriate usage of each model. In Figures 12 to 16 it is possible to locate both the average error and the error range generated against the experiments data.

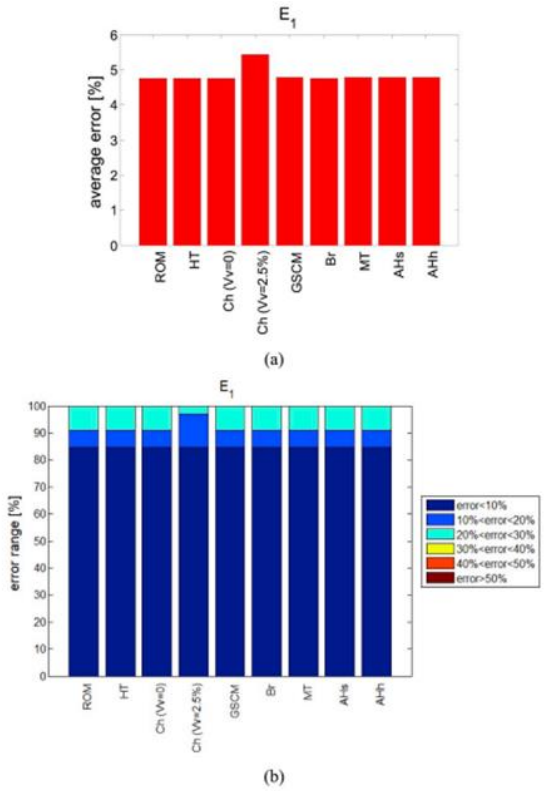

Figure 12: *(a) Average and (b) range error in axial elastic modulus [21].*

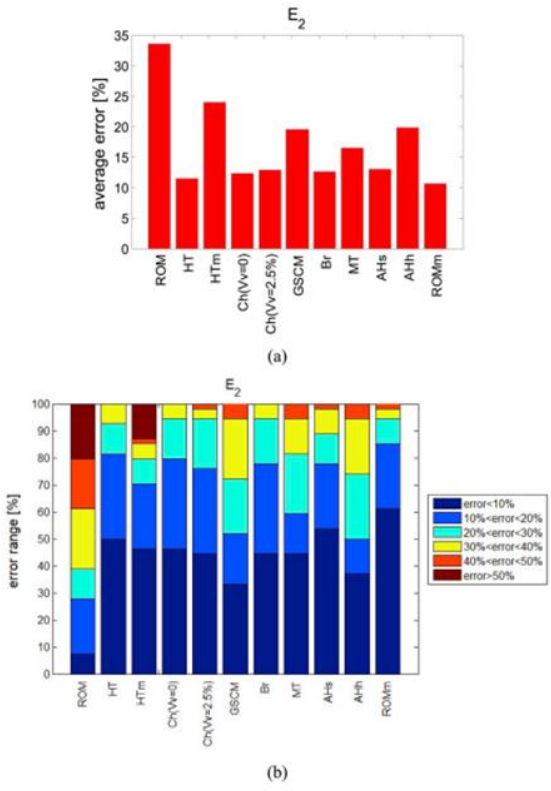

Figure 13: *(a) Average and (b) range error in transverse elastic modulus [21].*

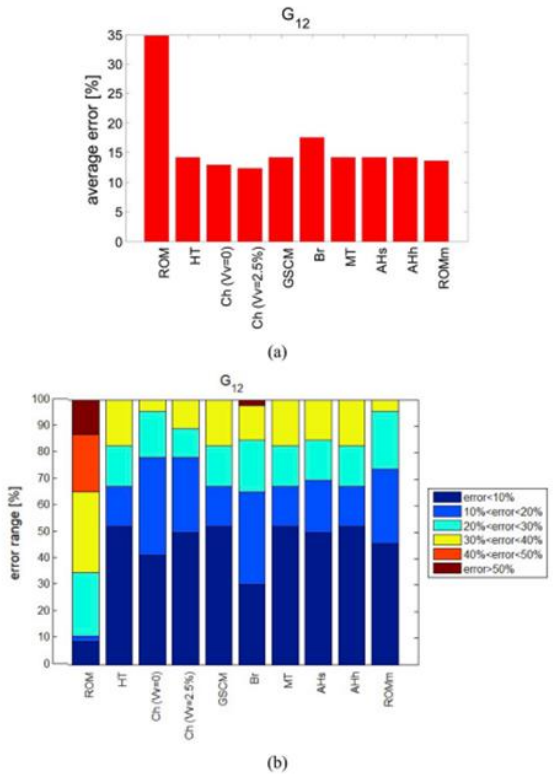

Figure 14: *(a) Average and (b) range error in axial elastic modulus. [21]*

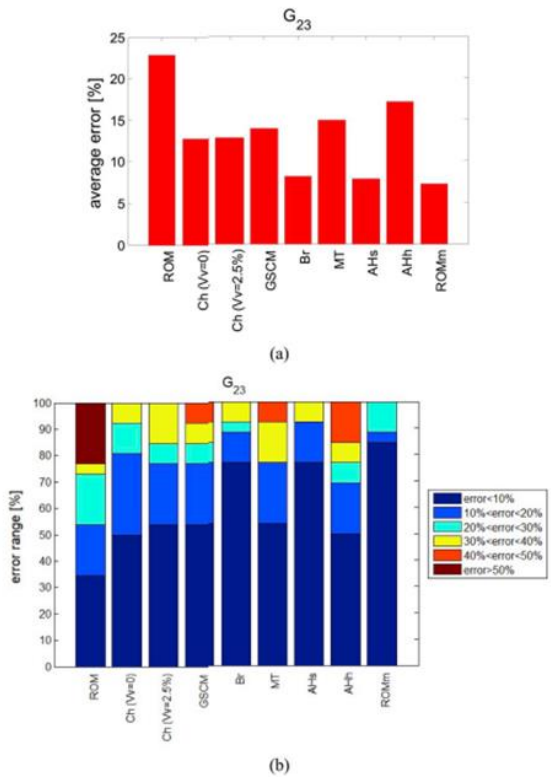

Figure 15: *(a) Average and (b) range error in transverse elastic modulus. [21]*

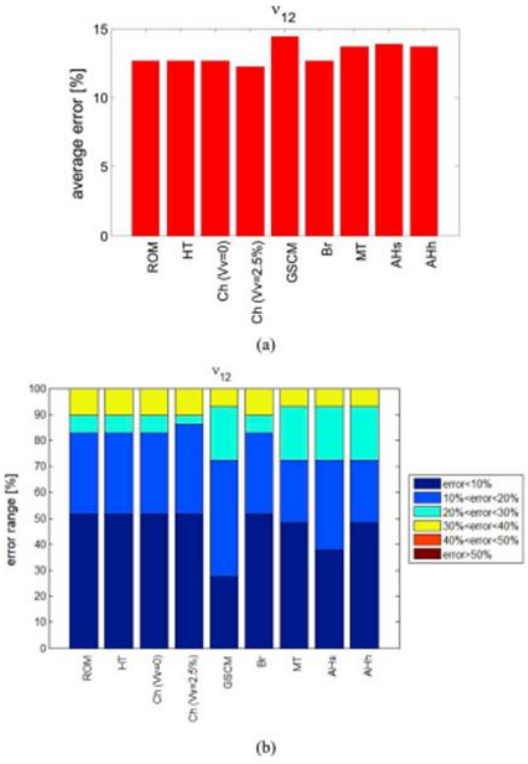

Figure 16: *(a) Average and (b) range error in axial Poisson's ratio. [21]*

Based on the data provided, Vignoli concluded that it's challenging to determine quantitatively which model offers the best predictions [21]. However, qualitative analysis of the provided graphs can offer insights. Notably, all models proved accurate in determining E_1, with ROM equations recommended for their simplicity.

For v_{12} , the Chamis model demonstrated superior accuracy, particularly when considering void volume V_v. Halpin-Tsai model provided the most precise representation of E_2.

ROM exhibited similar errors for axial properties, with notable discrepancies in representing E_2 and G_{12}, prompting the introduction of an experimental parameter, ξ, in ROMm to address this issue. The parallel assumption made in ROM contributes to its simplicity but leads to challenges in results accuracy, especially when analysing the transverse plane.

Among the considered models, the Chamis model yielded the lowest average errors for both G_{12} and G_{23}. Both the Chamis model and ROM/ROMm will be utilized for analytical modeling to compare and validate computational modeling of the RUC. This approach aims to identify ROM discrepancies compared to other models, despite its widespread popularity and simplicity.

2.6 FINITE ELEMENT ANALYSIS

To accurately capture the homogenized material properties and the distribution of stresses within a Repeating Unit Cell (RUC), implementing a periodic boundary condition is essential, as outlined in reference [23]. This approach allows for the simulation of an infinite lattice by replicating the RUC in a periodic arrangement. In the context of Abaqus/Standard, a Python script can be utilized to establish these boundary conditions effectively. By applying independent loading conditions to the RUC, the simulation can mimic real-world scenarios more accurately, enabling the assessment of both in-plane and out-of-plane tensile and shear stresses. This methodology not only aids in understanding the material behaviour under various loading conditions but also facilitates the extraction of meaningful data for further analysis and optimization in finite element analysis (FEA) studies.

2.7 MESH

In Abaqus/Standard, meshing plays a critical role in finite element analysis (FEA) as it directly impacts the accuracy and computational cost of simulations. Abaqus offers various meshing techniques, including standard, swept, and mapped meshing, each suitable for different types of geometries and analyses. The mesh quality is essential for obtaining reliable results; therefore, Abaqus/Standard provides tools for mesh diagnostics and optimization to ensure high-quality meshes. Additionally, Abaqus allows for the refinement of the mesh in regions of interest, where higher resolution is needed to capture complex phenomena accurately. Furthermore, Abaqus supports automatic mesh generation and adaptive meshing, which streamline the modelling process and enhance computational efficiency by dynamically adjusting the mesh during the analysis based on predefined criteria. Overall, the meshing capabilities in Abaqus empower users to generate robust and accurate finite element models for a wide range of engineering applications.

2.7.1 Mesh Element & Aspect Ratios

When meshing models for both 2D and 3D problems, the aspect ratio of elements serves as a metric for evaluating mesh quality, representing the ratio between the longest and shortest edge of an element (19), where x is the edge distance.

$$Element\ Aspect\ Ratio = \frac{\max\left(x_1, x_2, \dots, x_{12}\right)}{\min\left(x_1, x_2, \dots, x_{12}\right)} \tag{24}$$

Ideally, a ratio of 1 indicates a compact element, while higher ratios signify ‘elongated’ elements, which are undesirable due to potential issues during data collection. The primary disparity between a ratio of 1 and higher, undesired ratios like 3, lies in the discrepancy in distances between nodes along longer and shorter edges, leading to numerical challenges such as instability, ill-conditioning, reduced solution accuracy, compromised mesh convergence, and degraded mesh quality.

The illustration in Figure 18 also demonstrates various types of mesh elements, revealing similarities among the three depicted elements. Additionally, it's evident that in Figure 18 the elements (b) and (d) are both three-dimensional, whereas (a) and (c) are two-dimensional. The use of IDs in the Figure 17 title adds an intriguing element, particularly for those unfamiliar with mesh elements.

Additionally, in Abaqus, the 3D element types are referred to as C3D4 for 4-noded tetrahedrons, C3D6 for 6-noded wedges, and C3D8 for 8-noded bricks with full integration. These elements are commonly employed to mesh intricate geometries by combining them. Similarly, for 2D, the sequence is CPE3 and CPE4, where PE indicates plane strain [27]. CPE4 and C3D8 are typically utilized to model solid continuous bodies like an RUC due to their general-purpose linear brick element. In regions where geometry becomes more complex, the use of wedges tends to be more practical compared to C3D8. As mentioned earlier, these elements are full integration elements, but reduced integration elements are also introduced, often denoted with an 'R' after the mesh element code, such as 'C3D8R'. This feature assumes uniform strain across the elements by reducing the nodes within the element, from 4 to 1 for 2D and from 8 to 1 in 3D, for CPE4 and C3D8 respectively, thus reducing computational time.

When modelling RUC, a decision must be made when selecting an appropriate mesh element. Comparing C3D4 to C3D8, the former produces stiffer behaviour due to having fewer nodes. As mentioned in Section 4, the thickness of the 3D RUC equals the mesh size, hence a mesh element unit of thickness is used. Consequently, more C3D4 elements would be needed to mesh the 3D RUC entirely [28]. On the other hand, elements with a higher number of nodes, such as C3D20, pose a problem as full integration elements of this type are not suitable for materials with high Poisson's ratios like 'Flax' due to their plastic behaviour, which requires longer computational time [28].

C3D8R effectively captures stress concentrations throughout the geometry's boundaries as the node is situated in the middle of the mesh element. Thus, due to the RUC geometry in both its axial and transverse planes, C3D8R has proven to be a reasonable option to model both 2D and 3D RUCs. Meanwhile, C3D6 will be utilized to complete the mesh in geometrically complex areas such as curvatures. Below a breakdown of the mesh element naming is provided for further understanding.

$$\underset{(1)}{C}\quad\underset{(2)}{3D}\quad\underset{(3)}{8}\quad\underset{(4)}{R}$$

Figure 17: *Mesh Element ID breakdown.*

In this breakdown, (1) represents a continuum (solid) element, while (2) indicates its dimensionality (1D, Plane Strain (PE) or 3D), and (3) signifies the number of nodes.

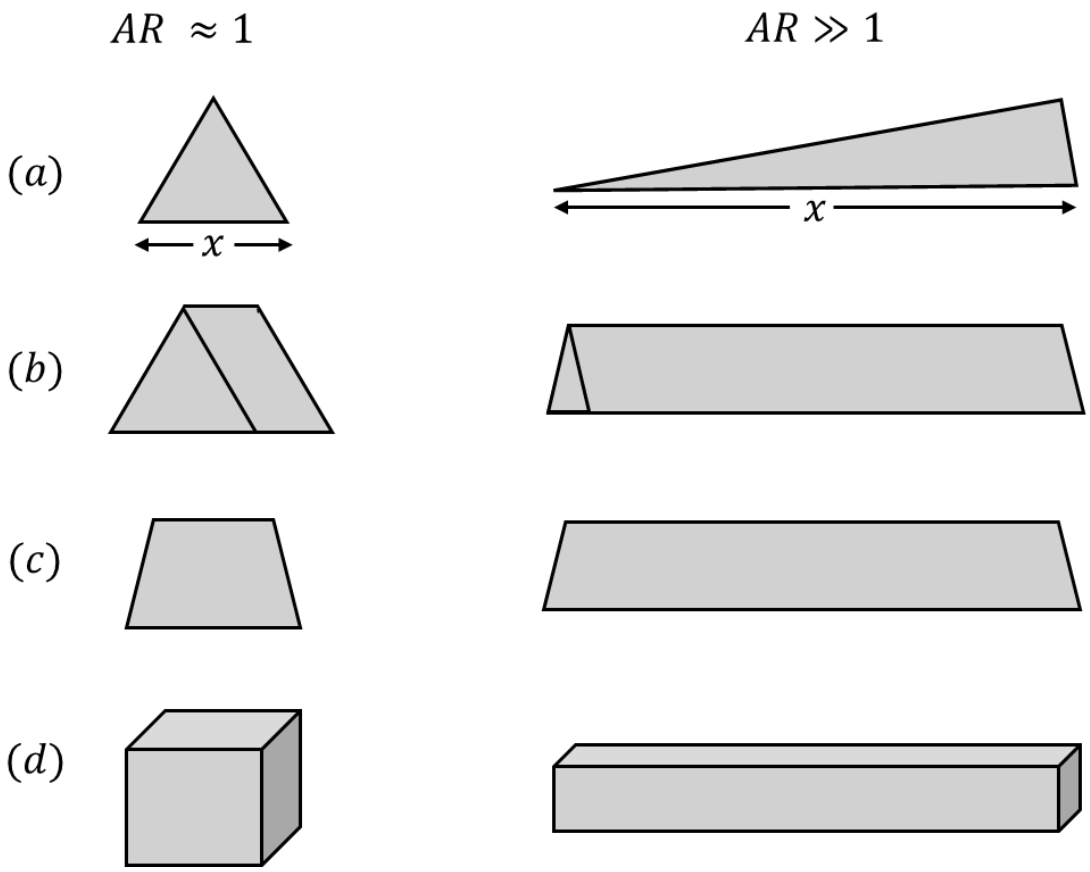

Figure 18: *Comparison of 2D and 3D Mesh Elements: (a) C2D3, (b) C3D6, (c) CPS4 and (d) C4D8 with Aspect Ratio, AR* ≈ 1*, (left) against high aspect ratio, AR* $\gg 1$*, (right).*

3 PROJECT OUTLINE

3.1.1 Project Rationale

In Section 2.2, it was noted that fiber-hybrid composites offer several advantages over single constituent materials, including enhanced strength-to-weight ratios, potential cost reduction, and reduced overall weight. Notably, the use of natural fibres discussed in Section 2.1 holds a significant environmental advantage over synthetic fibres, as the components of these composites are biodegradable. Therefore, this study aims to not only provide computational data on the fibres under consideration but also to facilitate a comparative analysis to elucidate the merits and drawbacks of natural and synthetic fibres. The selection of fibres for the study is somewhat arbitrary, with the sole criterion being their widespread usage across various industries.

The work of this dissertation encompasses both analytical and computational modelling of the behaviour of single fiber-reinforced polymer composites. This aims to confirm the

performance of each single fiber and establish a strong correspondence between the computational model discussed in Section 2.4 and the analytical model, with the use of *Python* Script located in 'Appendix B: PYTHON SCRIPT FOR VALIDATION USING ANALYTICAL MODELS FOR SINGLE-FIBER COMPOSITES', using equations from Section 2.5. This involves creating a table displaying the homogenized properties, including transverse elastic and shear modulus, as well as transverse Poisson's ratios, akin to the approach in Section 2.5.

Subsequent to validating the behaviour of fibre-hybrid materials, the next phase of the research involves modelling fibre-hybrid composites with the use of Abaqus/Standard and Digimat for both analytical and computation results. This encompasses various combinations of the four selected fibres with a chosen matrix material, as detailed in Section 4.1. Moreover, the combination of Natural-Synthetic fiber-hybrid composites, thus, Basalt/Carbon/Epoxy, Basalt/E-glass/Epoxy, Flax/Carbon/Epoxy and Flax/E-glass/Epoxy. These composite models will be tested at volume fraction of 0.6. This volume fraction is considered suitable based on the explanation provided in Section 2.4.

The research begins with 2D modelling utilizing the chosen RUC shape. It is essential to note the exclusion of axial parameters in this phase due to inherent constraints within 2D modelling stemming from the absence of thickness in the axial direction. This decision is made to establish a robust correspondence between analytical and computational models, while also facilitating the exploration of mesh strategies.

Following the aforementioned procedure, 3D modelling is employed to accurately capture transverse and axial parameters, along with the introduction of thickness, contingent upon time constraints not impeding progress, as outlined in Sub-section 2.4.1. It is noteworthy that the homogenized properties, crucial for deriving final results, are derived from the 3D modelling process, offering a more precise representation of the composite within these dimensions.

RUCs are favoured over RVEs in this investigation, primarily because of limitations within the Abaqus/Student Edition, which restricts the number of cells in a file, as delineated in Section 2.4. As the transition to 3D modelling commences, RUC modelling will persist as the preferred approach, especially when employing computer clusters with the full version of Abaqus/Standard Edition as the approach is known by the user. In RUCs

modelling a periodic boundary condition is applied, as shown in Section 4.1.1, using a *Python* Script, PBC plug-ins from GitHub.

It's also worth noting that the variety of transversely isotropic and isotropic constituents will be employed during data extraction. In this context, the use of RUCs is adequate to represent the composite material.

3.1.2 Aims and Objectives

The aim of the study is to predict the homogenised lamina properties and micro stress fields of natural synthetic fiber-hybrid composites.

Objectives:

1. Examine mechanical properties of different combinations of natural and synthetic fiber-hybrid composites.
2. Estimate mechanical properties of the natural synthetic fiber-hybrid composites using computational models in Abaqus/Standard.
3. Estimate mechanical properties of the natural synthetic fiber-hybrid composites using analytical methods in *Python*.
4. Validate the behaviour of composites comparing analytical models against computational models.
5. Provide 2D modelling data of the composites initially, with a potential expansion to 3D modelling to capture missing data.
6. Estimate the micro-stress fields of the natural synthetic composites using computational models in Abaqus/Standard.
7. Estimate the micro-stress fields of the natural synthetic composites using analytical models in *Python*.

4 METHODOLOGY

Using a *Python* script, the RUC's geometry will be generated and incorporated into ABAQUS/Standard's workspace. The script prompts various inputs such as fibre volume fraction and material properties detailed in subsection 4.3. The code can generate different volume fractions for both single fibres and fiber hybrid composites. In this project, a single polymer, Epoxy, is used. Volume fractions will be of 0.60. The selected volume fraction is based on its prevalence in modelling the micromechanics of composites as lower volume fraction may compete with conventional materials, and in the other hand, high volume fraction composites present inherent complications throughout the manufacturing processes. This volume fraction accurately reflects the proportions commonly observed in composites utilized across various sectors, as detailed in the corresponding Section 3.

To validate the model, Section 5.2 will implement and demonstrate an analytical comparison for single and fibre hybrid composites with the use of *Python* Script found in 'Appendix B: PYTHON SCRIPT FOR VALIDATION USING ANALYTICAL MODELS FOR SINGLE-FIBER COMPOSITES' and Digimat Software respectively. The model's variation from the coarsest mesh baseline computation model will be presented as a percentage of discrepancy.

Across the report, numerous assumptions have been made to simplify the RUC model, thus, a conglomerate of all the assumptions made is presented below in Table 2.

Table 2: RUC Model assumptions conglomerate.

	Fiber	**Matrix**	**Interphase**
Assumptions	• Continuous • Homogeneous • Transversely Isotropic • Defect-free. • Cylindrical fibres (Circular Cross-sections) • Linear Elastic	• Homogeneous • Isotropic • Void-free • Linear Elastic	• Perfect fiber-matrix interphase

To enable 3D modelling, a thin thickness is applied to the RUC (Representative Unit Cell), often set equal to the size of the mesh elements. This ensures uniformity throughout the mesh volume and helps maintain an ideal aspect ratio of 1 for the elements. This approach enhances the accuracy of the model by ensuring consistency and independence from the mesh resolution, thereby yielding reliable results.

For the 2D RUC, the matrix is meshed using 4-node elements (CPE4R) and 3-node elements (CPE3), along with a Hex-Dominated mesh. The fibres are divided and meshed using 4-node elements (CPE4R). Conversely, for the 3D RUC, the matrix employs 8-node elements (C3D8R) and 6-node elements (C3D6) within a Hex-Dominated mesh, while the fibres are divided and meshed using 8-node elements (C3D8R). To ensure result accuracy, a mesh convergence study is conducted, varying the mesh size as a percentage from the finest mesh with the most elements, and comparing the results to the total CPU time required for simulation runs across different mesh sizes. With a fiber radius of 5 μm, the current mesh sizes are set as fractions of this radius (25%, 15%, 10%, 5%, and 1% for both 2D and 3D). Notably, the thickness of the 3D RUC is adjusted to match the specified percentage, ensuring that the mesh becomes finer while maintaining an aspect ratio of 1 for the elements.

As previously stated, to ensure an accurate representation of the homogenized material properties of the composite material, a periodic boundary condition will be integrated into the Python script. This will be elaborated on and illustrated in Section 4.5, covering both the constraints and applied loads.

4.1 RUC MODELLING

A *Python* Script is made with the use of Macros, designed to generate 2D and 3D Repeating Unit Cell (RUC) models in Abaqus for both single-fiber and fiber-hybrid composites (with a maximum of 2 fibres) in both 2D and 3D configurations. The script assumes a Fiber Volume Fraction (V_f) of 0.60, where in hybrid fiber composites, the volume fraction of each fiber type is equal (i.e., $V_{f1} = V_{f2}$). A fixed fiber radius of 5 μm is applied uniformly across all materials and combinations.

The RUC's dimensions and meshing strategy are detailed thoroughly. This includes specifying the size of the part, the fibre's configuration and explaining the meshing

strategy employed to achieve mesh independence, ensuring accurate and reliable simulation results.

4.1.1 RUC Size

The RUC size, as outlined in Section 4.1, will remain constant for each composite, determined by the function: L (width of RUC), H (height of RUC), and R (radius of the fiber). Thus, an RUC of area $H \times L$. With the addition of thickness, t, as 3D RUC is introduced which is equal to the mesh size, to maintain a low aspect ratio element, thus a 3D RUC one mesh element thick.

$$L = R\sqrt{\frac{2\pi}{V_f\sqrt{3}}} \tag{25}$$

$$H = L\sqrt{3} \tag{26}$$

$$t = mesh\ size \tag{27}$$

Thus, the area of the RUC is dependent on the radius of the central fiber and volume fraction given for the fibres. It is worth mentioning that for both Fibre1 and Fibre2 in a fiber hybrid composite the radius is equal. This said, if E-Glass and Basalt are used for the modelling, Fibre1, being E-Glass, will be found in the corners partitioned as a quarter of fiber in each corner which combined will provide an entire fiber area, as for Fibre2, in this case the Basalt can be found in the centre of the RUC as a complete fiber. The completeness of quarter fibres found in edges will later be demonstrated in Subsection 4.5 Periodic Boundary Condition Implementation as the RUC is duplicated across the workspace as mentioned in Section 2.3 Periodic Boundary Condition.

4.1.2 Microstructure Geometry

Subsection 5.2.1 involves evaluating the impact of the RUC's microstructure by comparing it with analytical models. This comparison encompasses both 2D and 3D models and is conducted while maintaining constant volume fractions, as outlined in Section 4. The microstructure is structured using hexagonal packing, illustrated in Figure 19. Importantly, when incorporating fiber hybrid composites, a specific default order is

defined. For instance, in the case of Basalt/Carbon/Epoxy, the sequence within the RUC's structure is Fibre1/Fibre2/Epoxy, as depicted in Figure 19.

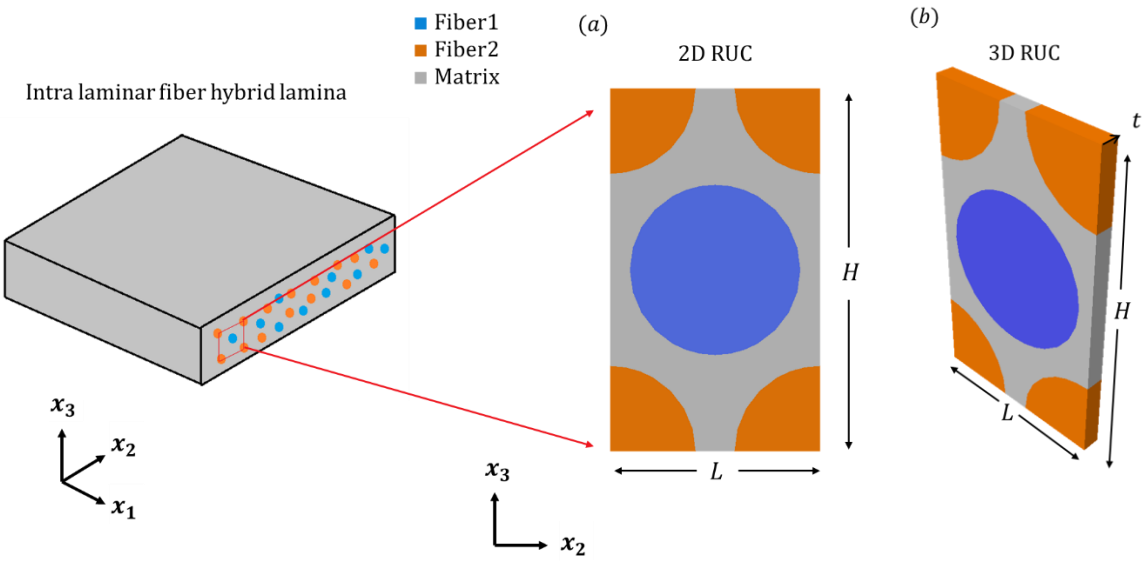

Figure 19: *(a) 2D and (b) 3D RUC microstructure geometry of composite Fiber1/ Fiber2/Matrix.*

4.2 Mesh Strategy and Element

Optimizing the mesh strategy is crucial for generating results that accurately represent the real composite material. As highlighted in section 3.1 and elaborated on in section 4.2, a mesh convergence analysis is conducted to ensure reliable outcomes, focusing on homogenized property E_2, as this engineering constant tends to be volatile during simulations in Abaqus/Standard between 2D and 3D due to the boundary conditions applied. This section delves into various aspects considered to attain mesh-independent results, including the selection of mesh elements, managing aspect ratios, partitioning within the RUC, employing Specimen IDs for mesh convergence analysis completion, and addressing potential mesh failures as initial mesh sizes are applied.

4.2.1 Mesh Elements

In sub-section 2.7.1, it was noted that the mesh utilized for both 2D and 3D RUC models employs a predominantly hexagonal structure, incorporating both hexahedral elements with four nodes and wedge elements with three nodes. This approach is maintained across both dimensions, with the main distinction being the addition of thickness for generating 3D parts, as elaborated in subsection 2.7.2. The Hex-Dominated mesh can utilize either reduced-integration elements to decrease simulation time or full-

integration elements, which offer higher accuracy but come with longer simulation durations.

4.2.2 Initial Global Mesh Size

After setting the RUC as illustrated in section 4.1, an initial global mesh will be applied to the unit cell with the use of the *Python* script. The mesh size range is made considering time processing, results accuracy, and mesh quality, focusing on maintaining element aspect ratios and physical interphases within the different materials.

During the generation of meshes within the specified range, potential errors/failed mesh may arise, necessitating iterative adjustments until a viable mesh is attained for each configuration. This enables subsequent testing for mesh sensitivity analysis. Up to five iterations will be undertaken to ensure comprehensive mesh refinement or ascertain the infeasibility of generating a suitable mesh for Finite Element Analysis (FEA) processing of the 3D Representative Unit Cell (RUC). Following each attempt, the mesh size will be decreased by 5%, thus multiplying prior mesh size by 0.95, providing the values as detailed in Table 3. This ensures that each global mesh is tested despite complications.

Table 3: Mesh Size feasibility convergence.

Initial Mesh Size	Iteration0	Iteration1	Iteration2	Iteration3	Iteration4
0.05	0.05	0.0475	0.045125	0.042869	0.040725
0.25	0.25	0.2375	0.225625	0.214344	0.203627
0.5	0.50	0.475	0.45125	0.428688	0.407253
0.75	0.75	0.7125	0.676875	0.643031	0.61088
1.0	1.00	0.95	0.9025	0.857375	0.814506

4.2.3 Partitioning

Partitioning has been implemented within the Representative Unit Cell (RUC) to enhance mesh quality, ensure symmetry within the unit cell, and address conflicts by constraining the mesh in problematic areas. This measure aims to prevent discrepancies in results, as depicted in Figure 21. Notably, the partitioning ensures alignment across the four faces divided by axes 2 and 3 in the transverse plane, with the partition datum positioned at the midpoint of fiber 2 (the centre of the RUC). However, Figure 20 reveals discrepancies

in element sizes between the left and right faces which consequently generates asymmetric stresses across opposite faces and edges despite the applied periodic boundary condition, and subsequently generating asymmetric and inaccurate results.

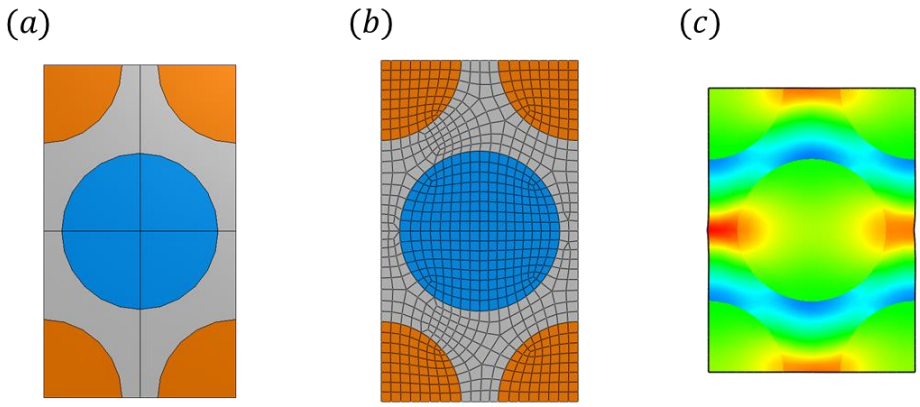

Figure 20: *Asymmetric RUC for fiber-hybrid composite at mesh size: (a) Part partition, (b) Mesh and (c) von Mises stress post-processing*

Figure 21 demonstrates how the introduction of a partition within the matrix has addressed the asymmetry observed across the mesh in Figure 20. By dividing the matrix into four equal parts rotated at 45°, symmetry is achieved across the mesh within the matrix, resulting in symmetric outcomes from Abaqus/Standard post-processing, as depicted in Figure X (c). This partitioning technique has significantly enhanced the accuracy of the results. The purpose of the Figures 21 (c) and 20 (c) is not to illustrate stress distribution across the RUC but rather to highlight the symmetry achieved through diagonal partitioning within the composite matrix for improved accuracy and mesh independent results.

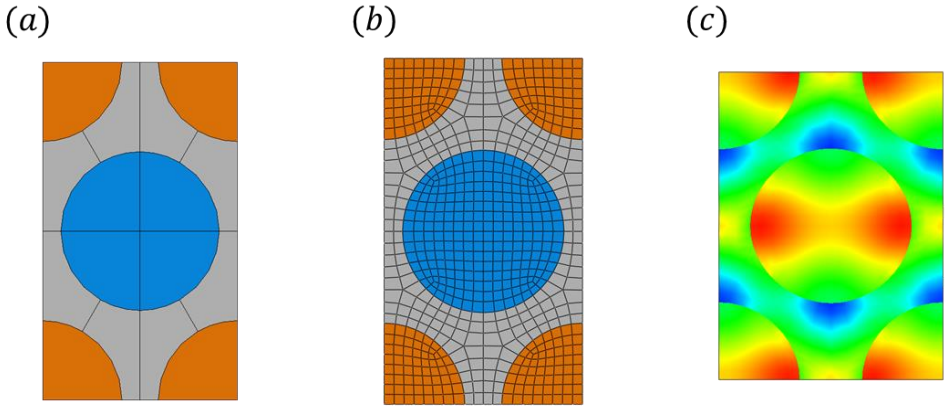

Figure 21: *Symmetric RUC for fiber-hybrid composite at mesh size: (a) Part partition, (b) Mesh and (c) von Mises stress post-processing.*

4.2.4 Mesh Strategy: Specimen ID

To conduct a mesh sensitivity analysis and systematically capture the influence of various factors on result accuracy, a Specimen ID system is introduced. This system encompasses factors such as material type (e.g., Basalt and Carbon), the type of fiber and matrix mesh elements, five different global mesh sizes, and volume fraction used. This configuration necessitates a total of 20 simulations to populate Table 4 comprehensively, representing the mesh sensitivity of the RUC. Subsection 5.1 later presents the results derived from these simulations.

$$\underset{(1)}{B}\ \underset{(2)}{E}\ \underset{(3)}{H}\ \underset{(4)}{H}\ \_\ \underset{(5)}{1.0}\ \_\ \underset{(6)}{0.6}\ \_\ \underset{(6)}{2}$$

Figure 22: *Mesh Specimen ID breakdown.*

1. Reinforced Fibre Material: (B: Basalt; BC: Basalt/Carbon)
2. Matrix Material: (E: Epoxy)
3. Fiber Mesh Element: (H: Hex-Dominate Element with Reduction CPE3/CPE4R; 3D: C3D6/C3D8R))
4. Matrix Mesh Element: (H: Hex-Dominate Element with Full Integration (2D: CPE3/CPE4R; 3D: C3D6/C3D8)
5. Global Mesh Size: (1.0, 0.75, 0.50)
6. Fibre Volume Fraction: (0.6: V_f = 0.60)
7. RUC dimension: (2: 2D; 3: 3D)

Table 4: Specimen ID strategy for Mesh Sensitivity Analysis.

Specimen ID	V_f	Global Mesh Size	Fiber Mesh Element	Matrix Mesh Element
BEHH_0.05_0.6_2	0.60	0.05 (0.01R)	Hex-Dom CPE3/CPE4R	Hex-Dom CPE3/CPE4R
BEHH_0.25_0.6_2	0.60	0.25 (0.05R)	Hex-Dom CPE3/CPE4R	Hex-Dom CPE3/CPE4R
BEHH_0.50_0.6_2	0.60	0.5 (0.10R)	Hex-Dom CPE3/CPE4R	Hex-Dom CPE3/CPE4R
BEHH_0.75_0.6_2	0.60	0.75 (0.15R)	Hex-Dom CPE3/CPE4R	Hex-Dom CPE3/CPE4R

BEHH_1.00_0.6_2	0.60	1.0 (0.20R)	Hex-Dom CPE3/CPE4R	Hex-Dom CPE3/CPE4R
BCEHH_0.05_0.6_2	0.60	0.05 (0.01R)	Hex-Dom CPE3/CPE4R	Hex-Dom CPE3/CPE4R
BCEHH_0.25_0.6_2	0.60	0.25 (0.05R)	Hex-Dom CPE3/CPE4R	Hex-Dom CPE3/CPE4R
BCEHH_0.50_0.6_2	0.60	0.50 (0.10R)	Hex-Dom CPE3/CPE4R	Hex-Dom CPE3/CPE4R
BCEHH_0.75_0.6_2	0.60	0.75 (0.15R)	Hex-Dom CPE3/CPE4R	Hex-Dom CPE3/CPE4R
BCEHH_1.00_0.6_2	0.60	1.0 (0.20R)	Hex-Dom CPE3/CPE4R	Hex-Dom CPE3/CPE4R
BCEHH_0.05_0.6_3	0.60	0.05 (0.01R)	Hex-Dom C3D6/C3D8R	Hex-Dom C3D6/C3D8R
BCEHH_0.25_0.6_3	0.60	0.25 (0.05R)	Hex-Dom C3D6/C3D8R	Hex-Dom C3D6/C3D8R
BCEHH_0.50_0.6_3	0.60	0.5 (0.10R)	Hex-Dom C3D6/C3D8R	Hex-Dom C3D6/C3D8R
BCEHH_0.75_0.6_3	0.60	0.75 (0.15R)	Hex-Dom C3D6/C3D8R	Hex-Dom C3D6/C3D8R
BCEHH_1.00_0.6_3	0.60	1.0 (0.20R)	Hex-Dom C3D6/C3D8R	Hex-Dom C3D6/C3D8R
BCEHH_0.05_0.6_3	0.60	0.05 (0.01R)	Hex-Dom C3D6/C3D8R	Hex-Dom C3D6/C3D8R
BCEHH_0.25_0.6_3	0.60	0.25 (0.05R)	Hex-Dom C3D6/C3D8R	Hex-Dom C3D6/C3D8R
BCEHH_0.50_0.6_3	0.60	0.50 (0.10R)	Hex-Dom C3D6/C3D8R	Hex-Dom C3D6/C3D8R
BCEHH_0.75_0.6_3	0.60	0.75 (0.15R)	Hex-Dom C3D6/C3D8R	Hex-Dom C3D6/C3D8R
BCEHH_1.00_0.6_3	0.60	1.0 (0.20R)	Hex-Dom C3D6/C3D8R	Hex-Dom C3D6/C3D8R

4.3 MATERIALS PROPERTIES

The natural synthetic fibres and matrix phase listed below in table 2, are the constituents subjected to modelling. To understand the behaviour of the constituents modelling of single fiber composites and combinations between the different natural and synthetic fibres will be performed and compared.

Table 5: Combination of fibre-hybrid composites used for simulations.

Combination	Fiber 1	Fiber 2	Matrix
1	Basalt	Carbon	Epoxy
2		E-Glass	
3	Flax	Carbon	
4		E-Glass	

The property's values allocated for each constituent and that will be used throughout the modelling are listed below, where E_1 is the axial elastic modulus and E_2 to the transverse elastic modulus, v_{12} and v_{13} correspond to the axial and transverse Poisson's ratios respectively, which are equal. Finally, G_{12} and G_{23}, represent the axial, transverse shear modulus of the phases separately. It is worth noting that some materials are transversely isotropic and therefore $E_2 = E_3$ for all constituents and $G_{12} = G_{23}$ specifically for E-Glass, Basalt and Epoxy.

Table 6: Elastic constants of reinforcement and matrix constituents [3].

Property	Carbon (IM7)	E-Glass	Basalt	Flax	Epoxy
$E_1\ (GPa)$	290	73	89	54.1	4.30
$E_2 = E_3\ (GPa)$	21	73	89	7	4.30
$G_{12} = G_{13}\ (GPa)$	14	30.20	21.70	3	1.29
$G_{23}\ (GPa)$	7.04	30.20	21.70	2	1.29
$v_{12} = v_{13}$	0.20	0.23	0.26	0.3	0.35
v_{23}	0.49	0.23	0.26	0.75	0.35

4.4 PERIODIC BOUNDARY CONDITIONS

PBC entails replicating a 3D modelled 'box,' often called a unit cell, infinitely across space to represent the composite material, ensuring the periodicity of mechanical fields and maintain continuity between neighbouring regions of the RUC. Implementing PBC in finite element analysis poses two main challenges that need to be overcome for successful simulation. The first challenge involves ensuring an equal number of nodes on opposite edges to maintain continuity and prevent artifacts as illustrated in Figure 20. The second challenge is to align corresponding nodes accurately to replicate the unit cell throughout space.

The type of boundary conditions imposed on Repeating Unit Cells (RUCs) significantly affects the estimated properties. Linear displacement and uniform traction boundary conditions establish upper and lower bounds for homogenized properties. However, the strain energies from these conditions may not fulfil the inequality $Ut \leq Up \leq Uu$, where Ut, Up, Uu represent strain energies obtained from uniform traction, periodic displacement, and linear displacement boundary conditions, respectively [29]. To address this, periodic displacement conditions, outlined by Equation (3), are often preferred for RUC models [29]. Despite challenges in ensuring periodic traction conditions with linear displacement or uniform traction conditions, Equation (3) ensures periodic traction conditions while enforcing periodic displacement conditions as shown in Figure 23.

$$u_i(x + \Delta x) - u_i(x) = \varepsilon_{ij}\Delta x_j \tag{3}$$

Where u_i is displacement in x_i direction, $x + \Delta x$ and x are position vectors of opposite RUC's faces, and ε_{ij} is the macro-strain component.

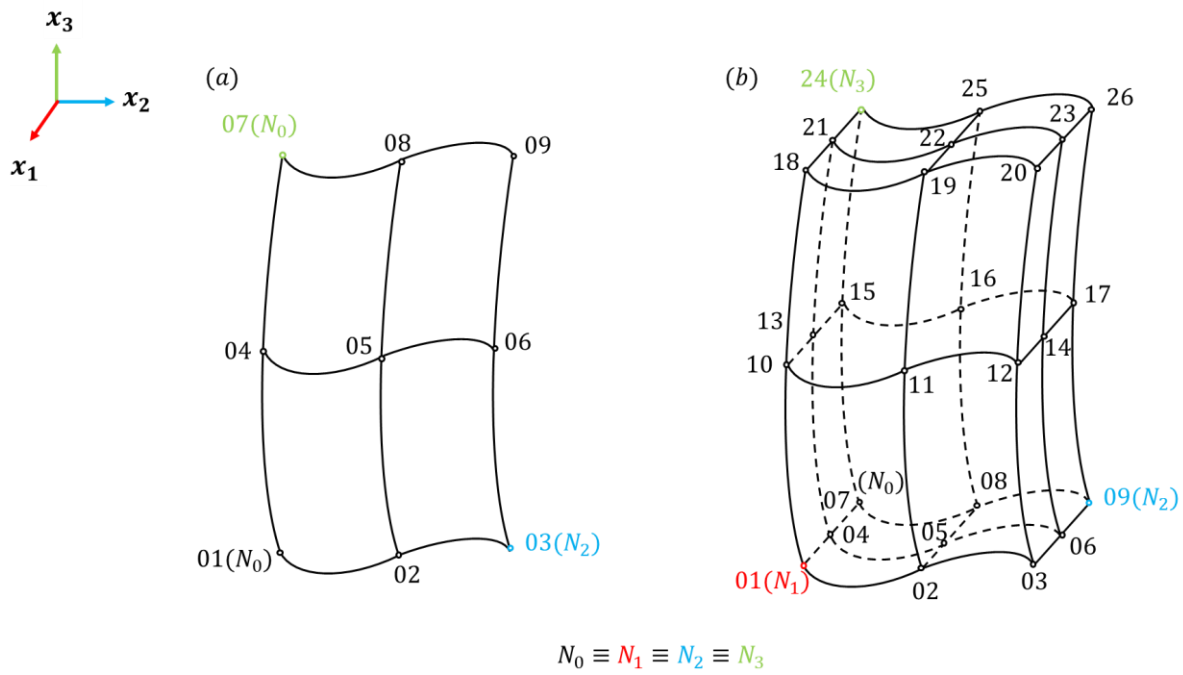

Figure 23: *Periodic Boundary Condition applied on (a) 2D and (b) 3D RUC*

Periodic Boundary Conditions are applied within the *Python Script* by the following equations (28) and (29), accounting for each edge, Γ_i, and corner node, N_i, of the RUC respectively:

$$\begin{cases} U_{2,\Gamma_{2-4}} - U_{2,\Gamma_{0-3}} = U_{2,N_2} \\ U_{3,\Gamma_{2-4}} - U_{3,\Gamma_{0-3}} = U_{3,N_2} \end{cases} \begin{cases} U_{2,\Gamma_{3-4}} - U_{2,\Gamma_{0-2}} = U_{2N_4} \\ U_{3,\Gamma_{3-4}} - U_{3,\Gamma_{0-2}} = U_{3N_4} \end{cases} \tag{28}$$

$$\begin{cases} U_{2,N_4} - U_{2,N_0} = U_{2,N_2} + U_{2,N_4} \\ U_{3,N_4} - U_{3,N_0} = U_{3,N_2} + U_{3,N_4} \end{cases} \tag{29}$$

The periodicity is applied as shown in Equations (28) and (29), using governing Equation (3) as base, for corner nodes and the RUC's edges as mentioned above. In this equation, variables U_2 and U_3 stand for the displacement across the transversal plane, 2 and 3, respectively. RUC's edges are denoted as followed Γ_{0-2}, Γ_{2-4}, Γ_{3-4} and Γ_{0-3}, as shown in Figure 24. Similarly, the RUC's nodes are denoted as N_0, N_2, N_2 and N_0. This convention is used in order to keep the node N_1 assigned to the axial plane when 3D is considered as shown in Figure 23.

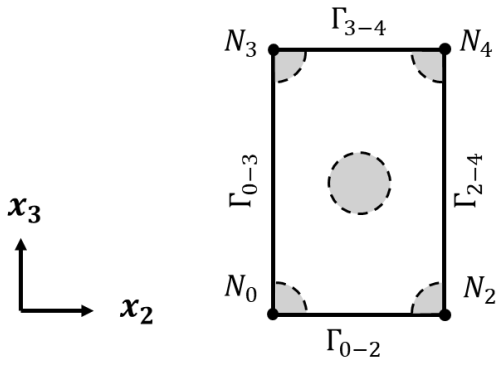

Figure 24: Periodic Boundary Conditions Applied to the RUC.

4.5 BOUNDARY CONDITIONS

Once the periodic boundary condition is implemented on the RUC, the macro mechanical behaviour of the composite is analysed using the finite element analysis software Abaqus/Standard. To derive the macro-stress from the microstructure, a macro-strain, denoted as U in the figures of Section 4.1, must be applied. Consequently, a relationship between stress and strain is essential, represented by an equation (30). Here, $\boldsymbol{\sigma}$, denotes the stress tensor, and $\boldsymbol{\varepsilon}$ signifies the strain tensor.

$$\boldsymbol{\sigma} = [C]\boldsymbol{\varepsilon} \tag{30}$$

$$[C] = \begin{bmatrix} C_{11} & C_{12} & C_{13} & 0 & 0 & 0 \\ C_{12} & C_{22} & C_{23} & 0 & 0 & 0 \\ C_{13} & C_{23} & C_{33} & 0 & 0 & 0 \\ 0 & 0 & 0 & C_{44} & 0 & 0 \\ 0 & 0 & 0 & 0 & C_{55} & 0 \\ 0 & 0 & 0 & 0 & 0 & C_{66} \end{bmatrix} \tag{31}$$

This is the case for unidirectional laminate, as it is assumed to be orthotopic and linearly elastic. Obtaining strain and stress C_{ij} can be derived [30]. Where the relation between C_{ij} and the homogenized constants are as depicted in equations (32).

$$\begin{aligned} E_1 &= 1/C_{11} \qquad v_{12} = C_{12}/C_{11} \qquad G_{12} = 1/2C_{44} \\ E_2 &= 1/C_{22} \qquad v_{13} = C_{13}/C_{11} \qquad G_{13} = 1/2C_{55} \\ E_3 &= 1/C_{33} \qquad v_{23} = C_{23}/C_{22} \qquad G_{23} = 1/2C_{66} \end{aligned} \tag{32}$$

It's important to acknowledge that for a general orthotropic material, determining nine independent material constants is necessary. However, equation (32) only incorporates

six, indicating the need for two additional sets of solutions. Notably, the bottom three equations in (32) yield the same modulus for both sets of solutions. [30]

Regarding the study in this paper, the information above holds true for 3D RUCs whereas for the 2D RUCs, the homogenized properties obtained from Abaqus/Standard and those located in the transverse plane thus: E_2, E_3, v_{23} and G_{23}. Required only from the stiffness matrix the following constants: C_{22}, C_{33}, C_{23} and C_{66}. Thus, four independent material constants that are evaluated from the 2D model.

Moreover, conducting a micromechanical study for larger-scale composites is impractical. Therefore, homogenization, also referred to as 'macro-micro' analysis, is carried out. This approach involves initially studying the micromechanics of local areas to predict the composite's behaviour at representative nodes, which is then scaled up to a common scale, such as the macro level, as demonstrated in Section 4.2.

In sub-section 4.1.1 and 4.1.2 the boundary conditions for 2D and 3D modelling are displayed. Figure 25: Schematic Illustration of the Boundary Condition applied to obtain the 2D RUC Homogenized property: Elastic Modulus (a)(1) E_2, (a)(2) E_3. and Figure 27: Schematic Illustration of the Boundary Condition applied to obtain the 3D RUC Homogenized property: Elastic Modulus (a)(1) $\mathbf{E_1}$, (a)(2) $\mathbf{E_2}$, (a)(3) $\mathbf{E_3}$. are under pure tension while Figure 26: Schematic Illustration of the Boundary Condition applied to obtain the 2D RUC Homogenized property: Shear Modulus (b)(1) G_{12}, (b)(2) G_{13}, (b)(3) G_{23} and Figure 28: Schematic Illustration of the Boundary Condition applied to obtain the 3D RUC Homogenized property: Shear Modulus (b)(1) G_{12}, (b)(2) G_{13}, (b)(3) G_{23} are pure simple shear in order to obtain both axial and transversal modulus individually and suggested by the title of the figures. Table 7: Boundary Condition applied to obtain Homogenized property: Elastic Modulus from the RUC, Table 8: Boundary Condition applied to obtain Homogenized property: Shear Modulus from the RUC, Table 9: Boundary Condition applied to obtain Homogenized property: Elastic Modulus from the RUC and Table 10: Boundary Condition applied to obtain Homogenized property: Shear Modulus from the RUC illustrates which homogenized properties are obtain for each loading setting, followed by the boundary conditions imposed in each node of the RUC. This said, a master Node (N_0), denoted as restrained Node is imposed from Abaqus/Standard. This is done to prevent any undesired movement from the part, and thus, generate feasible results. Regarding the remaining nodes: N_1 , N_2 and N_3 , a

maximum of 3 Degrees-of-freedom (DOF) for displacement are imposed in order to prevent rotation of the part from twisting and/or bending.

4.5.1 2D Boundary Conditions

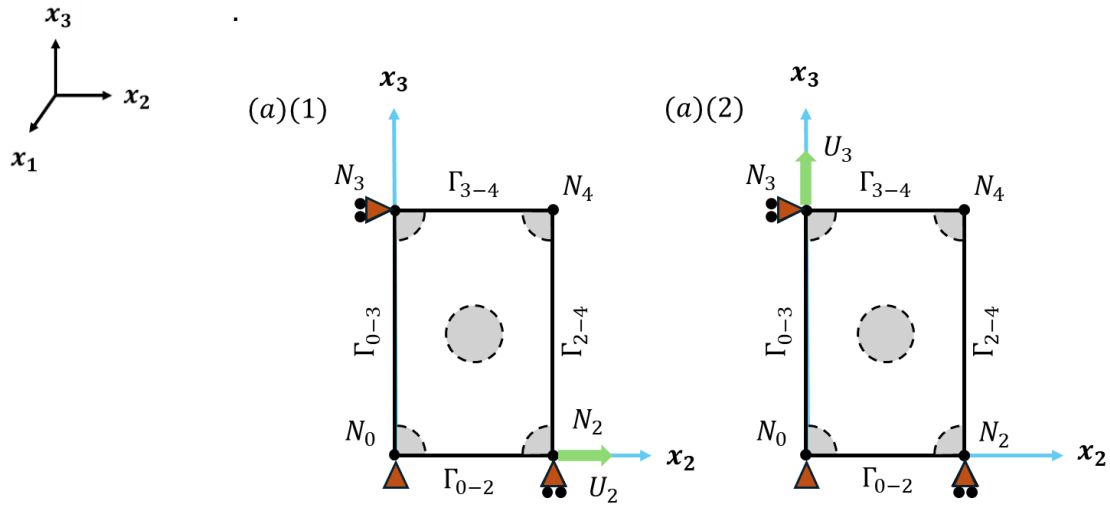

***Figure 25**: Schematic Illustration of the Boundary Condition applied to obtain the 2D RUC Homogenized property: Elastic Modulus (a)(1) E_2, (a)(2) E_3.*

Table 7: Boundary Condition applied to obtain Homogenized property: Elastic Modulus from the RUC.

Fig. X		*Elastic Modulus (E_{12}, E_{13}, E_{23})*		
Figure ID	Property	Retained Node N_0	Retained Node N_2	Retained Node N_3
Uniaxial deformation along x_2-axis				
b(1)	E_2	$U^{N_0} = 0$	$U_2^{N_2} = \delta_2$ $U_3^{N_2} = 0$	$U_3^{N_3} \neq 0$ $U_2^{N_3} = 0$
Uniaxial deformation along x_3-axis				
b(2)	E_3	$U^{N_0} = 0$	$U_2^{N_2} \neq 0$ $U_3^{N_2} = 0$	$U_3^{N_3} = \delta_3$ $U_2^{N_3} = 0$

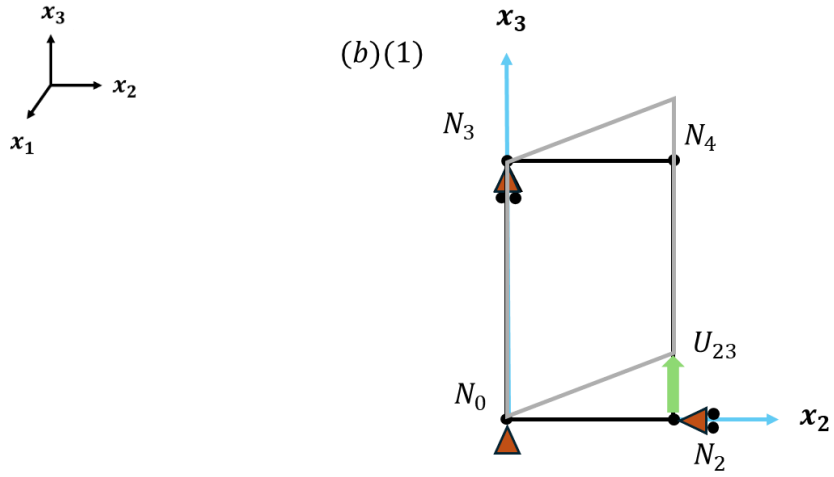

Figure 26: *Schematic Illustration of the Boundary Condition applied to obtain the 2D RUC Homogenized property: Shear Modulus (b)(1) G_{12}, (b)(2) G_{13}, (b)(3) G_{23}.*

Table 8: Boundary Condition applied to obtain Homogenized property: Shear Modulus from the RUC.

Fig. X		*Shear Modulus (G_{12}, G_{13}, G_{23})*		
Figure ID	Property	Retained Node N_0	Retained Node N_2	Retained Node N_3
Simple Shear deformation on x_2x_3-plane				
b(1)	G_{23}	$U^{N_0} = 0$	$U_2^{N_2} = 0$ $U_3^{N_2} = \delta_{23}$	$U_3^{N_3} = 0$ $U_2^{N_3} = 0$

4.5.1 3D Boundary Conditions

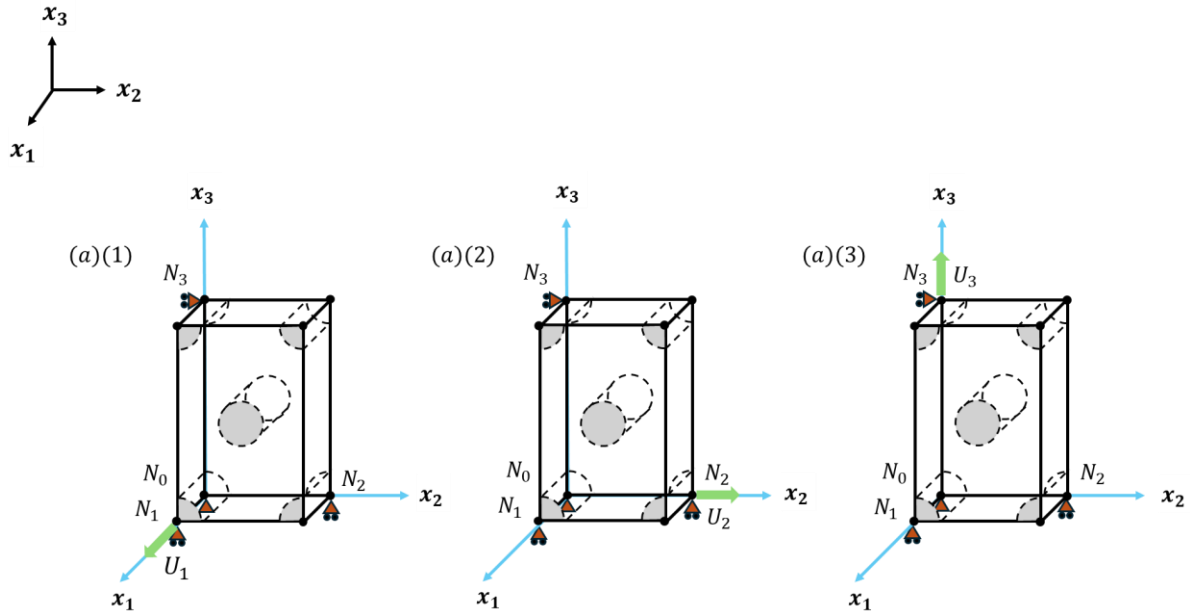

Figure 27: *Schematic Illustration of the Boundary Condition applied to obtain the 3D RUC Homogenized property: Elastic Modulus (a)(1) E_1, (a)(2) E_2, (a)(3) E_3.*

Table 9: Boundary Condition applied to obtain Homogenized property: Elastic Modulus from the RUC.

Fig. X		*Elastic Modulus (E_{12}, E_{13}, E_{23})*			
Figure ID	Property	Retained Node N_0	Retained Node N_1	Retained Node N_2	Retained Node N_3
Uniaxial deformation along x_2-axis					
b(1)	E_2	$U^{N_0} = 0$	$U_1^{N_1} \neq 0$ $U_2^{N_1} = U_3^{N_1} = 0$	$U_2^{N_2} = \delta_2$ $U_3^{N_2} = U_1^{N_2} = 0$	$U_3^{N_3} \neq 0$ $U_2^{N_3} = U_1^{N_3} = 0$
Uniaxial deformation along x_3-axis					
b(2)	E_3	$U^{N_0} = 0$	$U_1^{N_1} \neq 0$ $U_2^{N_1} = U_3^{N_1} = 0$	$U_2^{N_2} \neq 0$ $U_3^{N_2} = U_1^{N_2} = 0$	$U_3^{N_3} = \delta_3$ $U_2^{N_3} = U_1^{N_3} = 0$
Uniaxial deformation along x_1-axis					
b(2)	E_1	$U^{N_0} = 0$	$U_1^{N_1} = \delta_1$ $U_2^{N_1} = U_3^{N_1} = 0$	$U_2^{N_2} \neq 0$ $U_3^{N_2} = U_1^{N_2} = 0$	$U_3^{N_3} \neq 0$ $U_2^{N_3} = U_1^{N_3} = 0$

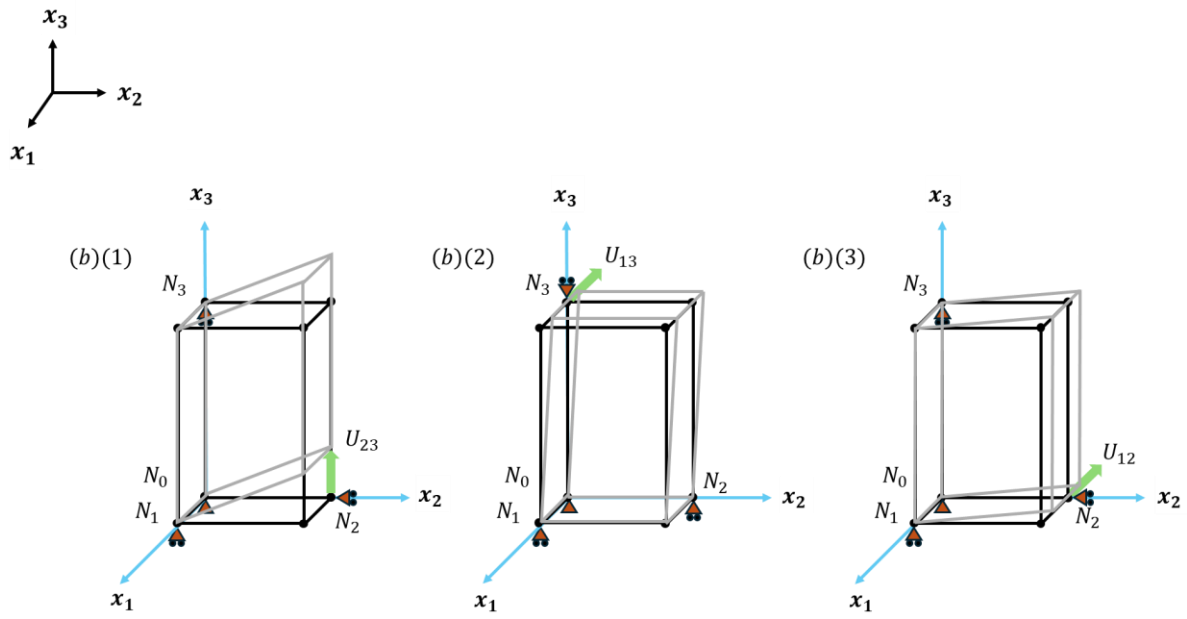

Figure 28: Schematic Illustration of the Boundary Condition applied to obtain the 3D RUC Homogenized property: Shear Modulus (b)(1) G_{12}, (b)(2) G_{13}, (b)(3) G_{23}.

Table 10: Boundary Condition applied to obtain Homogenized property: Shear Modulus from the RUC.

Fig. X		*Shear Modulus (G_{12}, G_{13}, G_{23})*			
Figure ID	Property	Retained Node N_0	Retained Node N_1	Retained Node N_2	Retained Node N_3
Simple Shear deformation on x_2x_3-plane					
b(1)	G_{23}	$U^{N_0} = 0$	$U_2^{N_1} = U_3^{N_1} = 0$ $U_1^{N_1} = 0$	$U_2^{N_2} = U_3^{N_2} = 0$ $U_3^{N_2} = \delta_{23}$	$U_2^{N_3} = U_3^{N_3} = 0$ $U_1^{N_3} = 0$
Simple Shear deformation on x_3x_1-plane					
b(2)	G_{13}	$U^{N_0} = 0$	$U_2^{N_1} = U_3^{N_1} = 0$ $U_1^{N_1} = 0$	$U_2^{N_2} = U_3^{N_2} = 0$ $U_1^{N_2} = 0$	$U_2^{N_3} = U_3^{N_3} = 0$ $U_1^{N_3} = -\delta_{13}$
Simple Shear deformation on x_2x_1-plane					
b(3)	G_{12}	$U^{N_0} = 0$	$U_2^{N_1} = U_3^{N_1} = 0$ $U_1^{N_1} = 0$	$U_2^{N_2} = U_3^{N_2} = 0$ $U_1^{N_2} = -\delta_{12}$	$U_2^{N_3} = U_3^{N_3} = 0$ $U_1^{N_3} = 0$

4.6 HOMOGENIZATIONS

In the context described, RUCs can be conceptualized as an array of identical units, with periodic boundary conditions ensuring consistency. This setup ensures uniform deformation modes throughout the RUCs, preventing overlap or separation [30]. To determine the composite material's properties, a uniform macro-strain, $\hat{\varepsilon}_{ij}$, is applied to each RUC. Since the collected properties are specific to individual nodes, calculating the unweighted volume average of micro-strains and micro-stresses is necessary to derive the macro-stresses and -strains of the entire composite, which encompasses all RUCs within the workspace. To upscale the homogenized properties from micro to macro level, Gauss's divergence theorem is utilized, alongside ensuring that the micro-stress field complies with the condition $\sigma_{ij,j} = 0$, indicating divergence-free outcomes.

With this approach, the micro-stresses are determined through Equation (31), considering the reaction forces and displacements at the relevant nodes, where the periodic boundary condition is enforced. Equation (32) represents an integration around the edges of the RUC. Likewise, for the unweighted volume average of micro-strain, Equation (32) is employed, leveraging the applied displacements at control nodes to enforce a macro-strain condition, $\hat{\varepsilon}_{ij}$, thus deriving the macro-strain components, $\hat{\sigma}_{ij}$.

$$\hat{\sigma}_{ij} = \frac{1}{\Omega}\int_{\Omega} \sigma_{ij}\, d\Omega = \int_{\partial\Omega=\Upsilon} \sigma_{ik}\overline{n}_k x_j d\Upsilon = \frac{(F_i)_j}{\Upsilon_j} \quad \text{(no summation over the index j)} \quad (31)$$

$$\hat{\varepsilon}_{ij} = \frac{1}{\Omega}\int_{\Omega} \varepsilon_{ij}\, d\Omega = \frac{1}{2\Omega}\int_{\partial\Omega=\Upsilon} (u_i\overline{n}_j + u_j\overline{n}_i) d\Upsilon \quad (32)$$

Where $\hat{\sigma}_{ij}$ and $\hat{\varepsilon}_{ij}$ are the macro-stress and micro-strain respectively. Ω stands for the volume of the RUC, $\overline{n}_i$ is the vector unit normal to the boundary, $(F_i)_j$ is the resultant force on the edge or surface (2D and 3D) normal to it in the x_j-direction.

Using the macro-strain state, the 2D RUC undergoes four independent loading conditions, including normal and shear loading along transverse directions. Similarly, the 3D RUC model experiences six independent loading conditions, comprising normal and shear loading along axial and transverse directions. The homogenized properties obtained for both the 2D, and 3D models are detailed as follows:

- 2D 'Plane Strain' RUC: $\hat{E}_2$, $\hat{E}_3$, $\hat{G}_{23}$, $\hat{v}_{23}$.
- 3D RUC: $\hat{E}_1$, $\hat{E}_2$, $\hat{E}_3$, $\hat{G}_{12}$, $\hat{G}_{13}$, $\hat{G}_{23}$, $\hat{v}_{12}$, $\hat{v}_{13}$, $\hat{v}_{23}$.

4.7 VALIDATION: ANALYTICAL MODELS

Validation is a crucial step when modelling as it ensures that the model produced from the Python Script to Abaqus Standard software is accurate and reliable. This practice is common across different software and disciplines and has become a standard procedure.

In the realm of computer-aided engineering (CAE), various approaches can be explored and implemented to ensure the integrity of the model, making it representative of the object being simulated.

The primary approach for validation in this project is utilizing analytical models, specifically focusing on both single fiber and fiber hybrid composites. Despite the emphasis on fiber hybrid composites, validating the single fiber combinations (such as Basalt/Epoxy, Flax/Epoxy, Carbon/Epoxy, and E-glass/Epoxy) is important for two reasons. Firstly, readily available data for these single fiber combinations allows for confident comparisons, as data is collected from this paper. Secondly, since the volume fraction remains consistent for each fiber (e.g., 0.6 Vf for Basalt/Carbon/Epoxy with 0.3 for Basalt and 0.3 for Carbon), comparing the homogenized properties of the fiber hybrid combination to those of its respective single fibre combinations ensures accuracy. This approach ensures that the homogenized properties generated from the fiber hybrid combination fall within the range of its individual single fiber combinations.

For single fibre validation, a Solver was developed, detailed in Appendix B, utilizing two analytical models: Chamis and ROM, along with the inclusion of ROMm. As noted earlier in the section, analytical models inherently introduce errors due to the assumptions made for each. Therefore, a subsequent discussion below outlines the anticipated behaviours of the collected values, as elaborated in the following Section 5.2.

Chamis, a widely recognized model stemming from the Rule of Mixture, shares assumptions related to linear elasticity and isotropic behaviour. Despite its foundation, Chamis faces challenges in accurately depicting the transverse plane of anisotropic composites. Though, as mentioned in sub-section 2.5.1 analytical models derived from the Rule of Mixture typically excel in representing axial parameters across straightforward geometries like the RUC.

Rule of Mixture (ROM) simplifies predictions of composite material properties by combining constituent properties linearly. While effective for simple geometries and

axial properties, ROM falls short in complex geometries due to variations in fibre distribution and interactions. It also struggles with transverse properties due to composites' anisotropic nature.

ROMm is an advancement over ROM as it integrates an experimental variable ξ to refine predictions. However, its effectiveness is hindered by the potential limitations of available data, raising concerns about the reliability of adjustments. Moreover, ROMm is likely to yield notable discrepancies in the transverse when compared to Finite Element Analysis (FEA) values.

The preference for using software like Digimat for validating fibre hybrid composites stems from the complexity inherent in implementing its formulas in the 'Analytical Solver'. In Digimat, the analytical model employed is Mori-Tanaka, which derives homogenized properties of the composites by averaging the behaviours of their constituents. Consequently, the values derived from Mori-Tanaka represent homogenized engineering constants obtained from averaging both stress and strain tensors, assuming linear elasticity.

4.8 FLOW DIAGRAM OF MODELLING

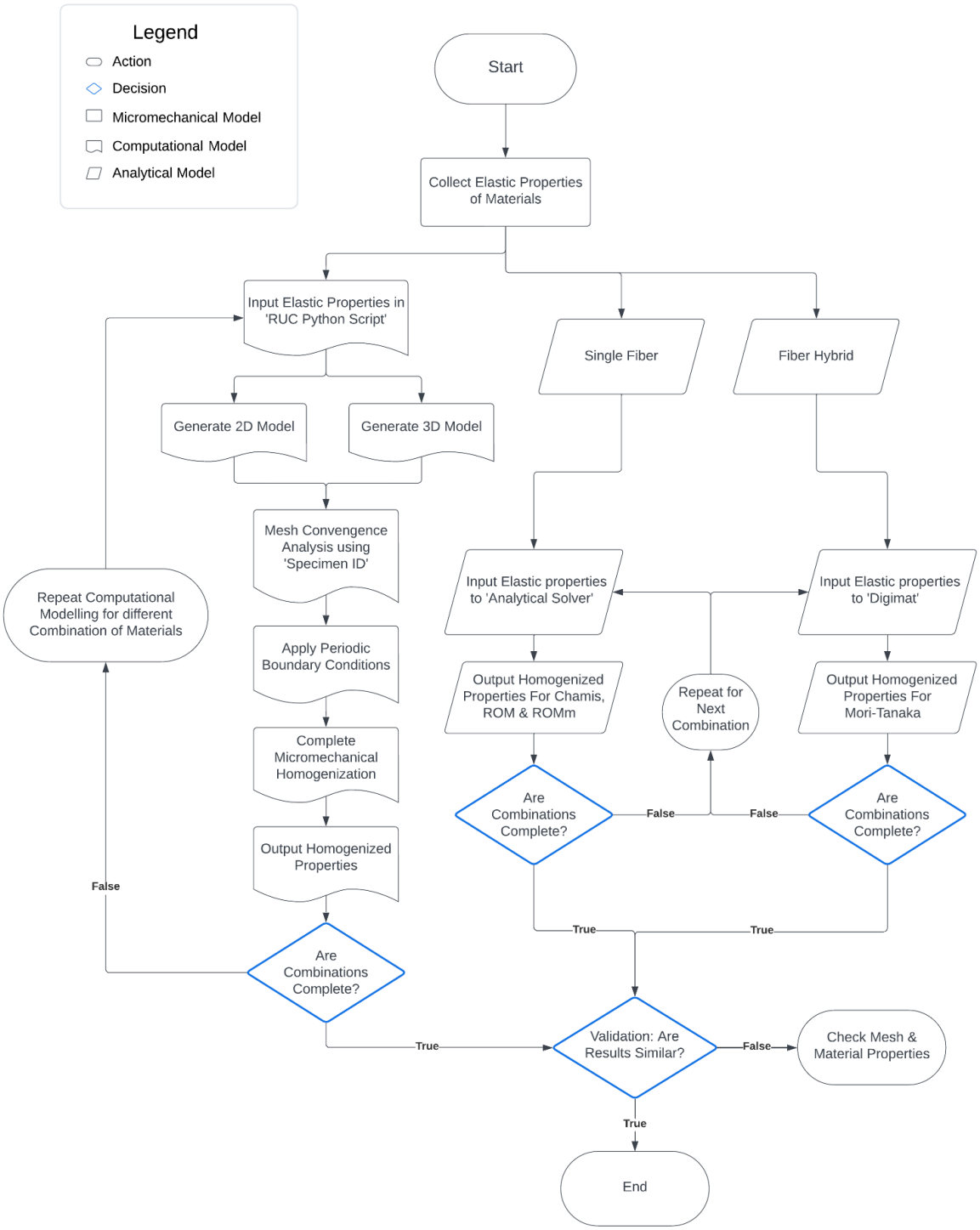

5 RESULTS AND DISCUSSION

Section 4 details the generation of 2D and 3D RUC models using a *Python* Script and Abaqus/Standard. The process involved the application of Periodic Boundary Conditions, Boundary Conditions, and Loading. The objective of this section is to comprehensively present all the data gathered from the Finite Element Analysis (FEA) simulations. The data is organized and presented as follows:

5.1 Mesh Sensitivity Analysis,

5.2 Validation: Repeating Unit Cells vs Analytical Models

5.3 Fibre Hybrid Composites: Mechanical Behaviour.

Section 5.2 possesses a single fiber and fiber hybrid validation, where FEA output data is compared side-by-side to commonly used analytical model across the industry. While Section 5.3 discusses the behaviour of the combination suggested in Section 3.

5.1 MESH SENSITIVITY ANALYSIS

Among the specimens utilized in the simulations, 'iEHH_0.05_0.6_i', employing the finest mesh with a mesh size of 0.05 and utilizing Hex-Dominated elements (CPE4R/CPE3 and C3D8R/C3D6) with reduced integration, is expected to yield the most accurate results. This choice aligns with the aim of achieving mesh-independent outcomes, as discussed in Section 4.2.4.

Table 11: Number of elements for mesh size.

	Global mesh Size (i)				
Specimen ID	1.0	0.75	0.5	0.25	0.05
BEHH_i_0.6_2	304	602	1054	4402	109013
BEHH_i_0.6_3	186	427	817	3319	82315

Table 12 displays the duration required to simulate each specimen across various mesh sizes. Unsurprisingly, as indicated in Table 11 and depicted in Figures 29 and 30, the total CPU time increases with the generation of more elements for the mesh. These simulations were conducted using an Intel i7-8700 @ 3.20GHz CPU. It's important to note that the provided time excludes tasks such as outputting material properties and post-processing.

Table 12: Total CPU time for mesh sizes 1.0, 0.75, 0.5, 0.25, and 0.05 using *Intel i7-8700 @ 3.20GHz.*

Global mesh Size (i)			1.0	0.75	0.5	0.25	0.05
Specimen ID	Fibre Mesh Element	Matrix Mesh Element	Time (s)				
BEHH_i_0.6_2	Hex-Dom C2D3/CPS4	Hex-Dom C2D3/CPS4	0.1	0.2	0.6	1.1	3.5
BCEHH_i_0.6_2	Hex-Dom C2D3/CPS4	Hex-Dom C2D3/CPS4	0.1	0.2	0.6	1.1	3.5
BEHH_i_0.6_3	Hex-Dom C3D6/C3D8	Hex-Dom C3D6/C3D8	0.3	0.4	0.8	1.9	60.8
BCEHH_i_0.6_3	Hex-Dom C3D6/C3D8	Hex-Dom C3D6/C3D8	0.3	0.4	0.8	1.9	60.8

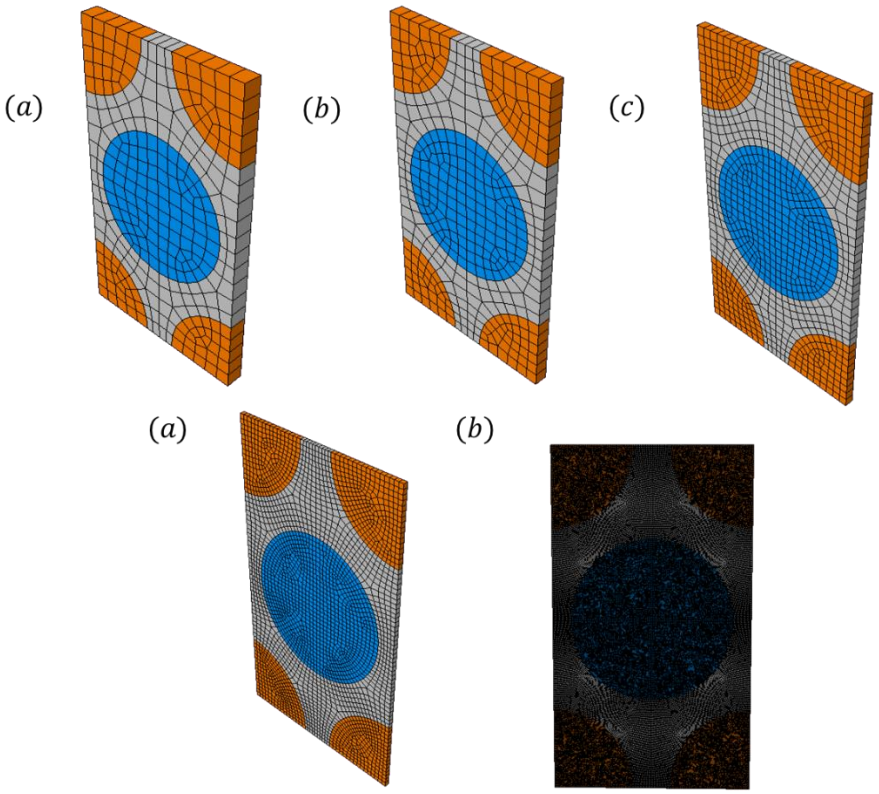

Figure 29: 3D Mesh of BEHH_i_0.6_3 for (a) 1.00, (b) 0.75, (c) 0.50, (d) 0.25, (e) 0.05.

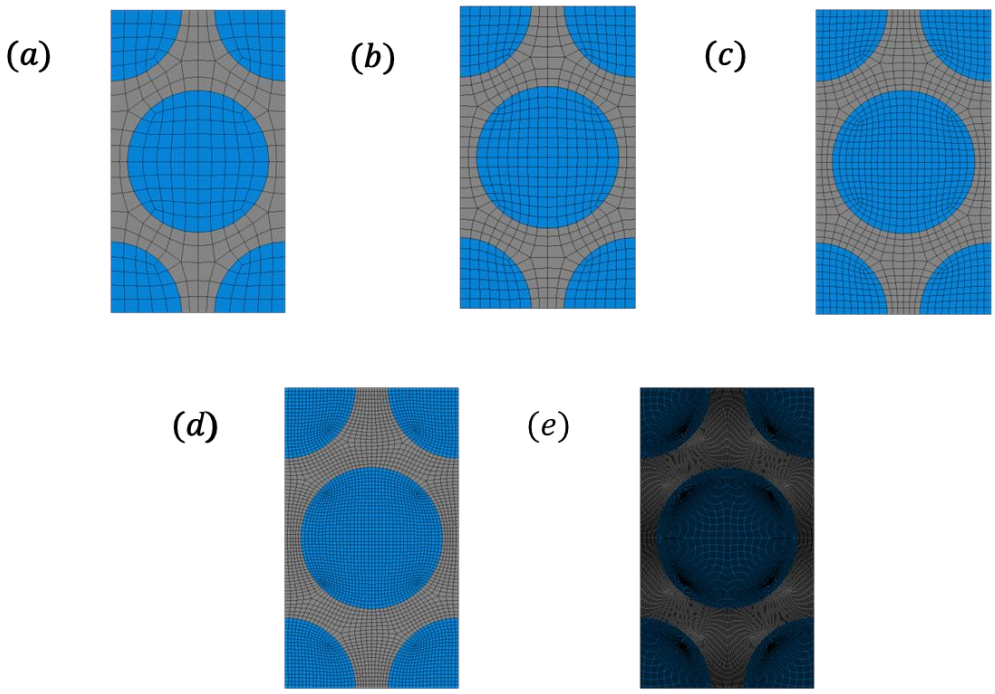

Figure 30: *2D Mesh of BEHH_i_0.6_2 for sizes: (a) 1.00, (b) 0.75, (c) 0.50, (d) 0.25, (e) 0.05.*

In Figures 31 to 34 at the largest mesh size of 1.00, there are slight indications of asymmetry, although not as pronounced as discussed in Section 4.2.3. This reduction of asymmetry is attributed to the diagonal partitioning applied throughout the mesh, which effectively mitigated asymmetry between the mirrored faces. The presence of periodicity becomes evident when analysing the von Mises stress (σ_{vm}) under the influence of a macro stress (σ_2) applied to both the 2D and 3D RUC, as demonstrated in Section 4.1. As the mesh size increases, it meets the requirements outlined in Section 4.2.3, addressing the 'two challenges' associated with periodic boundary conditions. This observed trend persists across all examined specimens *'iEHH_i_0.6_3'*.

Table 13 includes all the absolute values of the homogenized properties obtained for both 2D and 3D at all mesh settings considered in the mesh strategy. It is worth noting that for 2D axial parameters are not generated as no thickness in introduced, and $\hat{E}_2$ is equal to $\hat{E}_3$.

Table 13: Results of mesh sensitivity for Basalt/Epoxy and Carbon/Epoxy RUC with volume fraction (V_f) of 0.6 in GPa.

Specimen Set V_f = 0.60	$\hat{E}_1$	$\hat{E}_2$	$\hat{E}_3$	$\hat{G}_{12}$	$\hat{G}_{13}$	$\hat{G}_{23}$	$\hat{v}_{12}$	$\hat{v}_{13}$	$\hat{v}_{23}$
Baseline: *BEHH_0.05_0.6_2*	-	15.28	15.28	-	-	4.9			0.44
BEHH_0.25_0.6_2	-	15.26	15.26	-	-	4.93	-		0.44
BEHH_0.50_0.6_2	-	15.29	15.29	-	-	4.89	-	-	0.44
BEHH_0.75_0.6_2	-	15.26	15.26	-	-	4.9	-	-	0.44
BEHH_1.00_0.6_2	-	15.18	15.18	-	-	4.9	-	-	0.44
Baseline: *BCEHH_0.05_0.6_2*	-	12.87	12.87	-	-	4.04	-	-	0.46
BCEHH_0.25_0.6_2	-	12.86	12.86	-	-	4.05	-	-	0.46
BCEHH_0.50_0.6_2	-	12.87	12.87	-	-	4.03	-	-	0.46
BCEHH_0.75_0.6_2	-	12.84	12.84	-	-	4.04	-	-	0.46
BCEHH_1.00_0.6_2	-	12.8	12.8	-	-	4.03	-	-	0.46
Baseline: *BEHH_0.05_0.6_3*	55.2	14.95	14.95	5.04	5.04	4.9	0.29	0.29	0.41
BEHH_0.25_0.6_3	55.17	14.94	14.95	5.04	5.04	4.9	0.29	0.29	0.41
BEHH_0.50_0.6_3	55.09	14.9	14.93	5.02	5.03	4.89	0.29	0.29	0.4
BEHH_0.75_0.6_3	54.98	14.88	14.94	5	5.02	4.88	0.29	0.29	0.4
BEHH_1.00_0.6_3	54.86	14.76	14.83	4.97	5.01	4.88	0.29	0.29	0.41
Baseline: *BCEHH_0.05_0.6_3*	115.57	12.79	12.49	5	4.96	4.17	0.28	0.27	0.45
BCEHH_0.25_0.6_3	115.5	12.78	12.49	4.99	4.96	4.17	0.28	0.27	0.45
BCEHH_0.50_0.6_3	115.43	12.75	12.47	4.98	4.95	4.16	0.28	0.27	0.45
BCEHH_0.75_0.6_3	115.11	12.74	12.48	4.95	4.94	4.15	0.28	0.27	0.45
BCEHH_1.00_0.6_3	187.23	10.97	10.98	4.91	4.92	3.69	0.25	0.25	0.49

Table 14 displays the outcomes of the mesh sensitivity analysis, comparing the results of all mesh settings to the baseline. In the 2D analysis, the highest variation percentage occurs in the elastic modulus across the traverse plane, E_2 and E_3, with a value of 0.54%. Conversely, the lowest variation, 0%, is observed in the transverse Poisson's ratio, v_{23}. In

the 3D analysis, the largest variation, 2.44%, is observed in v_{23}, while the lowest variation, also 0%, is found in both Poisson's ratios, v_{12} and v_{13}. Therefore, based on these results, the discrepancies between different mesh settings are relatively small, indicating that the outcomes are not significantly influenced by the mesh strategy.

Table 14: FEA post-processing result variation compared to baseline mesh strategy BEHH_0.05_0.6_i in GPa.

Average Variation (%)	$\hat{E}_1$	$\hat{E}_2$	$\hat{E}_3$	$\hat{G}_{12}$	$\hat{G}_{13}$	$\hat{G}_{23}$	$\hat{v}_{12}$	$\hat{v}_{13}$	$\hat{v}_{23}$
Baseline: *BEHH_0.05_0.6_2*	-	-	-	-	-	-	-	-	-
BEHH_0.25_0.6_2	-	0.13	0.13	-	-	-0.61	-	-	0
BEHH_0.50_0.6_2	-	-0.07	-0.07	-	-	0.20	-	-	0
BEHH_0.75_0.6_2	-	0.13	0.13	-	-	0	-	-	0
BEHH_1.00_0.6_2	-	0.66	0.66	-	-	0	-	-	0
Baseline: *BCEHH_0.05_0.6_2*	-	-	-	-	-	-	-	-	-
BCEHH_0.25_0.6_2	-	0.08	0.08	-	-	-0.25	-	-	0
BCEHH_0.50_0.6_2	-	0	0	-	-	0.25	-	-	0
BCEHH_0.75_0.6_2	-	0.23	0.23	-	-	0	-	-	0
BCEHH_1.00_0.6_2	-	0.54	0.54	-	-	0.25	-	-	0
Baseline: *BEHH_0.05_0.6_3*	-	-	-	-	-	-	-	-	-
BEHH_0.25_0.6_3	0.05	0.07	0	0	0	0	0	0	0
BEHH_0.50_0.6_3	0.19	0.34	0.13	0.39	0.19	0.20	0	0	2.44
BEHH_0.75_0.6_3	0.39	0.47	0.07	0.79	0.39	0.41	0	0	2.44
BEHH_1.00_0.6_3	0.62	1.27	0.80	1.39	0.59	0.41	0	0	0
Baseline: *BCEHH_0.05_0.6_3*	-	-	-	-	-	-	-	-	-
BCEHH_0.25_0.6_3	0.061	0.08	0	0.2	0	0	0	0	0
BCEHH_0.50_0.6_3	0.12	0.31	0.16	0.4	0.20	0.24	0	0	0
BCEHH_0.75_0.6_3	0.39	0.39	0.08	1	0.40	0.48	0	0	0
BCEHH_1.00_0.6_3	0.63	1.02	0.64	1.4	0.61	0.48	0	0	0

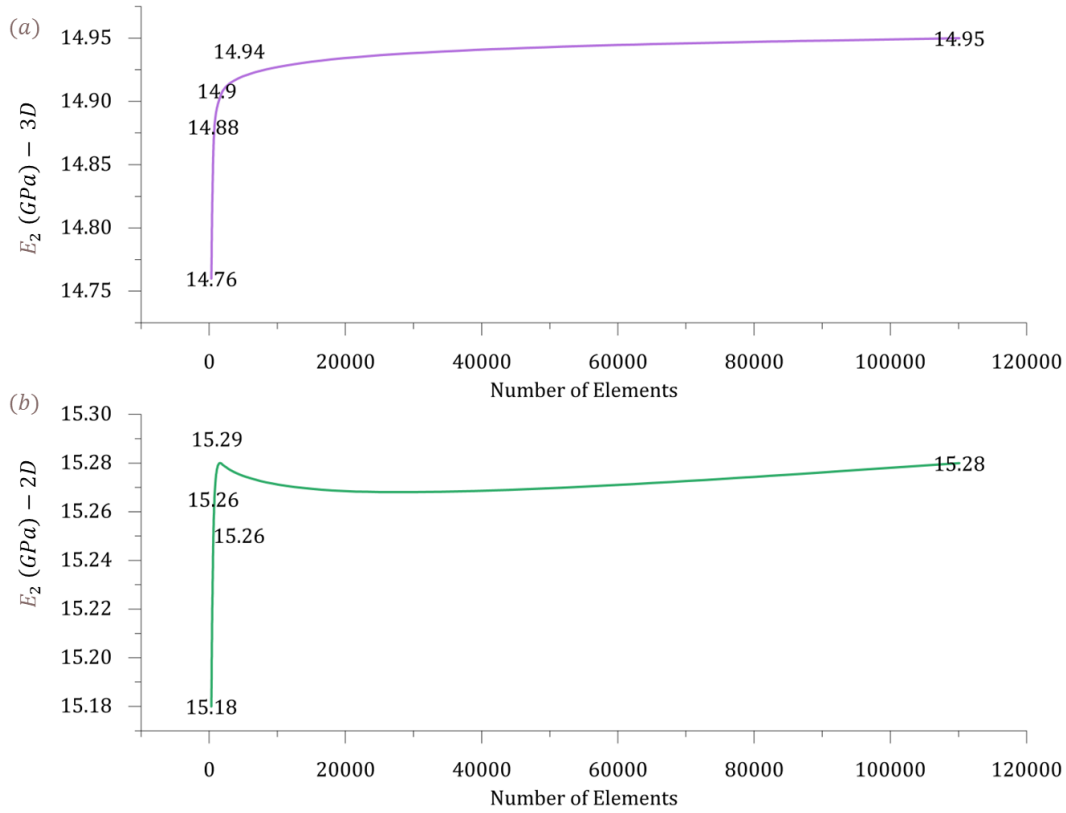

Figure 31: *Mesh Convergence of Transverse Elastic Modulus. E_2, for (a) 3D and (b) 2D RUCs.*

As outlined in Sub-Section 4.2, the engineering constant under consideration is particularly volatile. Notably, this constant is applicable to both 2D and 3D models, as depicted in Figure 31, illustrating mesh convergence for both model types.

Despite the minor disparities observed between mesh sizes of 0.25 and 0.05, it's notable that the finest mesh (0.05) necessitates a significantly larger number of elements. This increase directly correlates with a Total CPU time approximately 32 times longer than that required for the coarser mesh size (0.25).

In the context of human timeframes, simulations lasting approximately 1 minute are typically considered "short-timed simulations". Hence, if time permits, opting for the finest mesh could yield slightly more accurate results. However, this decision must be balanced against the constraints of time and computational resources. Additionally, the slight differences between 2D and 3D values can be attributed to 2D being Plane Strain. In a scenario where the material is analysed in two dimensions and the macro-stress applied doesn't affect all three dimensions, with negligible thickness, the confinement

within the axial plane restricts deformation across this plane. Consequently, this confinement results in a stiffer transverse elastic modulus (E_2).

As discussed in sub-Section 4.2, the engineering constant under scrutiny, given its fluctuating nature, is a crucial property for analysis to ensure accurate modelling. It's noteworthy that this engineering constant can be examined in both 2D and 3D simulations. Figure 31 illustrates the mesh convergence for both models.

5.2 VALIDATION: REPEATING UNIT CELLS VS ANALYTICAL MODELS

5.2.1 Validation for Single and Hybrid Fibers Composite

In order to assure accuracy from the RUC Model, an analytical validation is performed to compare results for the homogenized properties of the composite. For the first validation, the composite is assumed to be non-hybrid (i.e., Fiber 1 and Fiber 2 are assigned the same Material properties), thus single fiber composite and in addition to assumptions mentioned in Section 4 Methodology. For single fiber composites, Rule of Mixture (ROM), Modified Rule of Mixture (ROMm) and Chamis will be the analytical models of choice. Whereas for fiber-hybrid composites, Mori-Tanaka will be analytical model used for validation, following the order Fiber2/Fiber1/Matrix, thus, reversed. The values obtained from the analytical models are directly compared with the homogenized properties derived from both 2D and 3D RUCs. Subsequently, there is an examination of the efficacy of the RUC model, which is elaborated upon in Section 5.2.2 and 5.2.3.

5.2.2 Single Fiber Validation

In the validation process for single fibres, we examine four types of composites: Basalt/Epoxy, Carbon/Epoxy, Flax/Epoxy, and Flax/E-glass, each in both 2D and 3D RUCs. The fiber volume fraction remains consistent at around 0.60 for all composites. We evaluate the homogenized properties obtained from Abaqus/Standard and compare them directly with analytical models, including Chamis (Ch), Rule of Mixture (ROM), and modified Rule of Mixture (ROMm). Tables 15 through 18 contain the data for both computational and analytical models, corresponding to each composite as indicated in the table descriptions.

Table 15 Single Fiber Validation of Basalt/Epoxy composite shows the values from each model in absolute values, and in addition, the variation of each computational model in

comparison to each analytical model**.** Focusing on 2D RUC, which is capable of only generating transverse properties, a significant disagreement in visible when compared to ROM, with variation as high as 65%, and low as 36.50%. Whereas with Chamis model, lower variations are produced for elastic and shear modulus, ranging 3.11-6.61%, while a similar discrepancy to ROM is maintain with a variation of 38.97% for the transverse Poisson's ratio. Regarding 3D, ROM is capable of showcasing similar results for axial properties: E_1, v_{12} and v_{13} as expected, with variations ranging from 0 to 2.03%. Regarding the transverse properties, higher variations are produced, ranging from 30.11 to 40.8%. Though, the largest variation is located at the in-plane shear modulus: G_{12} and G_{13}, with 43.75%.

Figure 32 Maximum local von Mises stress for (a) 2D and (b) 3D RUC of Basalt/Epoxy, Figure 33 Maximum local von Mises stress for (a) 2D and (b) 3D RUC of Carbon/Epoxy, Figure 34 Maximum local von Mises stress for (a) 2D and (b) 3D RUC of Flax/Epoxy, and Figure 35 Maximum local von Mises stress for (a) 2D and (b) 3D RUC of E-glass/Epoxy for Mesh size 0.05 and Volume fraction 0.6 shows that within the von Mises stress distribution, an agreement on the concentration of stress is visible within the matrix, and different stresses maximums of 1.18 and 2.38 for Basalt/Epoxy, 1.05 and 2.33 for Carbon/Epoxy, 1.00 and 1.99 for Flax/Epoxy, and 1.17 and 2.40 for E-glass/Epoxy, for the 2D RUC and 3D RUC, respectively, are visible as expected due to the anisotropy reinforced polymers inherently possess from the fibre orientation, as the axial properties are captured in the 3D RUC.

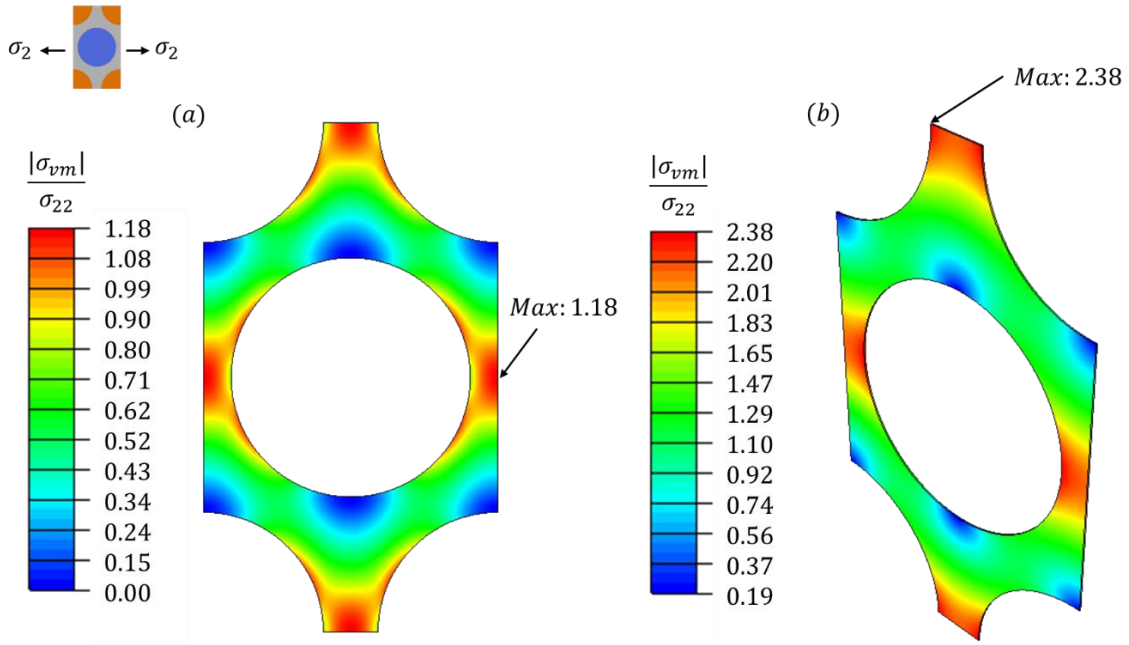

Figure 32: *Maximum local von Mises stress for (a) 2D and (b) 3D RUC of Basalt/Epoxy for Mesh size 0.05 and Volume fraction of 0.6.*

Table 15: Single Fiber Validation of Basalt/Epoxy composite**.**

	Basalt/Epoxy							
Property	ROM & ROMm (ξ=1)	Chamis	2D RUC	ROM Diff. (%)	Ch Diff. (%)	3D RUC	ROM Diff. (%)	Ch Diff. (%)
$E_1\ GPa$	55.120	55.12	-	-	-	55.2	0	0
$E_2\ GPa$	10.024	16.361	15.23	52.43	-6.61	14.95	30.11	-8.62
$E_3\ GPa$	10.024	16.361	15.23	52.43	-6.61	14.95	30.11	-8.62
$G_{12}\ GPa$	2.961	4.752	-	-	-	5.04	43.75	6.06
$G_{13}\ GPa$	2.961	4.752	-	-	-	5.04	43.75	6.06
$G_{23}\ GPa$	2.961	4.752	4.3	65.48	3.11	4.9	40.80	3.11
v_{12}	0.296	0.296	-	-	-	0.29	-2.03	-2.03
v_{13}	0.296	0.296	-	-	-	0.29	-2.03	-2.023
v_{23}	0.693	0.721	0.44	-36.50	-38.97	0.41	-39.25	-43.14

Table 16, which presents the Single Fiber Validation of Carbon/Epoxy composite, illustrates that the computational model aligns closely with the Chamis model across all homogenized properties, except for the transversal Poisson's ratio v_{23} ,. For this parameter, variations range from 0.14% to 7.93% across both 2D and 3D RUCs. However, when compared to the ROM model, the variations for E_1, v_{12} and v_{13} remain low at 0.14%, 3.85%, and 3.85%, respectively. Conversely, the variations for the other properties range between 21.72% and 59.55%.

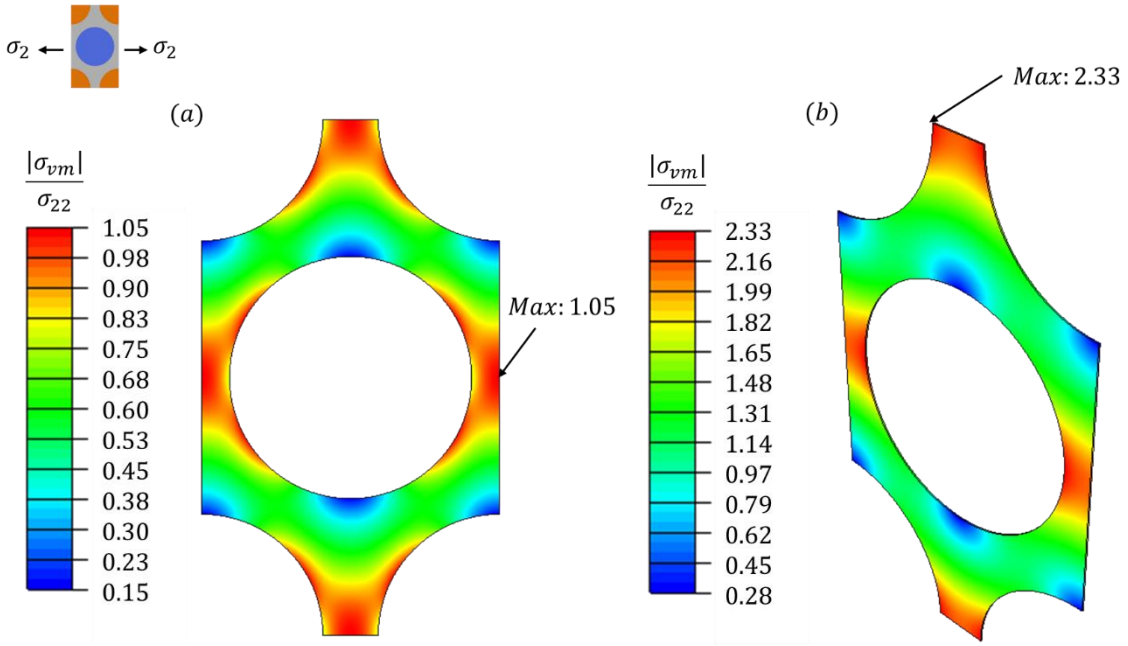

Figure 33: *Maximum local von Mises stress for (a) 2D and (b) 3D RUC of Carbon/Epoxy for mesh size 0.05 and Volume fraction of 0.6.*

Table 16: Single Fiber Validation of Carbon/Epoxy composite**.**

	Carbon/Epoxy							
Property	ROM & ROMm (ξ=1)	Chamis	2D RUC	ROM Diff. (%)	Ch Diff. (%)	3D RUC	ROM Diff. (%)	Ch Diff. (%)
$E_1\ GPa$	175.7	175.7	-	-	-	175.9	0.14	0.14
$E_2\ GPa$	8.224	11.198	10.32	25.73	-7.66	10.31	25.37	-7.93
$E_3\ GPa$	8.224	11.198	10.32	25.73	-7.66	10.31	25.37	-7.93
$G_{12}\ GPa$	2.833	4.347	-	-	-	4.52	59.55	3.98

$G_{13}\ GPa$	2.833	4.347	-	-	-	4.52	59.55	3.98
$G_{23}\ GPa$	2.530	3.512	3.1	36.76	-1.48	3.46	36.76	-1.48
v_{12}	0.26	0.26	-	-	-	0.25	-3.85	-3.85
v_{13}	0.26	0.26	-	-	-	0.25	-3.85	-3.85
v_{23}	0.626	0.723	0.49	-21.73	-17.51	0.49	-21.72	-17.51

In Table 17, which presents the Single Fiber Validation of Flax/Epoxy composite, it is observed that the computational and analytical results are quite similar. Variations across all homogenized properties, for ROM and Chamis, ranging from 0% to 11.48%, with the exception of the axial shear modulus G_{12} and G_{13}, which exhibit a variation of 17.86%.

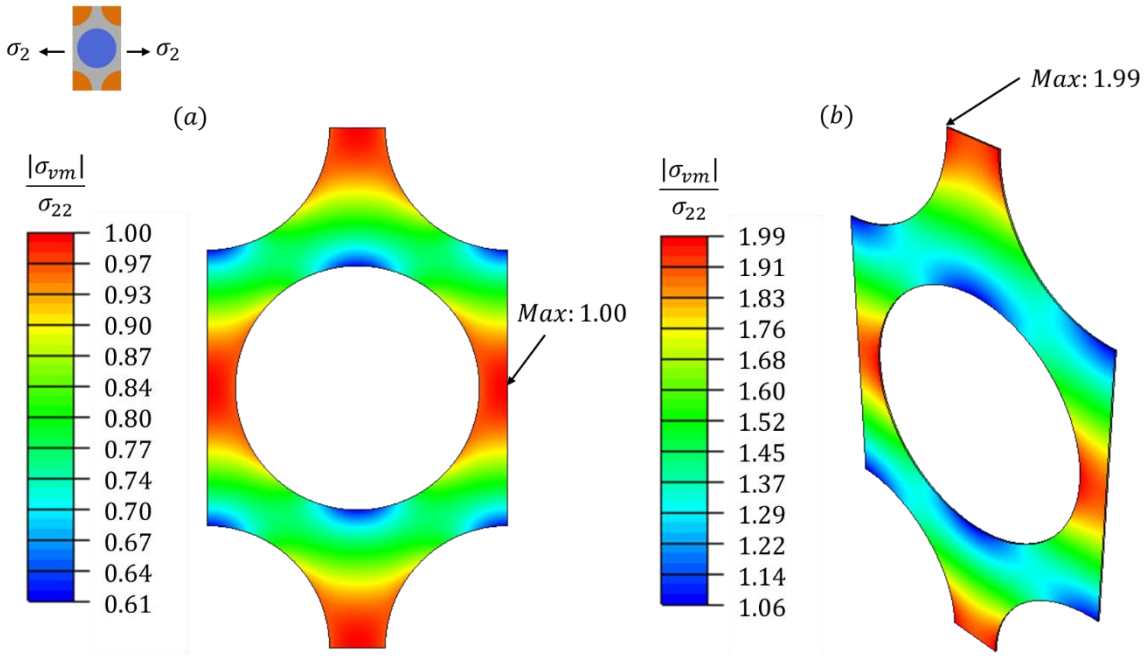

Figure 34: *Maximum local von Mises stress for (a) 2D and (b) 3D RUC of Flax/Epoxy for mesh size 0.05 and Volume fraction of 0.6.*

Table 17: Single Fiber Validation of Flax/Epoxy composite**.**

	Flax/Epoxy							
Property	ROM & ROMm (ξ=1)	Chamis	2D RUC	ROM Diff. (%)	Ch Diff. (%)	3D RUC	ROM Diff. (%)	Ch Diff. (%)
$E_1\ GPa$	34.180	34.180	-	-	-	34.22	0.12	0.12

$E_2\ GPa$	5.595	6.132	6.08	8.67	-0.85	5.97	6.70	-2.64
$E_3\ GPa$	5.595	6.132	6.08	8.67	-0.85	5.97	6.70	-2.64
$G_{12}\ GPa$	1.960	2.310	-	-	-	2.31	17.86	0
$G_{13}\ GPa$	1.960	2.310	-	-	-	2.31	17.86	0
$G_{23}\ GPa$	1.639	1.779	1.67	11.04	2.31	1.82	11.04	2.31
v_{12}	0.320	0.320	-	-	-	0.32	0	0
v_{13}	0.320	0.320	-	-	-	0.32	0	0
v_{23}	0.707	0.723	0.67	-5.23	-7.33	0.64	-9.48	-11.48

Finally, Table 18, illustrating the Single Fiber Validation of E-glass/Epoxy composite, reveals the most substantial variations among the four tables. Notably, the variation reaches as high as 76.84% for the axial shear modulus G_{12} and G_{13} in the ROM model. Conversely, when compared to the Chamis model, variations range from negligible to 2.64%, except for the transversal Poisson's ratio v_{23}, which exhibits variations of 11.48% and 7.33% for 3D and 2D models respectively.

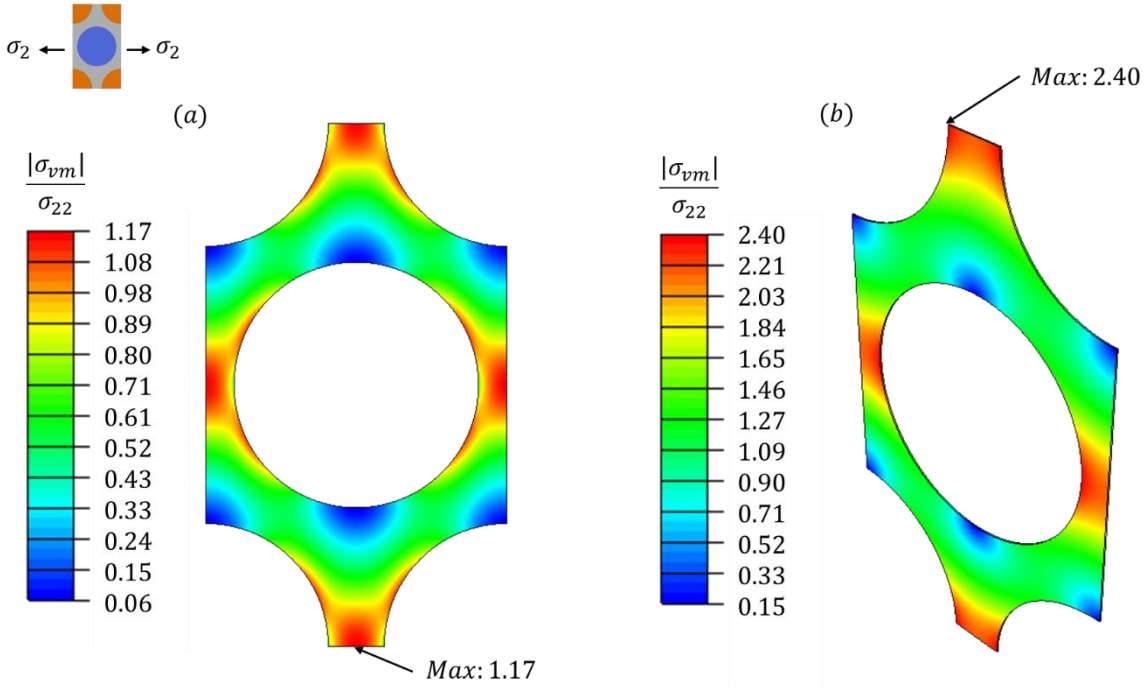

Figure 35: *Maximum local von Mises stress for (a) 2D and (b) 3D RUC of E-glass/Epoxy for mesh size 0.05 and Volume fraction of 0.6.*

Table 18: Single Fiber Validation of E-glass/Epoxy composite**.**

E-glass/Epoxy

Property	ROM & ROMm (ξ=1)	Chamis	2D RUC	ROM Diff. (%)	Ch Diff. (%)	3D RUC	ROM Diff. (%)	Ch Diff. (%)
$E_1\ GPa$	45.520	45.520	-	-	-	45.59	0.15	0.15
$E_2\ GPa$	9.877	15.865	14.77	50.15	-6.52	14.5	46.81	-8.60
$E_3\ GPa$	9.877	15.865	14.77	50.15	-6.52	14.5	46.81	-8.60
$G_{12}\ GPa$	3.031	4.991	-	-	-	5.36	76.84	7.39
$G_{13}\ GPa$	3.031	4.991	-	-	-	5.36	76.84	7.39
$G_{23}\ GPa$	3.031	4.991	4.54	71.23	3.99	5.2	71.56	4.19
v_{12}	0.278	0.278	-	-	-	0.27	-2.88	-2.88
v_{13}	0.278	0.278	-	-	-	0.27	-2.88	-2.88
v_{23}	0.629	0.590	0.43	-31.64	-27.12	0.4	-36.41	-32.20

5.2.3 Fiber Hybrid Validation

Table 19 Fiber-hybrid Validation of Basalt/Carbon/Epoxy composite shows the data for both Mori-Tanaka's analytical model and both 2D and 3D RUCs where it is possible to see that a large agreement between the 3 is captured across the tables where the variation ranges from 0.09 to 6.21%. Concluding that both computation and analytical models were capable of representing accurately the mechanical behaviour of the composite at hand (Basalt/Carbon/Epoxy).

Figure 36: Maximum local von Mises stress for (a) 2D and (b) 3D RUC of Basalt/Carbon/Epoxy and Figure 37: Maximum local von Mises stress for (a) 2D and (b) 3D RUC of Flax/E-glass/Epoxy for mesh size 0.05 and Volume fraction 0.6 show that within the von Mises stress distribution, an agreement on the concentration of stress is visible within the matrix, and different stresses maximums of 1.38 and 2.66 for Basalt/Carbon/Epoxy and 1.57 and 3.47 for Flax/E-glass/Epoxy for the 2D RUC and 3D RUC, respectively, are visible as expected due to the anisotropy reinforced polymers inherently possess as the axial properties are captured in the 3D RUC. paraphrase

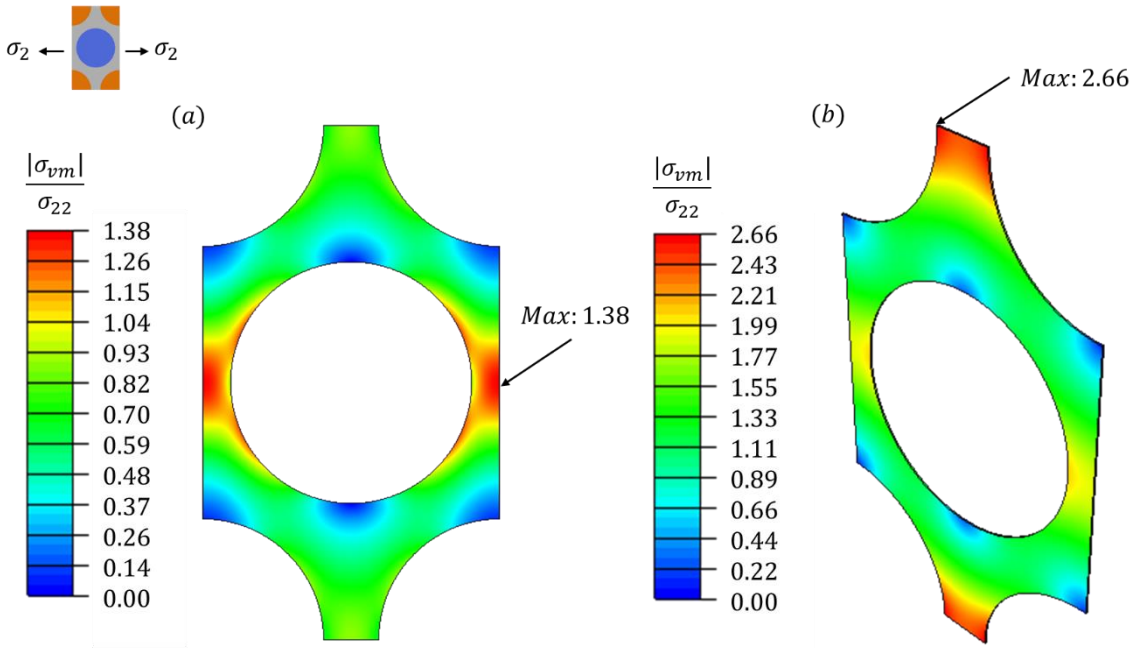

Figure 36: *Maximum local von Mises stress for (a) 2D and (b) 3D RUC of Basalt/Carbon/Epoxy for mesh size 0.05 and Volume fraction of 0.6.*

Table 19: Fiber-hybrid Validation of Basalt/Carbon/Epoxy composite.

Basalt/Carbon/Epoxy					
Property	Mori-Tanaka	2D RUC	Variation (%)	3D RUC	Variation (%)
$E_1\ (GPa)$	115.46	-	-	115.57	0.09
$E_2\ (GPa)$	12.118	12.87	6.21	12.79	5.55
$E_3\ (GPa)$	12.118	12.87	6.21	12.49	3.07
$G_{12}\ (GPa)$	4.9802	-	-	5.00	0.39
$G_{13}\ (GPa)$	4.9802	-	-	4.96	-0.41
$G_{23}\ (GPa)$	4.109	4.04	-1.68	4.17	1.48
v_{12}	0.2748	-	-	0.28	1.89
v_{13}	0.2748	-	-	0.27	-1.74
v_{23}	0.4746	0.46	-3.08	0.45	-5.18

Table 20 Fiber-hybrid Validation of Flax/E-glass/Epoxy composite shows a direct comparison between Flax/E-glass/Epoxy for 2D and 3D RUCs against Mori-Tanaka analytical model. For 2D, variations from 5.47 to 20.55%. Where the largest variation is

attributed to the out-of-plane shear modulus. While an agreement between the 2D model and Mori-Tanaka model is captured from out-of-plane Poisson's ratio as well as elastic modulus E_2 and E_3.

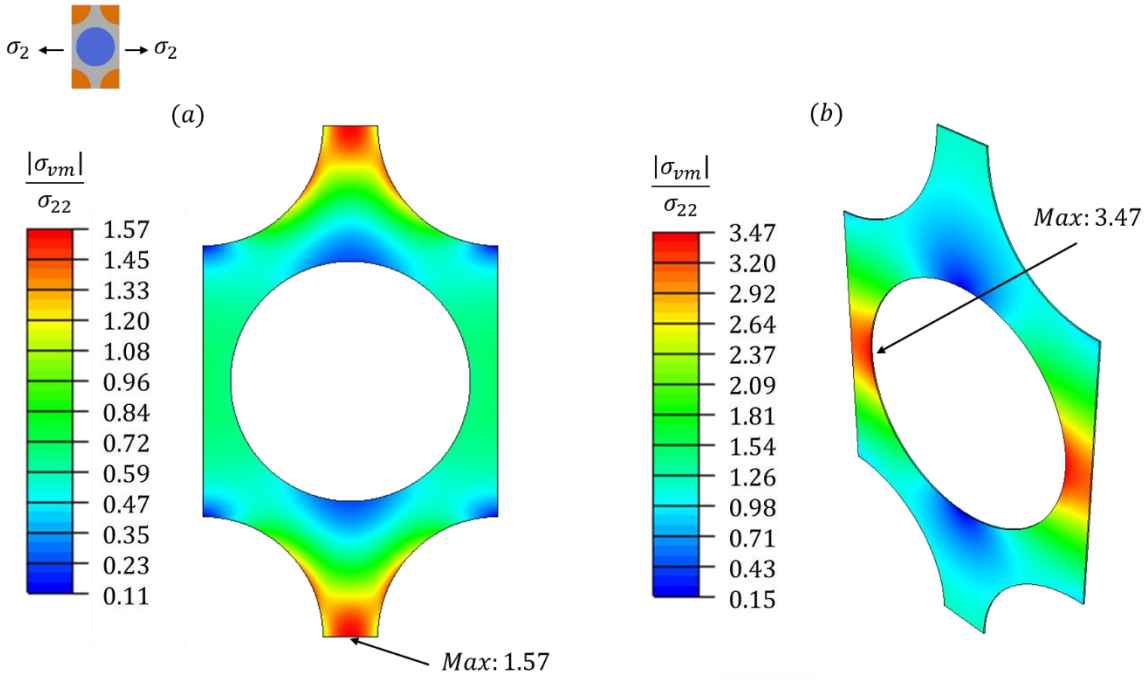

Figure 37: *Maximum local von Mises stress for (a) 2D and (b) 3D RUC of Flax/E-glass /Epoxy.*

Table 20: Fiber-hybrid Validation of Flax/E-glass/Epoxy composite.

Flax/E-glass/Epoxy					
Property	Mori-Tanaka	2D RUC	Variation (%)	3D RUC	Variation (%)
$E_1\ (GPa)$	39.876	-	-	39.91	0.09
$E_2\ (GPa)$	9.9343	10.70	7.71	10.47	5.39
$E_3\ (GPa)$	9.9343	10.70	7.71	9.85	-0.85
$G_{12}\ (GPa)$	3.8125	-	-	3.74	-1.90
$G_{13}\ (GPa)$	3.8125	-	-	3.26	-14.49
$G_{23}\ (GPa)$	3.2851	2.61	-20.55	2.61	-20.55
v_{12}	0.2645	-	-	0.29	9.64
v_{13}	0.2645	-	-	0.3	13.42
v_{23}	0.51202	0.54	5.47	0.5	-2.35

5.2.4 Discussion of Single and Fiber Hybrid for 2D and 3D RUCs

In Section 5.2.2 and Section 5.2.3, both 2D and 3D RUCs undergo validation using analytical models outlined in Section 2.5. However, an additional examination delves into the significant discrepancies observed in the transverse homogenized properties for single fiber validation, particularly regarding the ROM and ROMm models. While Chamis' models generally exhibit lower variations across most homogenized properties, there's a notable exception with the transverse Poisson's Ratio, v_{23} , necessitating further investigation. In the context of Fiber Hybrid validation, there's a stronger agreement between computational and analytical models, except for considerable variations observed in the axial shear moduli G_{12} and G_{13} for Flax/E-glass/Epoxy composites, warranting a detailed discussion.

Table 21 presents the aggregated data from single fiber validation, where we calculated the average variation across all four combinations for both the Rule of Mixture and Chamis models. This approach aims to capture the overall trend observed in the analytical models.

Table 21; Average Variation from 2D and 3D RUCs against ROM, ROMm, Chamis and Mori-Tanaka.

Average Variation (%)			
Property	ROM & ROMm (ξ=1)	Chamis	Mori-Tanaka
$E_1\ (GPa)$	0.1025	0.1025	0.09
$E_2\ (GPa)$	30.74625	6.17875	6.215
$E_3\ (GPa)$	30.74625	6.17875	4.46
$G_{12}\ (GPa)$	49.5	4.3575	1.145
$G_{13}\ (GPa)$	49.5	4.3575	7.45
$G_{23}\ (GPa)$	43.08375	2.81	11.065
v_{12}	2.19	2.19	5.765
v_{13}	2.19	2.18825	7.58
v_{23}	25.24625	24.4075	4.02

Table 21 illustrates the notable consistency among analytical models in accurately predicting the axial Young's Modulus (E_1), with variations hovering around ~0.1%. This stability arises from the shared assumption across models, where fibres and matrices are presumed to align parallelly, minimizing volatility in this property. However, due to the inadequate representation of the transverse plane in the Rule of Mixture (ROM), significant disparities emerge for E_2, E_3, G_{23}, and ν_{23}. In contrast, the Chamis model demonstrates reduced variation in these properties, owing to its utilization of a nonlinear relationship between fiber volume fraction and transversal properties. As anticipated, ROM exhibits subpar performance in computing in-plane shear moduli (G_{12} and G_{13}), attributed to the nonlinear behaviour of unidirectional laminae under high shear stress levels, particularly in materials like Carbon/Epoxy with high carbon strength. Substantial variations are evident in out-of-plane properties (G_{23} and ν_{23}), primarily due to experimental parameters where suboptimal values were selected for adjustment.

To visually depict the trends observed across all considered models, Figures 38 to 43 were generated, showcasing the nine independent homogenized properties derived. Notably, the 2D RUC model generates only four constants instead of nine, as detailed in Section 4.1. Consequently, instead of a connecting line, green triangles are employed to indicate the constants produced by the 2D RUC model.

Single fiber validation reveals that the Chamis model and Finite Element Analysis (FEA) models generate comparable contours, with slight over and underestimations. Conversely, the Rule of Mixture (ROM) values align closely with the majority of models for axial Young's Modulus but exhibit significant underestimation across transverse properties. Specifically, the ROM model underestimates all shear moduli, transverse Young's Modulus, and overestimates the transverse Poisson's ratio in comparison to the FEA models.

In the realm of composite materials, characterized by extensive microscale assumptions, the observed variations resulting from the comparison between computational and analytical models align with expectations. Notably, a robust agreement between the two is attained, affirming that the design of RUCs models effectively captures the behaviour of composite laminae with accuracy.

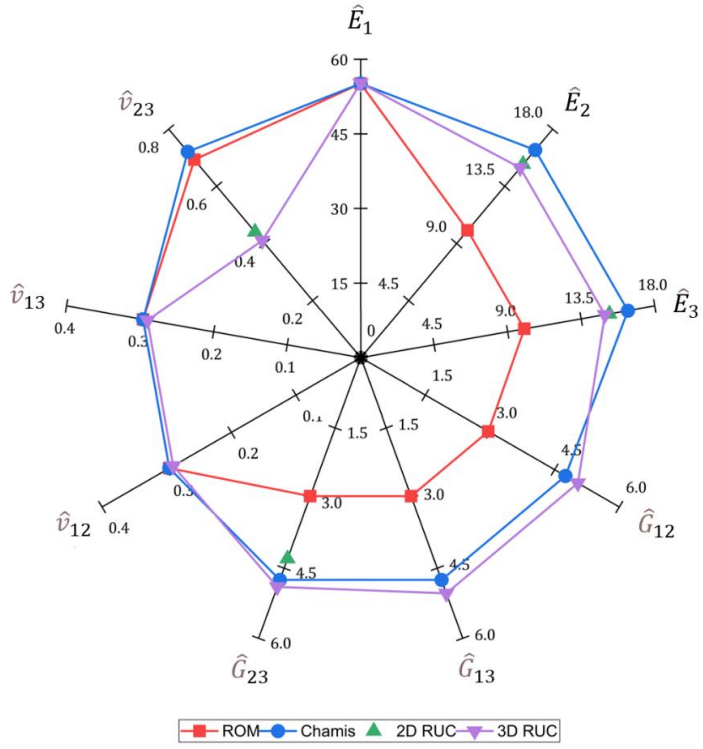

Figure 38: *Spider plot for the homogenised properties of Basalt/Epoxy for Volume fraction 0.6.*

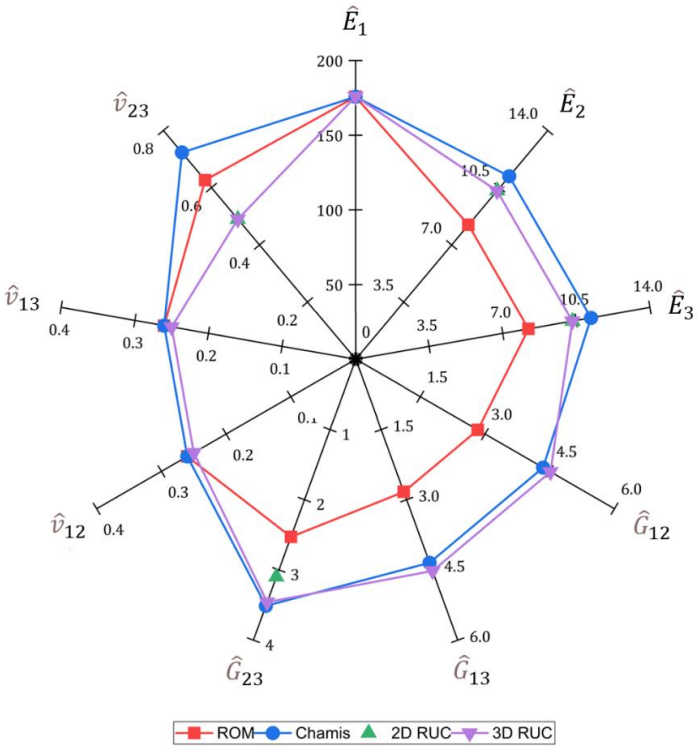

Figure 39: Spider plot for the homogenised properties of Carbon/Epoxy *for Volume fraction 0.6.*

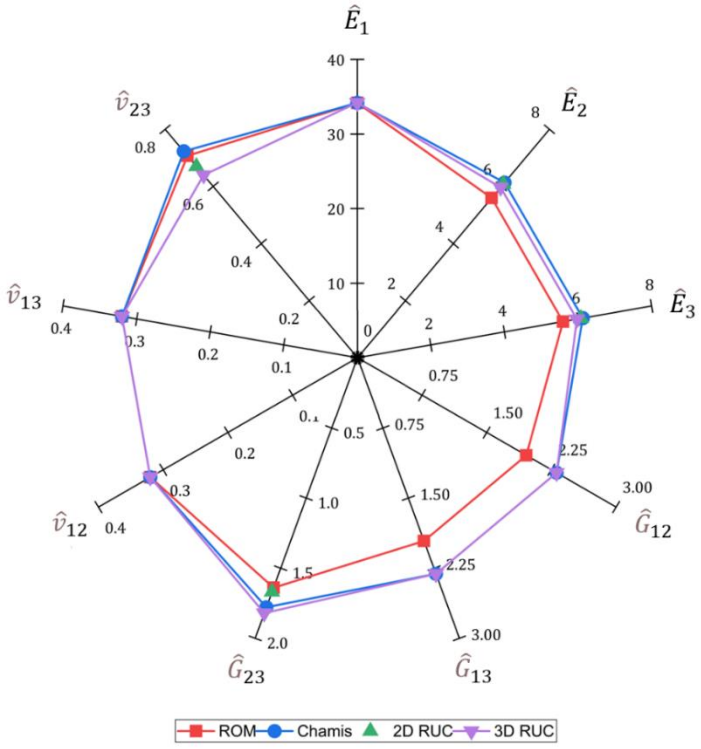

Figure 40: Spider plot of the homogenised properties of Flax/Epoxy *for Volume fraction 0.6*.

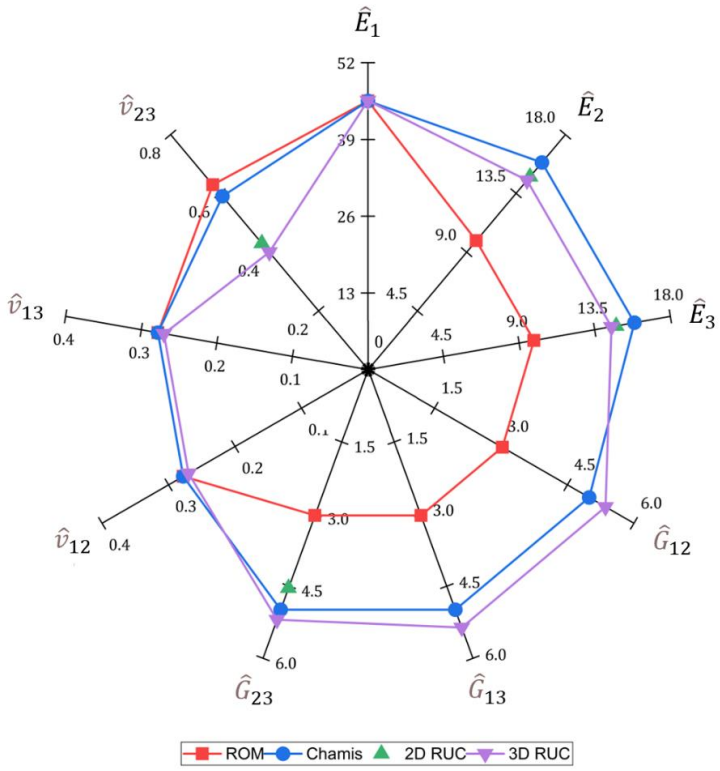

Figure 41: *Spider plot of the homogenised properties of E-glass/Epoxy* for *Volume fraction* 0.6.

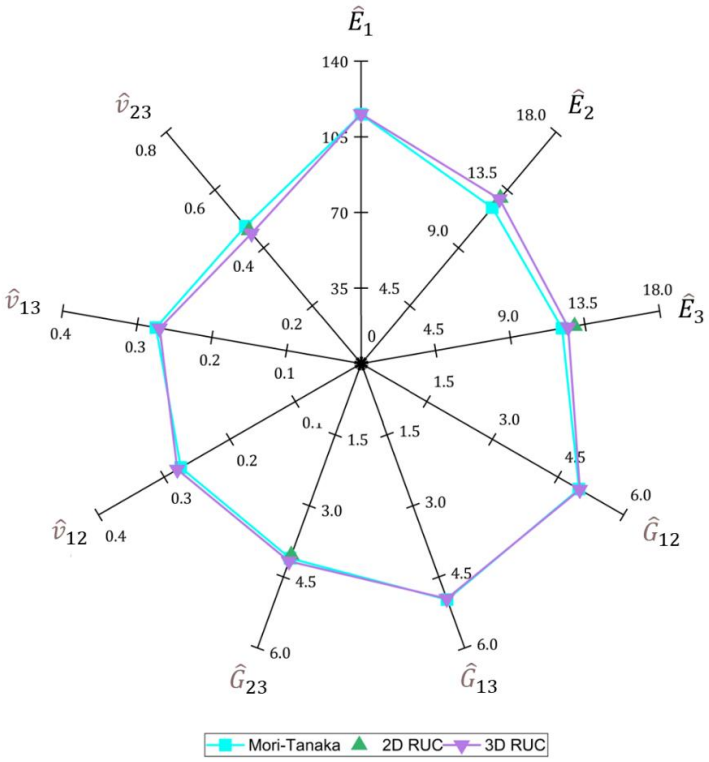

Figure 42: Spider plot of the homogenised properties of Basalt/Carbon/Epoxy *for Volume fraction 0.6.*

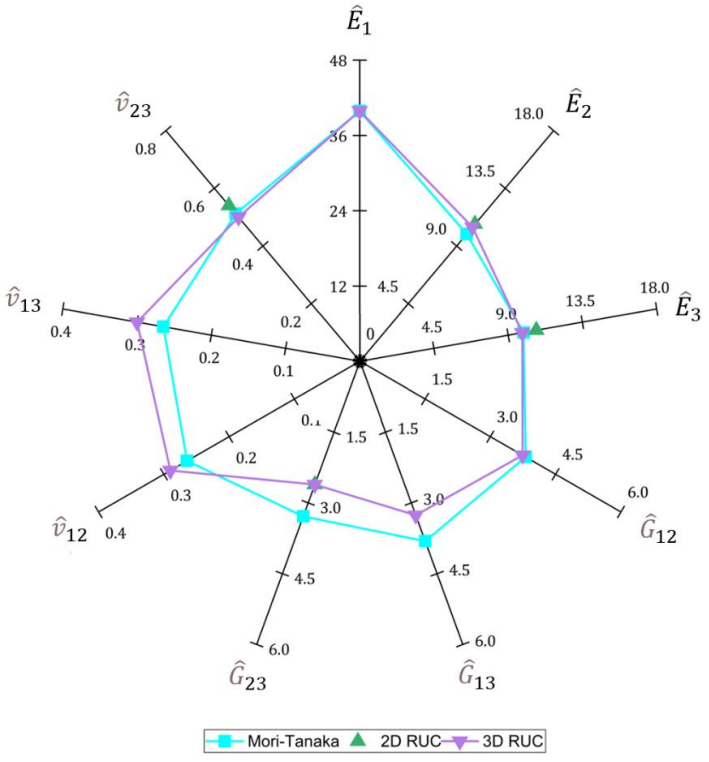

Figure 43: Spider plot of the homogenised properties of Flax/E-glass/Epoxy *for Volume fraction 0.6*.

5.3 MICRO STRESS FIELD WITHIN RUC UNDER TENSION LOADING

Figure 44: Maximum local von Mises under tension loading for composites: (a) Basalt/Carbon/Epoxy, (b) Flax/E-glass/Epoxy, (c) Basalt/E-Glass/Epoxy , and (d) Flax/Carbon/Epoxy using 2D RUC and Figure 45: Maximum local von Mises under tension loading for composites: (a) Basalt/Carbon/Epoxy, (b) E-glass/Flax/Epoxy, (c) Basalt/E-Glass/Epoxy , and (d) Carbon/Flax/Epoxy using 3D RUC shows the von Mises stress distribution under pure tension by applying macro-stress $\hat{\sigma}_2$, for all four combinations of fibre hybrid composites. The maximum stress points are shown by the arrows located in each plot.

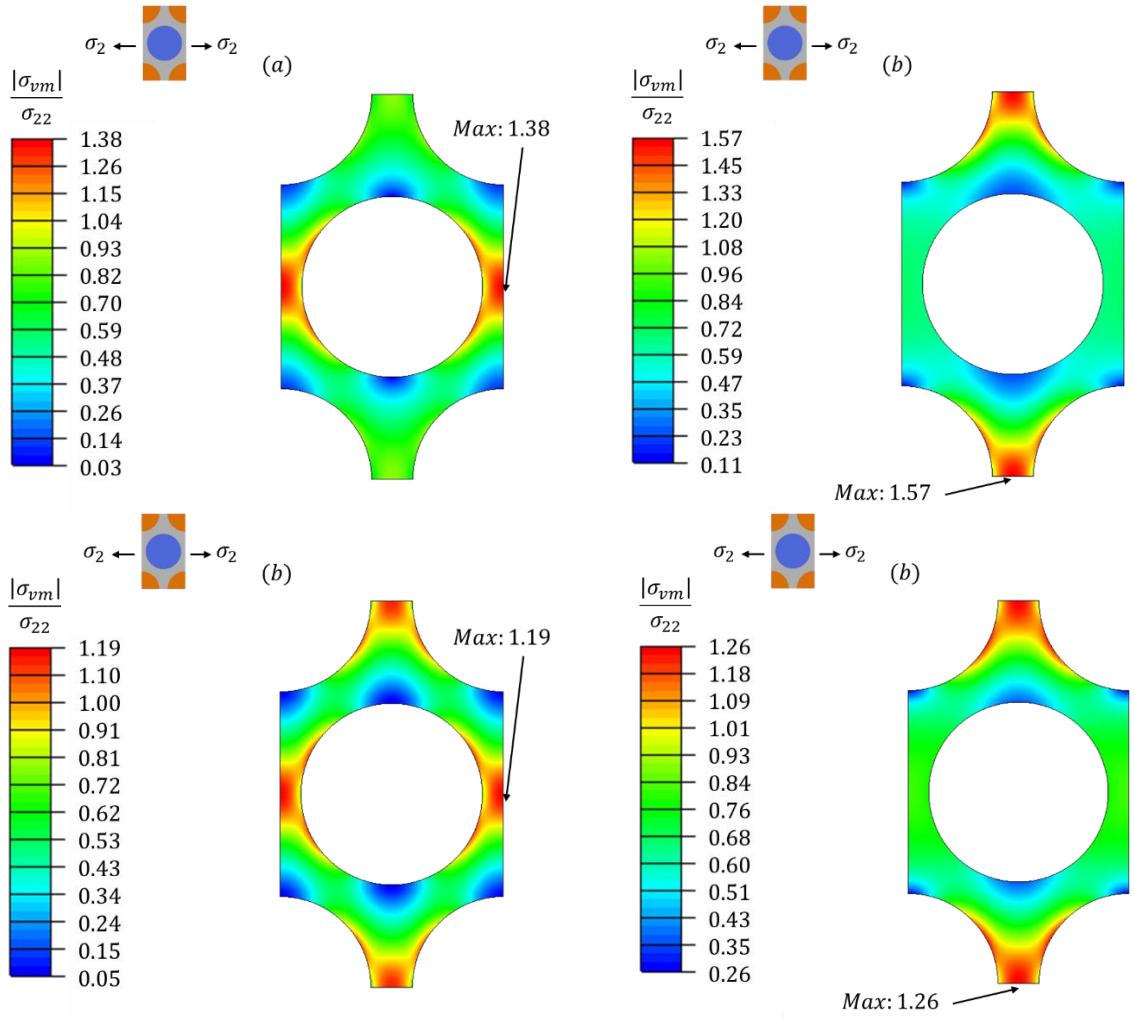

Figure 44: *Maximum local von Mises under tension loading for composites: (a) Basalt/Carbon/Epoxy, (b) Flax/E-glass/Epoxy, (c) Basalt/E-Glass/Epoxy , and (d) Flax/Carbon/Epoxy using 2D RUC.*

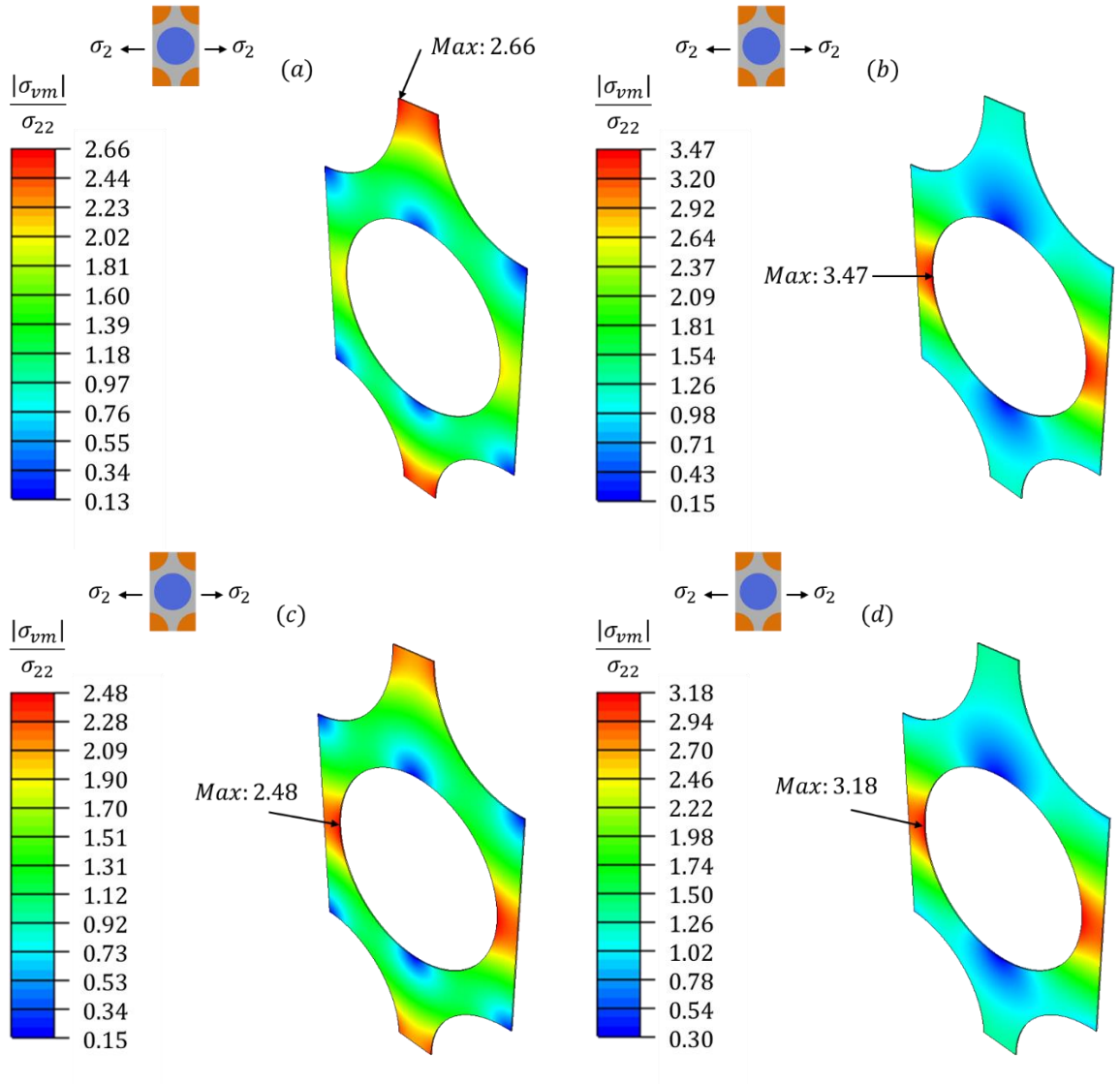

Figure 45: *Maximum local von Mises under tension loading for composites: (a) Basalt/Carbon/Epoxy, (b) E-glass/Flax/Epoxy, (c) Basalt/E-Glass/Epoxy , and (d) Carbon/Flax/Epoxy using 3D RUC.*

Table 22 provides the homogenized properties for the four combinations considered in this paper for Natural and Synthetic fiber hybrid composite laminae for the two Repeating Unit Cells considered: 2D and 3D.

Table 22: Homogenized Properties of Basalt/Carbon/Epoxy, Flax/E-glass/Epoxy, Basalt/E-Glass/Epoxy , and Flax/Carbon/Epoxy.

Homogenized Properties	$\hat{E}_1$	$\hat{E}_2$	$\hat{E}_3$	$\hat{G}_{12}$	$\hat{G}_{13}$	$\hat{G}_{23}$	$\hat{v}_{12}$	$\hat{v}_{13}$	$\hat{v}_{23}$
2D RUC									
Basalt/Carbon/ Epoxy	-	12.87	12.87	-	-	4.04	-	-	0.46
Flax/ E-glass/Epoxy	-	10.70	10.70	-	-	2.61	-	-	0.54
Basalt/ E-Glass/Epoxy	-	15.06	15.06	-	-	5.04	-	-	0.43
Flax/Carbon/ Epoxy	-	8.13	8.13	-	-	2.59	-	-	0.58
3D RUC									
Basalt/Carbon/ Epoxy	115.6	12.79	12.49	5.00	4.96	4.17	0.28	0.27	0.45
Flax/ E-glass/Epoxy	39.91	10.47	9.85	3.74	3.26	2.61	0.29	0.30	0.50
Basalt/ E-Glass/Epoxy	50.4	14.74	14.73	5.43	5.43	5.27	0.28	0.28	0.40
Flax/Carbon/ Epoxy	105.1	8.24	8.15	3.36	3.08	2.35	0.28	0.29	0.57

Similarly, Table 22 is visually added by the Spider plots Figure 46: Spider Plot for the homogenized properties of Basalt/Carbon/Epoxy, Flax/E-glass/Epoxy, Basalt/E-Glass/Epoxy, and Flax/Carbon/Epoxy using 2D RUC and Figure 47: Spider Plot for the homogenized properties of Basalt/Carbon/Epoxy, Flax/E-glass/Epoxy, Basalt/E-Glass/Epoxy , and Flax/Carbon/Epoxy using 3D RUC where the homogenized proportion for each combination, and each axis is normalized for the appropriate range of each engineering constant.

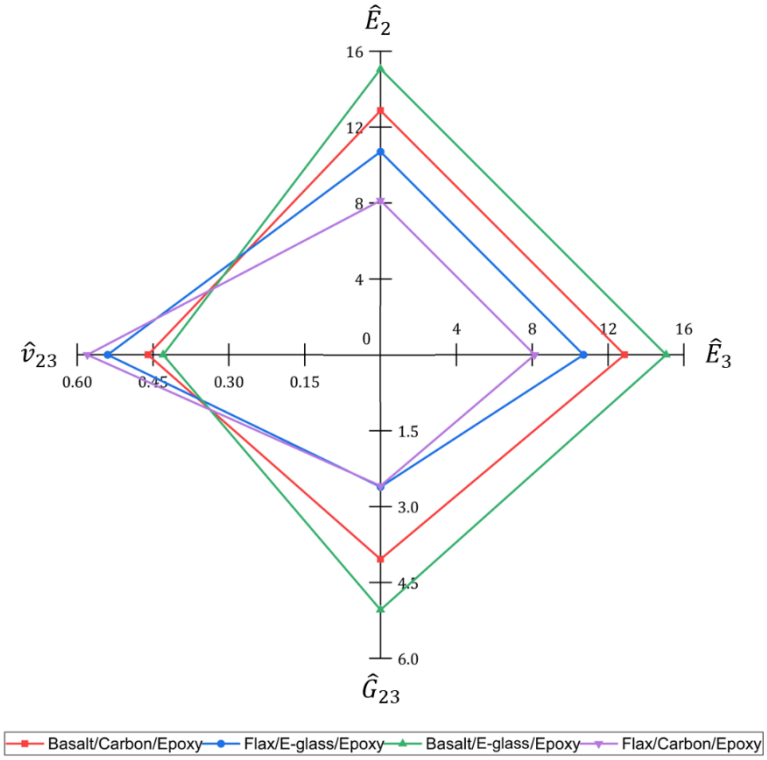

Figure 46: *Spider Plot for the homogenized properties of Basalt/Carbon/Epoxy, Flax/E-glass/Epoxy, Basalt/E-Glass/Epoxy, and Flax/Carbon/Epoxy using 2D RUC.*

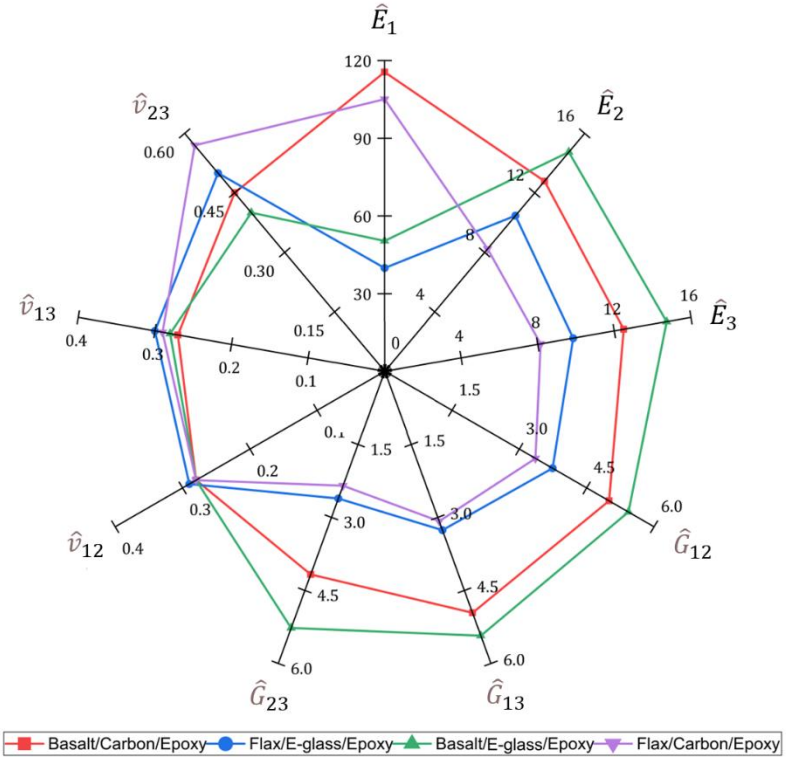

Figure 47: *Spider Plot for the homogenized properties of Basalt/Carbon/Epoxy, Flax/E-glass/Epoxy, Basalt/E-Glass/Epoxy, and Flax/Carbon/Epoxy using 3D RUC.*

5.3.1 Discussion and Conclusions

In this section, we analyse the results derived from the simulations conducted using Abaqus/Standard. We interpret how the selection of different fibres influences the von Mises stresses experienced by the matrix, which remains consistent across all simulations (i.e., Epoxy). Specifically, the locations of local maximum stresses encountered are pinpointed.

The discussion will focus on contrasting the effects of single-fiber and fiber-hybrid composites when subjected to a macro-stress, specifically in pure tension. As well as the individual capabilities of each combination of fiber-hybrid composites to others.

The disparity in local maximum von Mises stresses between the 2D representation of the transverse plane and the 3D model with thickness stems from several factors. In the simplified 2D RUC, stress concentrations at discontinuities, such as fiber-matrix interfaces, lead to localized areas of high stress, resulting in elevated von Mises stresses as shown in Figure 44. Additionally, the 2D model neglects out-of-plane effects present in the 3D model, such as bending and shear stresses, leading to an underestimation of stresses. Moreover, boundary conditions applied to the models influence stress distributions, with the 2D model restricting deformation in the out-of-plane direction due to the Boundary Condition applied, in Section 4.5. Consequently, the transition to a 3D representation with thickness allows for a more comprehensive analysis of material behaviour, facilitating a better understanding of stress distributions and potential von Mises stress concentrations. It is worth noting that von Mises stresses are used as it is particularly useful for ductile materials such as Epoxy resin, exhibiting its linear deformation prior to fracture, which is not studied in this paper.

This said, a discussion between the von Misses stresses exhibited by the matrix (i.e. Epoxy) in both single fiber and fiber-hybrid composites is conducted below.

When Basalt is paired with Carbon fibres, local von Mises stresses peak at 1.38 and 2.66 for 2D and 3D setups respectively, close to the Basalt region, as depicted in Figure 45 (a). In contrast, single fiber Carbon/Epoxy configurations register maximums of 1.05 and 2.33. This indicates that the matrix experiences higher stress levels of 31.4% and 14.1% respectively, owing to the differential load sharing among fibres. These elevated stresses are observed nearer to the fiber with the higher transversal elastic modulus (E_2),

indicating that a stiffer component offers greater resistance to deformation. For instance, near Basalt, which has an E_2 of 89 GPa compared to Carbon's 21 GPa, this difference is more than fourfold. A similar pattern is evident in Flax/Carbon/Epoxy combinations, where Flax, with an E_2 of 7 GPa (three times smaller than Carbon's), contributes to higher von Mises stresses of 20% and 36.5% in 2D and 3D respectively, compared to Carbon/Epoxy setups. These stress peaks are typically found near the Carbon fiber, as illustrated in Figure 45 (c).

Similarly, both Basalt and Flax are combined with E-glass, yielding the following results. Basalt/E-glass/Epoxy setups show a slight increase in maximum local von Mises stresses of 1.7% and 3% for 2D and 3D configurations respectively, compared to E-glass/Epoxy setups. However, with Flax, the increase is more significant, with maximum local von Mises stresses rising by 34.2% and 44.6% for 2D and 3D configurations respectively. In the case of Basalt, the higher stresses are typically located near the Basalt due to a 1.2 times greater increase in E_2 compared to E-glass. Conversely, for Flax setups, the highest stresses occur near the E-glass because E-glass has a transversal elastic modulus several times higher than that of Flax. It's important to note that the increase in stresses for Basalt/E-glass/Epoxy setups is relatively small, mainly due to the minor difference in transversal elastic modulus (E_2) between Basalt and E-glass. On the other hand, Flax/E-glass setups experience a more substantial increase in stresses, primarily because of the significant differences between their E_2 values.

As all combinations are compared, a discussion about each homogenized property and the trends captured from the combinations is provided below.

- Axial Elastic Modulus ($\hat{E}_1$):

The combinations with carbon fibres achieved the highest axial Young's modulus ($\hat{E}_1$). Carbon fibers are known for their exceptionally high stiffness and strength, contributing significantly to the overall stiffness of the composite across the axial plane.

The high modulus of carbon fibres results in stiffening the composite along the axial direction, leading to higher values of $\hat{E}_1$ of 115.6 and 105.1 GPa when combined with Basalt and Flax respectively. When compared to single fiber composites Basalt/Epoxy and Flax/Epoxy an improvement in $\hat{E}_1$ of 109.4% and 208.5% is visible, respectively.

As for E-glass, its fibres are known for their moderate stiffness and are typically not as stiff as carbon fibre. Thus, composites containing E-glass fibres exhibited lower axial Young's modulus values of 39.91 and 50.4 GPa when combined with Flax and Basalt, respectively. This said, an improvement from single fiber E-glass/Epoxy is capture when the use of basalt fibres is used for hybridization, of 10.6%. Whereas a reduced in transversal of Young's modulus by 14.2% is visible when combined with Flax.

- Transversal Young's Modulus ($\hat{E}_2$, $\hat{E}_3$):

Basalt combinations also scored better properties for transversal Young's modulus ($\hat{E}_2$, $\hat{E}_3$), with values of 12.79 and 12.49 GPa for $\hat{E}_2$ and $\hat{E}_3$ respectively when combined with Carbon fibres, and 14.74 and 14.73 for $\hat{E}_2$ and $\hat{E}_3$ respectively when combined with E-glass. Basalt fibres contribute to the overall stiffness of the composite in the transverse direction when compared to a single fiber E-glass/Epoxy composite, scoring 14.5 GPa for both E_2 and E_3, thus a slight improvement of 1.5% percent.

The higher transversal Young's modulus values in basalt combinations reflect the enhanced stiffness and rigidity of the composite in directions perpendicular to the fiber orientation.

Similar to the axial Young's modulus, the low scoring of flax combinations in transverse Young's modulus ($\hat{E}_2$, $\hat{E}_3$) can be attributed to the lower stiffness of flax fibres compared to carbon and basalt fibres. Flax fibres are less effective in resisting breakage in the transverse direction, resulting in lower transverse Young's modulus values.

- Transverse Poisson's Ratio ($\hat{v}_{23}$):

The combinations with flax fibres scored the highest transverse Poisson's ratio ($\hat{v}_{23}$). Flax fibers typically have a higher transversal Poisson ratio compared to carbon or basalt fibres as shown in table 6, where Flax has 0.75 and Carbon 0.49.

Flax fibres possess intrinsic flexibility and compliance, allowing them to accommodate transverse deformations more effectively, and thus expand, resulting in a higher transverse Poisson ratio. Improving single fiber Carbon/Epoxy by 16.3% when Flax is introduced for hybridization.

Basalt combinations scoring the lowest transversal Poisson's ratios suggesting a potential lack of deformation in these materials. Basalt fibres are isotropic, and in

addition to this, they offer excellent strength and stiffness properties, scoring low deformation across both its axial and transversal plane, and thus, influencing in this way to the fiber-hybrid composites where it is introduced. When it comes to the transverse deformation, E-glass/Epoxy and Basalt/E-glass/Epoxy remain with the same Poisson's ratio of 0.40, while in comparison to Carbon/Epoxy, Basalt/Carbon/Epoxy produces a less deformable material with a reduction of 8.8%.

- Axial Poisson's Ratio ($\hat{v}_{12}$, $\hat{v}_{13}$):

Flax combinations achieved a slight advantage in axial Poisson's ratio. This is attributed to the natural compliance and flexibility of Flax fibres as mentioned above, allowing them to undergo greater deformation in response to axial loading, which can eventually work as bridging elements if fracture occurs. Flax shows improvement to Carbon and E-glass single fiber composites of 16% and 7.4% respectively.

The slight advantage of flax combinations in axial Poisson's ratio suggests a higher degree of axial compressibility compared to Carbon or Basalt combinations.

Basalt combinations scoring the lowest Poisson's ratios (both axial and transverse) suggests a potential lack of transverse isotropy in these materials. This said, Basalt is keener to deformation in the axial plane than Carbon and E-glass still improving its deformation when Carbon/Epoxy and E-glass/Epoxy are considered, by 12% and 3.7% respectively.

- Axial and Transverse Shear Modulus ($\hat{G}_{12}$, $\hat{G}_{13}$, $\hat{G}_{23}$):

Basalt combinations exhibited better properties for both axial and transversal shear modulus ($\hat{G}_{12}$, $\hat{G}_{13}$, and $\hat{G}_{23}$). Basalt fibres have excellent shear resistance and interfacial bonding with the epoxy matrix.

The higher shear modulus values in basalt combinations indicate greater resistance to shear deformation, resulting in improved structural stability and stiffness in both axial and transverse directions. Moreover, when combined with Carbon fibres an improve of 10.6%, 9.7% and 20.5% is captured for $\hat{G}_{12}$, $\hat{G}_{13}$, and $\hat{G}_{23}$ respectively. Similarly, when combined with E-glass an improvement of 1.3%, 1.3% and 1.3% is visible for $\hat{G}_{12}$, $\hat{G}_{13}$, and $\hat{G}_{23}$ respectively, to their single fiber counterparts.

Flax combinations scoring the lowest shear modulus (both axial and transverse) is consistent with the lower stiffness of flax fibres compared to Carbon and Basalt fibres, scoring reductions of 25.7%, 31.9% and 32% for $\hat{G}_{12}$, $\hat{G}_{13}$, and $\hat{G}_{23}$ respectively against the single fiber Carbon/Epoxy and 30.2%, 39.2% and 49.8% for $\hat{G}_{12}$, $\hat{G}_{13}$, and $\hat{G}_{23}$ respectively against the single fiber E-glass/Epoxy. Shear modulus is related to the material's resistance to deformation under shear stress, and the lower stiffness of Flax fibres contributes to lower shear modulus values in the composite.

The observed trends can be attributed to the inherent properties of each constituent material and their interactions within the composite structure. Carbon fibres provide high stiffness and strength, Flax fibres offer flexibility and compliance, Basalt fibres contribute to shear resistance and stiffness and E-glass a moderate stiffness. The combination of these materials in different configurations leads to variations in mechanical properties, highlighting the importance of material selection and composite design in achieving desired performance characteristics. Additionally, the presence of multiple fiber types in each combination may lead to complex interactions, resulting in unique mechanical behaviour such as anisotropy (i.e. Flax/Carbon/Epoxy) or isotropy (i.e. Basalt/E-glass/Epoxy) depending on the specific arrangement and orientation of fibres within the composite structure.

6 CONCLUSIONS AND FURTHER RESEARCH

6.1 CONCLUSIONS

The comparative analysis of transverse and axial elastic lamina constants, conducted through computational models 2D and 3D Repeating Unit Cells capable of generating the intra-laminar fiber hybrid unidirectional composite laminae, and analytical models such as Rule of Mixture, modified Rule of Mixture, Chamis, and Mori-Tanaka, demonstrates a robust agreement between computational and analytical methodologies. This alignment underscores the reliability and accuracy of both approaches in predicting the transverse behaviour of fiber hybrid composites, and more importantly the reliability of the models created for this paper.

This study sheds light on the behaviour of fibre hybrid composites with Fibre Volume fraction of 60% ($V_f = 0.60$), showcasing the advantages of incorporating

environmentally friendly fibres alongside synthetic ones and highlighting their performance capabilities of the following composites: Basalt/Carbon/Epoxy, Flax/E-glass/Epoxy, Basalt/E-glass/Epoxy, and Flax/Carbon/Epoxy. By demonstrating the potential for enhanced structural applications during pure tension, this research expands our understanding of utilizing natural fibres in composite materials.

When comparing homogenized properties, the introduction of natural fibres in hybridization with commonly used synthetic fibres reveals both improvements and reductions. Basalt fibres exhibit a consistent increase in composite stiffness ($\hat{E}_1$, $\hat{E}_2$ and $\hat{E}_3$), deformation reduction ($\hat{v}_{12}$, $\hat{v}_{12}$ and $\hat{v}_{23}$) and improved shear resistance ($\hat{G}_{12}$, $\hat{G}_{13}$, and $\hat{G}_{23}$).

While flax fibres, known for their deformable and 'ropey' nature, provide enhancements in the deformation across the axial and transverse Poisson's ratios ($\hat{v}_{12}$, $\hat{v}_{12}$ and $\hat{v}_{23}$), while significantly decreasing the material stiffness ($\hat{E}_1$, $\hat{E}_2$ and $\hat{E}_3$) and shear resistance ($\hat{G}_{12}$, $\hat{G}_{13}$, and $\hat{G}_{23}$) across its two combinations when compared to the single fibre of its partnered constituents.

Considering the advantages and disadvantages of each fibre type, the combinations presented in this study offer attractive prospects for a wide range of applications across various sectors. The conglomerate of combinations utilizing both natural and synthetic fibres in fiber hybrid reinforced polymer composites showcases diverse mechanical properties, encouraging discussions on their capabilities and stimulating ideas for potential applications. From energy absorption to thermal, electrical, and acoustic insulation, as well as high or low deformability applications, presenting promising opportunities for innovation and advancement in composite materials technology.

6.2 LIMITATIONS

The simplification of volume fraction constraints for fibres and matrix materials, although necessary for computational modelling, assumes uniform distribution and perfect bonding, potentially neglecting real-world variability and interface complexities. Similarly, the assumption of homogeneous fibres and matrix materials simplifies analysis but may overlook variations in material properties arising from manufacturing processes, impurities, or inhomogeneities. Moreover, ignoring potential hollowness and defects within fibres leads to an oversimplified representation of the composite's

mechanical behaviour, overlooking factors crucial for stiffness and strength. Additionally, the limited material selection, while encompassing materials like flax, basalt, carbon, and E-glass fibres with an epoxy matrix, may restrict the generalizability of findings to a broader range of fiber-hybrid composites. Recognizing that Repeating Unit Cells may not fully capture composite behaviour compared to more complex representative volumes is pivotal. Discussing discrepancies and limitations between unit cells and representative volume elements (RVEs) would bolster the dissertation's rigor. Furthermore, acknowledging the simplifying assumptions about continuous, defect-free, cylindrical fibres with perfect interphase bonding is essential, as they may oversimplify the real-world complexities of fiber-hybrid composites, affecting the accuracy and applicability of findings. Addressing modelling limitations inherent in finite element analysis, such as mesh dependency, convergence issues, and numerical artifacts, is crucial for result interpretation. Moreover, navigating the complex interactions between fibres, matrix, and interphase presents interpretation challenges, underscoring the importance of discussing both experimental and computational results within this context to glean valuable insights. Additionally, reliance on analytical models, while beneficial, comes with inherent errors. Therefore, incorporating experimental data for validation could enhance the accuracy of Finite Element Analysis (FEA) models, ensuring they faithfully represent the discussed composites. This integration of experimental validation would further bolster confidence in the FEA models, validating their ability to accurately capture the behaviour of the composite materials under consideration.

6.3 FURTHER RESEARCH

Basalt is a sustainable raw material sourced from volcanic stone, known for its fire resilience, high durability, dimensional stability, and resistance against moisture. Basalt reinforced bars, crafted from high-strength basalt fiber and epoxy resin through spinning, winding, surface coating, and compound molding, offer a novel building material characterized by exceptional strength, excellent acid and alkali resistance, and long-lasting durability.

When combined with carbon fibres, a multitude of potential applications emerge, particularly in aerospace components where the combination's high stiffness, strength, and thermal stability are highly desirable. Similarly, in automotive parts manufacturing,

the amalgamation of basalt and carbon fibres enables the production of lightweight yet robust components, thereby enhancing fuel efficiency and crash safety performance.

For infrastructure and construction projects, the corrosion resistance and durability inherent in basalt composites make them ideal for structural reinforcement applications. Similarly, Basalt/E-glass/Epoxy composites offer advantages in automotive components, leveraging their thermal stability, impact resistance, and lightweight structure to improve vehicle performance and safety.

In the case of Flax/E-glass/Epoxy composites, the combination excels in providing electrical, thermal, and acoustic insulation, with synergistic mechanical properties. While the high stiffness and strength of E-glass fibres contribute to structural integrity, the toughness and energy absorption capabilities of flax fibres enhance overall performance.

The Flax/Carbon combination presents intriguing possibilities for the automotive industry, with flax fibres offering high elongation at break and superior energy absorption compared to carbon fibres. This combination can act as a crack arrester or bridging element, preventing crack propagation and shattering. Moreover, flax's lower density compared to carbon reduces weight, thereby enhancing fuel efficiency.

It's noteworthy that both Basalt and Flax fibres can be harvested sustainably, supporting circular manufacturing practices. However, further research is needed to understand the energy requirements for fiber production and ensure sustainable sourcing practices. Additionally, the lower cost of natural fibres like flax, sourced from renewable plants, compared to carbon fibres derived from complex and energy-intensive processes, makes them an attractive option for composite manufacturing.

In terms of simulations, studying fracture behaviour and thermal expansion in these combinations is crucial for assessing their capabilities in real-world industrial applications. Understanding fracture mechanics will provide insights into the performance and durability of hybrid composites, informing design and manufacturing processes for optimal results. A broader spectrum of fibre volume fractions is sought, encompassing both the overall fibre volume fraction of the fibres based on commonly used values ($0.30 < V_f < 0.70$), and the ability to adjust the volume fraction of each individual fiber type, such as Fiber1 and Fiber2 (For example: $V_f = 0.60$; $V_{f1} = 0.25$, $V_{f2} = 0.35$). Regarding the modelling approach, improvement could be made by replacing

RUCs by RVEs, or including eccentricities withing the RUC, in order to ‘represent’ the randomness of real composites.

REFERENCES

1. Aboudi, J., Arnold, S. M., & Bednarcyk, B. A. (2013). *Chapter 3 - Fundamentals of the Mechanics of Multiphase Materials*. Butterworth-Heinemann. https://doi.org/10.1016/B978-0-12-397035-0.00003-3
2. Aboudi, J., Arnold, S. M., & Bednarcyk, B. A. (2021). *Practical Micromechanics of Composite Materials*. Elsevier Science. https://books.google.co.uk/books?id=ADYXEAAAQBAJ
3. Al-Ostaz, A. and Cai, L. (2014) Applying Periodic Boundary Conditions in Finite Element Analysis, *iMechanica*, 1-13. https://imechanica.org/fites/pbc.pdf.
4. Banerjee, S., & Sankar, B. V. (2014). Mechanical properties of hybrid composites using finite element method based micromechanics. *Composites Part B: Engineering*, *58*, 318–327. https://doi.org/10.1016/j.compositesb.2013.10.065
5. Bednarcyk, B. A., & Arnold, S. M. (2003). Micromechanics-Based Modeling of Woven Polymer Matrix Composites. *AIAA Journal*, *41*(9), 1788–1796. https://doi.org/10.2514/2.7297
6. Bakhvalov, N.S., Panasenko, G.P., 1984. Homogenization in Periodic Media, Mathematical Problems of the Mechanics of Composite Materials.
7. Benssousan, A., Lions, J.L., Papanicoulau, G. (1978). Asymptotic Analysis for Periodic Structures.
8. Chawla, K. K. (2012). *Composite Materials: Science and Engineering*. Springer New York. https://books.google.co.uk/books?id=rbuNxwzM27cC
9. Clyne, T. W., & Hull, D. (2019). *An Introduction to Composite Materials*. Cambridge University Press. https://books.google.co.uk/books?id=4oKWDwAAQBAJ
10. D'Mello, R. J., & Waas, A. M. (2019). Influence of Unit Cell Size and Fiber Packing on the Transverse Tensile Response of Fiber Reinforced Composites. *Materials*, *12*(16). https://doi.org/10.3390/ma12162565
11. Dvorak, G. (2012). *Micromechanics of Composite Materials*. Springer Netherlands. https://books.google.co.uk/books?id=9m96aIdLwKQC
12. Katnam, K. B., Dalfi, H., & Potluri, P. (2019). Towards balancing in-plane mechanical properties and impact damage tolerance of composite laminates using quasi-UD woven fabrics with hybrid warp yarns. *Composite Structures*, *225*, 111083. https://doi.org/10.1016/j.compstruct.2019.111083

13. Li, S. (2001). General unit cells for micromechanical analyses of unidirectional composites. *Composites Part A: Applied Science and Manufacturing*, *32*(6), 815–826. https://doi.org/10.1016/S1359-835X(00)00182-2
14. Mohammed, M., Oleiwi, J. K., Mohammed, A. M., Jawad, A. J. M., Osman, A. F., Adam, T., Betar, B. O., Gopinath, S. C. B., Dahham, O. S., & Jaafar, M. (2023). Comprehensive insights on mechanical attributes of natural-synthetic fibres in polymer composites. *Journal of Materials Research and Technology*, *25*, 4960–4988. https://doi.org/10.1016/j.jmrt.2023.06.148
15. Natali, A., Manzi, S., & Bignozzi, M. C. (2011). Novel fiber-reinforced composite materials based on sustainable geopolymer matrix. *Procedia Engineering*, *21*, 1124–1131. https://doi.org/10.1016/j.proeng.2011.11.2120
16. Needleman, A., Tvergaard, V. (1993). Comparison of crystal plasticity and isotropic hardening predictions for metal-matrix composites. *ASME Journal of Applied Mechanics 60,* 70–76.
17. Sanchez-Palencia, E. (1980). Non-homogeneous Media and Vibration Theory. In: Lecture Notes in Physics, vol. 127. *Springer Verlag*, *Berlin.*
18. Sun, C.T., Vaidya, R.S. (1996). Prediction of composite properties from a representative volume element. *Composite Science and Technology 56*, 171–179.
19. Suquet, P. (1987). Elements of homogenization theory for inelastic solid mechanics. In: Sanchez-Palencia, E., Zaoui, A. (Eds.), *Homogenization Techniques for Composite Media. Springer-Verlag, Berlin,* 194–275.
20. Swolfs, Y., Gorbatikh, L., & Verpoest, I. (2014). Fibre hybridisation in polymer composites: A review. *Composites Part A: Applied Science and Manufacturing*, *67*, 181–200. https://doi.org/10.1016/j.compositesa.2014.08.027
21. Vignoli, L. L., Savi, M. A., Pacheco, P. M. C. L., & Kalamkarov, A. L. (2019). Comparative analysis of micromechanical models for the elastic composite laminae. *Composites Part B: Engineering*, *174*, 106961. https://doi.org/10.1016/j.compositesb.2019.106961
22. Wriggers, P., & Hain, M. (2007). Micro-Meso-Macro Modelling of Composite Materials. In E. Oñate & R. Owen (Eds.), *Computational Plasticity* (pp. 105–122). Springer Netherlands. https://doi.org/10.1007/978-1-4020-6577-4_7
23. Xia, Z., Zhang, Y., & Ellyin, F. (2003). A unified periodical boundary conditions for representative volume elements of composites and applications. *International*

Journal of Solids and Structures, *40*(8), 1907–1921. https://doi.org/10.1016/S0020-7683(03)00024-6

24. Xia, Z., Zhou, C., Yong, Q., & Wang, X. (2006). On selection of repeated unit cell model and application of unified periodic boundary conditions in micro-mechanical analysis of composites. *International Journal of Solids and Structures*, *43*(2), 266–278. https://doi.org/10.1016/j.ijsolstr.2005.03.055
25. Yang, Y., Boom, R., Irion, B., Heerden, D.-J. van, Kuiper, P., & Wit, H. de. (2012). Recycling of composite materials. *Chemical Engineering and Processing: Process Intensification*, *51*, 53–68. https://doi.org/10.1016/j.cep.2011.09.007
26. Daniel, I. M., & Ishai, O. (2006). *Engineering Mechanics of Composite Materials*. (Second ed.) Oxford University Press.
27. X. Su, Z. Yang, G. Liu, "Finite Element Modelling of Complex 3D Static and Dynamic Crack Propagation by Embedding Cohesive Elements in Abaqus", Acta Mechanica Solida Sinica, Volume T, Issue 3, 2010, Pages 271-282, ISSN 0894-9166, https://doi.org/10.1016/S0894-9166(10)60030-4.
28. ZienkiEWicz, O.C. and Taylor, R.L., The finite element method.McGraw-Hill Book Company (1989).
29. Sádaba, S., Herráez, M., Naya, F., González, C., Llorca, J., Lopes, C.S.: Special-purpose elements to impose Periodic Boundary Conditions for multiscale computational homogenization of composite materials with the explicit Finite Element Method. Composite Structures. 208, 434–441 (2019).
30. Okereke, M.I., Akpoyomare, A.I.: A virtual framework for prediction of full-field elastic response of unidirectional composites. Computational Materials Science. 70, 82–99 (2013). https://doi.org/10.1016/j.commatsci.2012.12.036

APPENDIX A: PROJECT MANAGEMENT

INITIAL PROJECT GANTT CHART

		Sem 1												Sem 2											
Wp0	**PM**	**W1**	**W2**	**W3**	**W4**	**W5**	**W6**	**W7**	**W8**	**W9**	**W10**	**W11**	**W12**	**W1**	**W2**	**W3**	**W4**	**W5**	**W6**	**W7**	**W8**	**W9**	**W10**	**W11**	**W12**
0.1	Weekly Meeting	0.5	0.5	0.5	0.5	0.5	0.5	0.5	0.5	0.5	0.5	0.5	0.5	0.5	0.5	0.5	0.5	0.5	0.5	0.5	0.5	0.5	0.5	0.5	0.5
Wp1	**Preliminar Research**																								
1.1	Literature Review																								
1.2	Background Research																								
1.3	Identify Gaps																								
Wp2	**Build Model of Composites**																								
2.1	Unsupervised Learning																								
2.2	Composite model creation																								
2.3	Testing and Results																								
2.4	Graphing and Comparing																								
Wp3	**Analysis**																								
3.1	Data Analysis																								
3.2	Overall Analysis																								
Wp4	**Reporting / Deliverables**																								
4.1	Aims and objectives		Fri-6pm																						
4.2	Project proposal							Mon-6pm																	
4.3	Poster																								
4.4	Dissertation																								
Actual resource remaining (hours)		7.5	7.5	7.5	7.5	7.5	7.5	7.5	7.5	7.5	7.5	7.5	7.5	11.5	11.5	11.5	11.5	11.5	11.5	13.5	13.5	13.5	11.5	11.5	11.5	0
Resource Budget (hours)		8	8	8	8	8	8	8	8	8	8	8	8	12	12	12	12	12	12	14	14	14	12	12	12	0

INITIAL PROJECT GANTT CHART: INITIAL PLAN AND REFLECTIONS

INITIAL PLAN

As mentioned in the project's title, my individual project will be focused on the microscale of the fibre-hybrid reinforced polymer composites. This is a computational-driven project. Therefore, knowledge in certain software and programmes will be required. Moreover, ABAQUS will be utilized for modelling and testing of such fibre-hybrid composites, followed by a complimentary programming language such as Python, to handle, collect and plot extensive data. Therefore, unsupervised learning regarding the software of choice will be required. Parallel, literature review and background research will be expected to identify gaps regarding fibre-hybrid reinforced polymer composites and locate a focus of interest. After discussing with supervisor Kali Katnam, demonstrating general knowledge of the micromechanics of such composites is as desired as filling gaps in the research community to achieve a feasible final report. Enumerating the initial **objectives** follows:

1. Describe the structure of the composites to introduce the micro-scale of such.
2. Analyse the behaviour of the composites when transverse tensile, compressive and shear stress is applied to both individual fibres and conglomerates of fibre and polymer such as residual stress shrinkage.
3. Compare the behaviour of the composites when different volume fraction of different fibres is used like stiffness strength.
4. Locate limitations of each composite, individual fibres, and polymers.
5. Identify manufacturing defects/limits such as porosity and change in temperature for different fibre-hybrid composites.

To have a better understanding of the approach of the project, the following **questions** will complement the objectives and description of the report:

1. What are the gaps within the studies related to the micromechanics of fibre-hybrid reinforced polymer composites?
2. What are the uses of such composites, what combinations of different fibres have been used and which ones have stayed undiscovered or untested?

3. What are the limitations of currently used composites and what could be the limitations of undiscovered composites?
4. What are the limitations during the manufacturing of such composites?

it is worth remarking that previous objectives/questions have been described from a weak base of understanding of the topic, and objectives and questions might be subjected to change as the weeks progresses and either advise from my supervisor reaches myself, information 'gaps' are identified and/or crucial information is missing or if the project lacks depth.

REFLECTIONS

The initial Project Gantt Chart was swiftly created in the early weeks of Semester 1 to establish a framework for future iterations. However, due to the limited understanding of both the project and the semester's activities and assessments, the divisions and sub-divisions of tasks appear vague and ambiguous. The project's tasks are broadly categorized into four sections:

- Weekly Meetings: A standard 30-minute weekly meeting was set up initially, subject to adjustments as workload and schedules evolve throughout the academic year. The aim was to maintain records of these meetings over time.
- Composite Modeling: There was a basic grasp of Modeling using Abaqus Standard and Python Scripts, resulting in a somewhat vague breakdown of tasks necessary for completing the Modeling of composites.
- Analysis: Similarly, due to the unfamiliarity with FEA Software and Modeling composite materials, there's a lack of detailed steps for completing the analysis.
- Reporting/Deliverables: The deadlines provided by the 'Individual Project' module coordinators were incorporated as the final section of the Gantt chart, outlining the project's deliverables.

Overall, while the initial representation of time and project management is lacking in specificity, it serves as a starting point for continuous improvement as I immerses themselves in the academic year 2023-2024.

PROPOSAL GANTT CHART

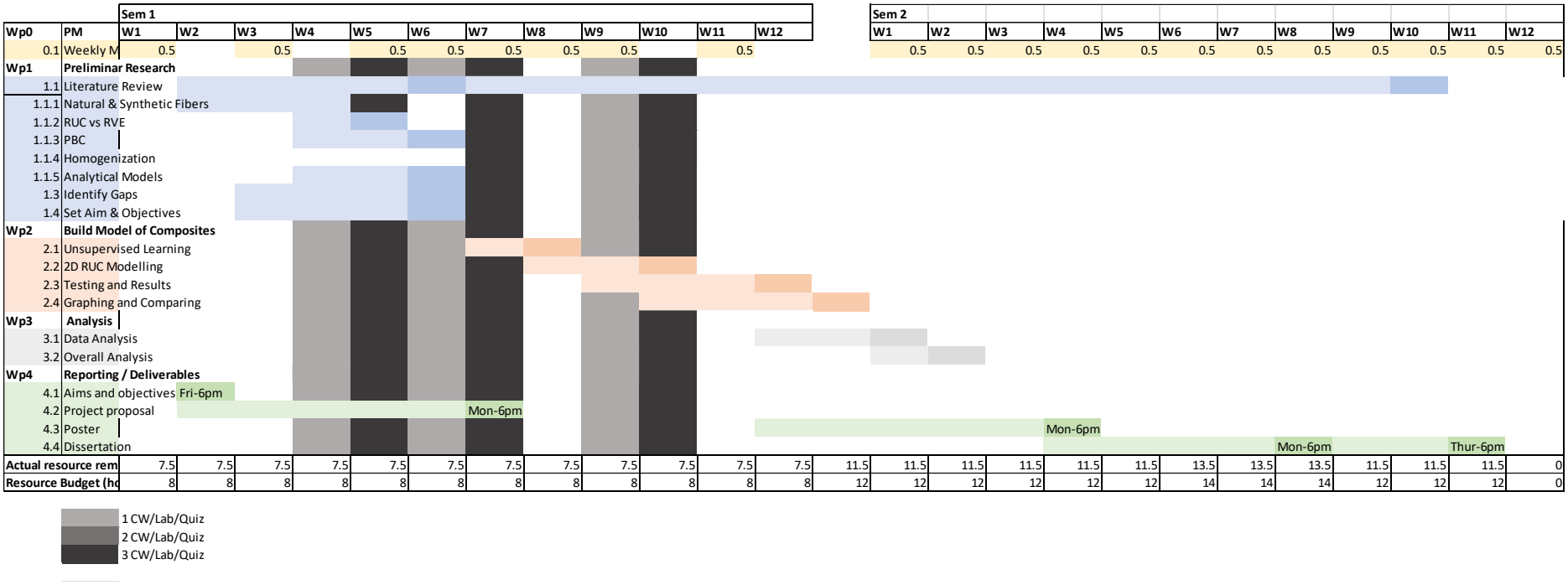

PROPOSAL GANTT CHART: REFLECTIONS

As time progressed, the coursework deadlines for Semester 1 were finalized and communicated to students, providing valuable insights into the expected workload throughout the semester. This allowed us to plan effectively, considering the evaluations that were part of the planning process. Additionally, deeper learning about the dissertation unfolded, offering not only a better grasp of the project's structure but also highlighting the most challenging areas within it.

Changes:

- Wp1:
    - Literature Review: Working for the proposal submission, an almost complete literature was tried to be achieved, thus, the newer 'Literature Review' intends to show the subdivision within it for its completion, containing all the topics I should delve into for a better understanding of the project's development.

Version: Proposal	
1.1	Literature Review
1.1.1	Natural & Synthetic Fibers
1.1.2	RUC vs RVE
1.1.3	PBC
1.1.4	Homogenization
1.1.5	Analytical Models
1.3	Identify Gaps
1.4	Set Aim & Objectives

Version: Initial	
1.1	Literature Review
1.2	Background Research
1.3	Identify Gaps

    - Setting Aim & Objectives: The project plan and the milestone for completion were clearly articulated in the Aims & Objectives section of the Proposal report submitted in W7. This laid the groundwork for both the Methodology and Results & Discussion sections.
- Wp2: 2D RUC Modeling: Following discussions with PhD student Giuseppe Romano and supervisor Kali-Babu Katnam and gaining insights into different approaches for modelling composite microstructures, particularly RUCs and/or RVEs, a modelling approach (RUC) was decided upon for this project. This

specificity is reflected in the change to 2.2. Initially, due to time constraints, only 2D modelling was considered, with a plan to expand to 3D if time permitted. However, by the completion of the proposal, 3D simulation had not been added as it remained relatively unexplored.

Additions:

- Integration of Coursework: The Gantt Chart for Semester 1 now includes coursework, laboratories, and quizzes, represented by three different scales of grey depending on the quantity of activities scheduled for each week. The legend indicates that 1, 2, or 3 colours represent the workload, with various combinations depicting the workload distribution throughout the semester.

	Evaluations: 1		
	CW		
	Lab		
	Quiz		
	Evaluations: 2		
	CW/CW	CW/Lab	
	Lab/Lab	Lab/Quiz	
	Quiz/Quiz	Quiz/CW	
	Evaluations: 3		
	CW/CW/CW	CW/CW/Lab	CW/CW/Quiz
	Lab/Lab/Lab	Lab/Lab/CW	Lab/Lab/Quiz
	Quiz/Quiz/Quiz	Quiz/Quiz/CW	Quiz/Quiz/Lab
	CW/Lab/Quiz		

In wrapping up this reflection, it's evident that there has been a substantial enhancement in the level of detail across all aspects of the Gantt Chart. There's a heightened awareness of the comprehensive workload necessary for a successful completion of Semester 1. Additionally, there's a glimpse into what needs to be accomplished for the individual project by Semester 2.

SEMESTER 2 GANTT CHART

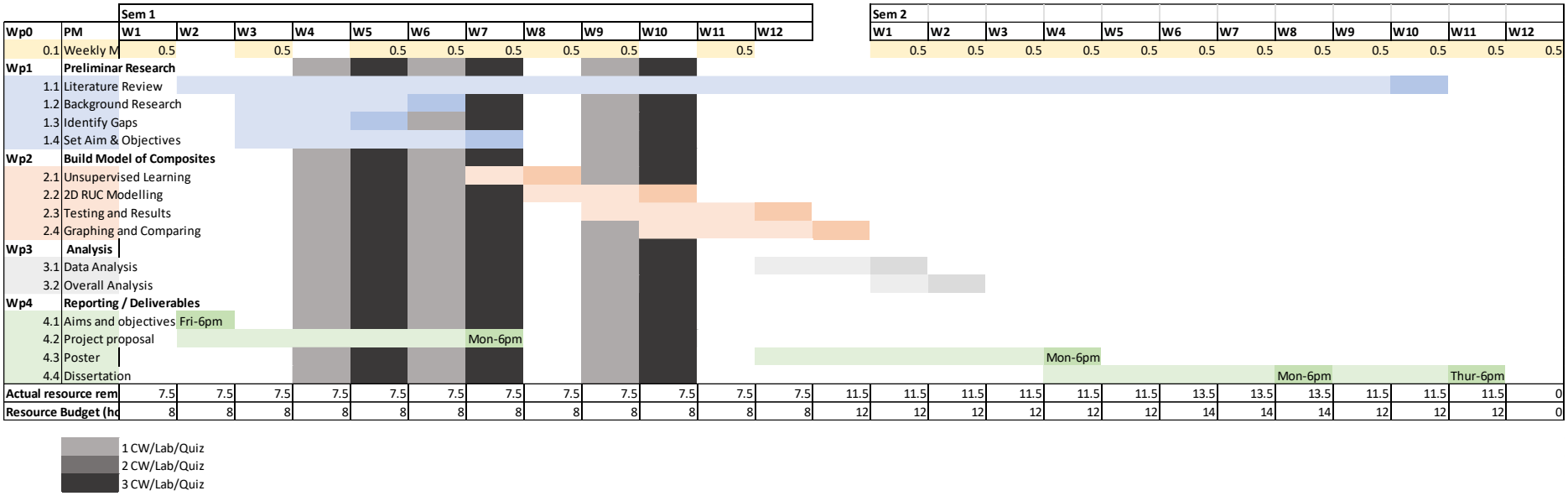

		Sem 1												Sem 2											
Wp0	**PM**	**W1**	**W2**	**W3**	**W4**	**W5**	**W6**	**W7**	**W8**	**W9**	**W10**	**W11**	**W12**	**W1**	**W2**	**W3**	**W4**	**W5**	**W6**	**W7**	**W8**	**W9**	**W10**	**W11**	**W12**
0.1	Weekly M	0.5		0.5		0.5	0.5	0.5	0.5	0.5		0.5		0.5	0.5	0.5	0.5	0.5	0.5	0.5	0.5	0.5	0.5	0.5	0.5
Wp1	**Preliminar Research**																								
1.1	Literature Review																								
1.2	Background Research																								
1.3	Identify Gaps																								
1.4	Set Aim & Objectives																								
Wp2	**Build Model of Composites**																								
2.1	Unsupervised Learning																								
2.2	2D RUC Modelling																								
2.3	Testing and Results																								
2.4	Graphing and Comparing																								
Wp3	**Analysis**																								
3.1	Data Analysis																								
3.2	Overall Analysis																								
Wp4	**Reporting / Deliverables**																								
4.1	Aims and objectives	Fri-6pm																							
4.2	Project proposal							Mon-6pm																	
4.3	Poster																Mon-6pm								
4.4	Dissertation																				Mon-6pm			Thur-6pm	
Actual resource rem		7.5	7.5	7.5	7.5	7.5	7.5	7.5	7.5	7.5	7.5	7.5	7.5	11.5	11.5	11.5	11.5	11.5	11.5	13.5	13.5	13.5	11.5	11.5	11.5	0
Resource Budget (ho		8	8	8	8	8	8	8	8	8	8	8	8	12	12	12	12	12	12	14	14	14	12	12	12	0

1 CW/Lab/Quiz
2 CW/Lab/Quiz
3 CW/Lab/Quiz

SEMESTER 2 GANTT CHART: REFLECTIONS

As Semester 2 commenced, a clearer plan and allocation of the workload needed for project completion emerged. Consequently, a more refined and detailed description of tasks was outlined. This distribution not only afforded me a broader overview but also fragmented tasks into manageable segments that could be accommodated within the personal weekly calendar. This approach aimed to facilitate continuous progress and alleviate the workload strain, particularly as parallel coursework labs and quizzes intensified. Similar to previous reflections, a compilation of changes and additions is elaborated below, along with their respective rationales and objectives.

Changes:

As mentioned above, significant revisions have been made to the task breakdown in both the Modeling and Analysis sections of the Gantt Chart. These revisions signify an improved comprehension of the necessary steps for effectively executing both the Modeling and Simulation of the Composites, as well as identifying pertinent discussion points based on the obtained results, also referred to as 'Discussion/Analysis.' Below are detailed explanations behind these changes.

Version: Draft	
Wp2	**Modelling**
2.1	Unsupervised Learning
2.2	Analytical Solver for Validation
2.3	Learning Python Scripts for RUC Mod.
2.4	Mesh Sensitivity
2.5	2D RUC Mod. & Collect Data
2.6	3D RUC Mod. & Collect Data
2.7	Validate Simulations

Version: Proposal	
Wp2	**Build Model of Composites**
2.1	Unsupervised Learning
2.2	2D RUC Modelling
2.3	Testing and Results
2.4	Graphing and comparing

Wp3	**Analysis**
3.1	Plotting of Results
3.2	Discussion of Mesh Sensitivity
3.3	Discussion of Validation
3.4	Discussion of Homogenised Properties

Wp3	**Analysis**
3.1	Data Analysis
3.2	Overall Analysis

- Modelling: The task section in the Gantt Chart has been meticulously detailed, encompassing the understanding that unsupervised learning remains a consistent element throughout the project despite its widespread comprehension. Even minor aspects, such as refining the imaging of figures from Abaqus/Standard to enhance result quality in the report, are continuously learned and improved upon, underscoring the significance of seemingly subtle efforts. While a Python Script for the analytical method wasn't deemed necessary, dedicating early semester time to initiating this supplementary project facilitated data generation and collection as the project progressed. Incorporating Mesh Sensitivity and Validation, denoted as 2.4 and 2.7 respectively, became imperative for ensuring sound simulation practices, hence their inclusion. Acquiring proficiency in Python and understanding Macros within Abaqus/Standard was essential for adapting the Python Script sourced from GitHub for project purposes. Notably, the code itself is not included in this document, as it wasn't authored by the writer. Furthermore, the data collection for 2D and 3D RUCs was split into two sub-tasks (2.5 and 2.6) due to each model utilizing different code, necessitating separate time allocations for each task.
- Analysis: Sub-task 3.1 for Analysis and Plotting was introduced to accommodate the considerable time needed for crafting custom figures, refining images from Abaqus/Standard simulations using MS PowerPoint, and mastering Origin Pro for generating Mesh Convergence plots and Spider Plots depicting the Homogenized properties of both Single and Hybrid-Fiber Composites. Like the modelling tasks, each sub-task necessitated thorough discussion to interpret simulation results, prompting a staggered division of tasks over time to alleviate the workload.

Additions:

- PhD Student Meeting: As depicted in the Gantt Chart, meetings with the PhD Student, Giuseppe Romano, became increasingly frequent towards the end of Semester 1 and continued throughout Semester 2. This adjustment was made based on the recognition that such meetings enhanced my performance within the project and increased my engagement, allowing me to stay on track with tasks and consistently receive valuable feedback across different project sections, thereby maximizing learning opportunities.

- Semester 2 Coursework: Similarly, the Coursework's deadline week were added, and the Laboratories required for the successful completion of Semester 2, following the same legend to prior update 'PROPOSAL GANTT CHART: REFLECTIONS'.

SEMESTER 2 GANTT CHART WITH EXTERNAL INFLUENCES

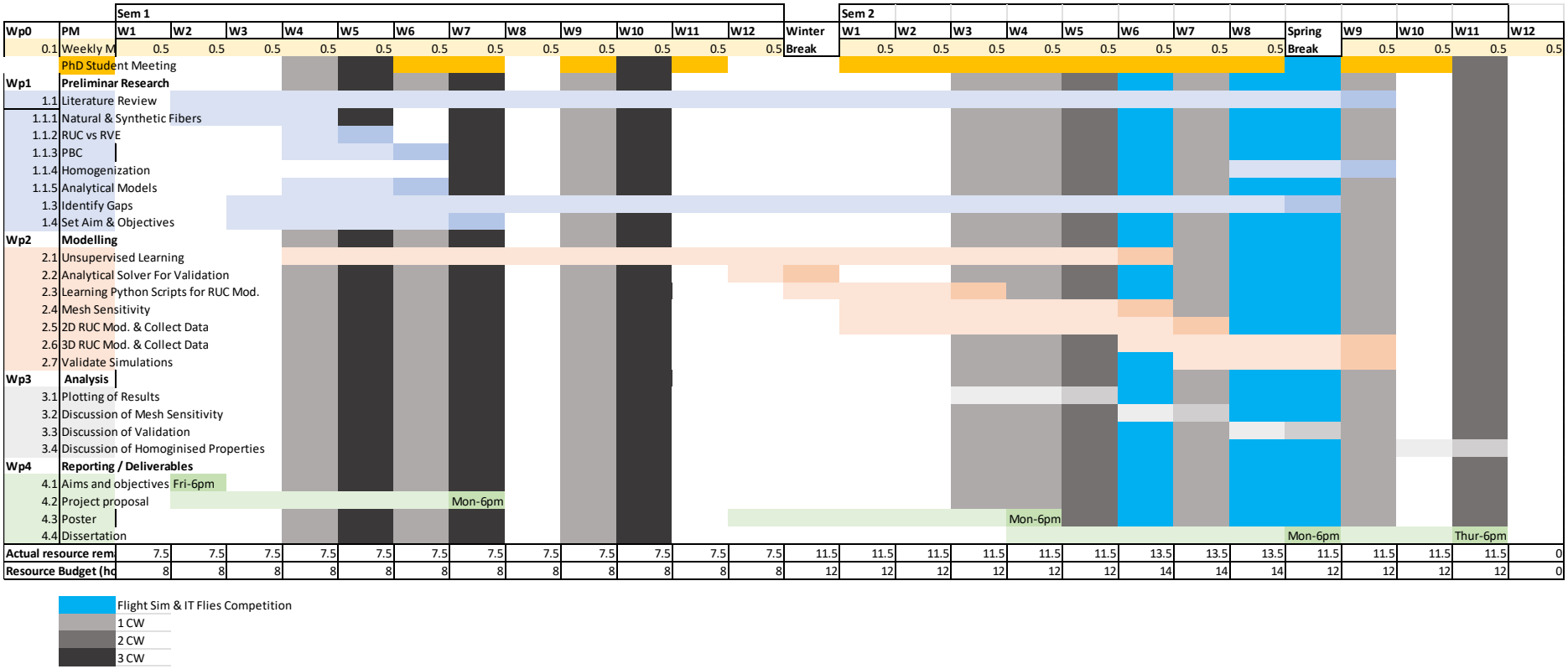

SEMESTER 2 GANTT CHART WITH EXTERNAL INFLUENCES: REFLECTIONS

Finally, the last update, where the same Gantt Chart of Semester 2 is kept equal with the exception of the addition of the society I am part of 'Flight Sim'. The Flight Sim activities occupied part of my time across weeks 6 to 9, as preparation was required in order to complete a model for competition. The competition, called IT Flies 2024 was hosted at The University of Dayton, Ohio. Required travelling delaying dissertation task further. Despite this, I was able to complete my tasks as expected as work was done throughout the trip.

APPENDIX B: PYTHON SCRIPT FOR VALIDATION USING ANALYTICAL MODELS FOR SINGLE-FIBER COMPOSITES

```
#Rule of Mixture & Chamis Models
'''
author: Juan Doval

     x2          x2 |o   o|
     |              |  o  |           RUC Model
     |____ x1       |o   o| x1
    /
x3 /

Variables
E1 is the Longitudinal Elastic Modulus
E2 is the Transversal Elastic Modulus

G12 is in-plane shear modulus
G23 is out of plane shear modulus

v12 is in-plane Poisson's ratio

V is volume fraction

K23 is the plane strain bulk moduli

Subscripts
f is fiber
m is matrix
'''

def rom(Em, Vf, E1f, vm, v12f, Gm, G12f, E2f, G23f):
    E1=E1f*Vf+(1-Vf)*Em #E1 Longitudinal Elastic Modulus
    E2=(E2f*Em)/(E2f*(1-Vf)+Em*Vf) #E2 Transversal Elastic Modulus
    v12=v12f*Vf+(1-Vf)*vm #v12 in-plane Poisson's ratio
    G23=Gm*(1/(1+((Gm/G23f)-1)*Vf))#G23 out-of plane shear modulus ROMm
    v23=(E2/(2*G23))-1 #v23 out-of-plane Poisson's ratio, #Not capable of
capturing tranverse isotropy due to poor representation to arrangement of
fibers
    G12=(G12f*Gm)/(G12f*(1-Vf)+Gm*Vf)#G12 in-plane shear modulus
    #G12=Gm*(1/(1+((Gm/G12f)-1)*Vf))#G12 in-plane shear modulus ROMm
    #K23=(K23f*Km)/(K23f*(1-Vf)+Km*Vf) #K23 in-plane strain bulk moduli
    #K23o=E1/(4*((E1/E2)-v12**2)-(E1/G23)) #K23o out-of-plane strain bulk
    print(f'ROM Values')
    # print(f'in-plane strain bulk moduli: {K23:.3f} GPa')
    #print(f'out-of-plane strain bulk modulus{K23o}')
    #print(f'out-of-plane shear modulus{G23}')
```

```
    print_results(f'{E1:.3f}', f'{E2:.3f}', f'{v12:.3f}', f'{v23:.3f}',
f'{G12:.3f}', f'{G23:.3f}')

def chamis(Em, Vf, E1f, vm, v12f, Gm, G12f, E2f, G23f):
    E1=Em+Vf*(E1f-Em) #No Vv as its assumed Void-Free
    E2=Em/(1-(1-(Em/E2f))*Vf**(1/2))
    v12=vm+Vf*(v12f-vm)
    G12=Gm/(1-(1-(Gm/G12f))*Vf**(1/2))
    G23=Gm/(1-(1-(Gm/G23f))*Vf**(1/2))
    v23=(E2/(2*G23))-1 #v23 out-of-plane Poisson's ratio, #Not capable of
capturing tranverse isotropy due to poor representation to arrangement of
fibers

    print(f'Chamis Values')
    # print(f'in-plane Shear Modulus: {G12:.3f}')
    # print(f'out-of-plane Shear Modulus: {G23:.3f}')

    print_results(f'{E1:.3f}', f'{E2:.3f}', f'{v12:.3f}', f'{v23:.3f}',
f'{G12:.3f}', f'{G23:.3f}')

def print_results(lem, tem, inv, outv, g12, g23):
    print(f'Longitudinal Elastic Modulus: {lem} Gpa')
    print(f'Transversal Elastic Modulus: {tem} GPa')
    print(f'in-plane Poisson ratio: {inv}')
    print(f'out-of-plane Poisson ratio: {outv}')
    print(f'Longitudinal Shear Modulus: {g12} Gpa')
    print(f'Transversal Shear Modulus: {g23} GPa')

def select_fiber(fibers_material_properties):
    # Fibers Dictionary
    print('0: E-Glass, 1: Basalt, 2: Carbon Fiber, 3: Flax')
    print('Choose a fiber material:')
    for i in fibers_material_properties:
        print(f'{i}: {fibers_material_properties[i]}')

    selected_fibers_material = int(input("Enter the index of the fiber
material: "))

    selected_fibers_properties =
fibers_material_properties[selected_fibers_material]

    return (selected_fibers_properties['E1f'],
selected_fibers_properties['E2f'], selected_fibers_properties['v12f'],
            selected_fibers_properties['K23f'],
selected_fibers_properties['G12f'], selected_fibers_properties['G23f'])
```

```
def select_matrix(matrix_material_properties):
    # Matrix Dictionary
    print('0: Epoxy')
    print('Choose a matrix material:')
    for i in matrix_material_properties:
        print(f'{i}: {matrix_material_properties[i]}')

    selected_matrix_material = int(input("Enter the index of the matrix
material: "))

    return (matrix_material_properties[selected_matrix_material]["Em"],
            matrix_material_properties[selected_matrix_material]["vm"],
            matrix_material_properties[selected_matrix_material]["Gm"],
            matrix_material_properties[selected_matrix_material]["Km"])

def select_method(selection_choices):
    print(selection_choices)
    return int(input("Enter the index of the method: "))

def getVf():
    while True:
        Vf = float(input("Enter Vf (between 0.45 and 0.65): "))
        if 0.45 <= Vf <= 0.65:
            return Vf
        else:
            print("Vf must be between 0.45 and 0.65. Please try again.")


def fiber_single(fibers_material_properties, matrix_material_properties):

    E1f, E2f, v12f, K23f, G12f, G23f =
select_fiber(fibers_material_properties)
    Em, vm, Gm, Km = select_matrix(matrix_material_properties)
    Vf = getVf()

    # Matrix Volume Fraction
    Vm=1-Vf

    # Ask the user to choose the method
    method = select_method(
        """
          Choose a method:\n
          1: Rule of Mixtures (ROM) \n
          2: Chamis Method
        """)
    #Em, Vf, E1f, vm, v12f, Gm, G12f, E2f, G23f
    if method == 1:
       rom(Em=Em, Vf=Vf, E1f=E1f, vm=vm, v12f=v12f, Gm=Gm, G12f=G12f, E2f=E2f,
G23f=G23f)
```

```
    elif method == 2:
        chamis(Em=Em, Vf=Vf, E1f=E1f, vm=vm, v12f=v12f, Gm=Gm, G12f=G12f,
E2f=E2f, G23f=G23f)
    else:
        print('Invalid Method Selection')

def fiber_double(fibers_material_properties):
    E1f1, E2f1, v12f1, K23f1, G12f1, G23f1 =
select_fiber(fibers_material_properties)
    E1f2, E2f2, v12f2, K23f2, G12f2, G23f2 =
select_fiber(fibers_material_properties)
    Em, vm, Gm, Km = select_matrix(matrix_material_properties)


    print('Not finished')


print("""
      Choose a Single Fiber or Fiber Hybrid: \n
      "1: Single Fiber" \n
      "2: Fiber Hybrid"
      """)

fibers_amount = int(input("Enter the type of composite: "))

fibers_material_properties = {
        0: {'E1f': 73, 'E2f': 73, 'v12f': 0.23,'G12f': 30.2, 'G23f': 30.2,
'K23f': 50},  # E-Glass
        1: {'E1f': 89, 'E2f': 89,'v12f': 0.26, 'G12f': 21.7, 'G23f': 21.7,
'K23f': 60},  # Basalt
        2: {'E1f': 290, 'E2f': 21, 'v12f': 0.2, 'G12f': 14, 'G23f': 7.04,
'K23f': 70},   # Carbon Fiber
        3: {'E1f': 54.1, 'E2f': 7, 'v12f': 0.3, 'G12f': 3, 'G23f': 2, 'K23f':
0}    # Flax
}

matrix_material_properties = {
    0: {'Em': 4.30, 'vm': 0.35,'Gm': 1.29, 'Km': 3.0}  # Epoxy
}

if fibers_amount == 1: # Single Fiber
    fiber_single(fibers_material_properties, matrix_material_properties)
elif fibers_amount == 2:
    fiber_double()
    pass
else:
    print('Invalid Composite type')
```

Fin